LOSS OF *BRCA1* INDUCES SENESCENCE OF MURINE OVARIAN FIBROBLASTS AND MAY CONTRIBUTE TO FIBROBLAST-MEDIATED OVARIAN AGING

Submitted by Het Vaishnav

A thesis submitted in partial fulfillment of the requirements for the degree of Master of Science, Specialization in Cellular and Molecular Medicine

Department of Cellular and Molecular Medicine

University of Ottawa

Ottawa, Ontario, Canada

May 2023

Supervised by Dr. Barbara C. Vanderhyden

© Het Vaishnav, Ottawa, Canada, 2023

Abstract

Ovarian cancer, primarily diagnosed at advanced stages of the disease, is the most lethal of all gynaecological malignancies, with a 5-year survival of only 45%. Increasing age and number of ovulations are the primary non-hereditary risk factors, with the median age of onset being 63 years. Considering that risk peaks upon onset of menopause and that 50% of all cases of ovarian cancer have non-ovarian origins, it is believed that the physiological aging of the ovary renders it an appealing pre-metastatic niche. Mutations in the tumor suppressor genes *BRCA1* and *BRCA2* are the primary hereditary risk factors, accounting for 20-25% of all cases. We have preliminary data showing that *BRCA1* mutation carriers tend to develop ovarian fibrosis, a phenomenon that naturally accompanies ovarian aging, at premenopausal ages, whereas age-associated fibrosis becomes evident after menopause in non-carriers. Consistently, *BRCA1*/*2* mutation carriers are at elevated risk for premature cessation of ovarian function. With the median age of cancer onset decreasing from 63 to 50 years of age in *BRCA1* mutation carriers, these data collectively suggest accelerated ovarian aging in these women and highlights an association between ovarian aging and increased risk for cancer. As such, we hypothesized that loss of *Brca1* in murine ovarian fibroblasts (MOFs) may accelerate the onset of ovarian fibrosis through fibroblast hyperactivation, contributing to ovarian aging. Using primary MOFs isolated from *Brca1* LoxP/LoxP mice and adenoviral cre mediated recombination, we generated *Brca1* deficient MOFs. RNA sequencing was used to characterize the transcriptomic changes associated with the loss of *Brca1*. Our findings suggest that *Brca1* deficiency in MOFs induces cellular senescence and enhances their myofibroblastic function, likely yielding increased stiffness of the ovarian extracellular matrix due to the dysregulated synthesis and degradation of its constitutive components, contributing to accelerated ovarian aging.

Acknowledgments

I would like to take this opportunity to thank all the individuals who have not only supported me every step in my research journey, but without whom this body of work would not have been possible. First and foremost, I would like to thank my supervisor, Dr. Barbara Vanderhyden for her critical guidance and mentorship that have taught me invaluable skills, such as scientific writing, good experimental design and planning, the value of team-work, among many others that have shaped me into a scientist capable of tackling any roadblock. Your never-ending support, optimism, love and curiosity for science have made it possible for me to persistently work on this project despite all the failures and continue to inspire me to look for answers and get to the bottom of scientific questions. I'd especially like to thank you for always patiently listening to my crazy ideas, fueling, and channeling my passion for science, despite having barged into your office unannounced, countless times over the past 5 years.

I thank Dr. David Landry for his time, invaluable guidance, and mentorship for not only teaching me all the hands-on techniques I know and lab bookkeeping, but also for training me to be become a thorough scientist, and for helping me troubleshoot and pilot this project from the very beginning. It would not have been possible for me to get this far into the project without your expertise and support. Many thanks to members of my thesis advisory committee, Drs. Jay Baltz and Angela Crawley, for challenging me, and for providing guidance, direction, and important scientific perspectives. Special thanks for Dr. Keith Wheaton for always listening to and helping me resolve roadblocks along this project and for encouraging and challenging me to always think critically and out of the box.

I'd like to acknowledge Elizabeth Macdonald- for always having a solution for all problems, and for hers and Humaira Murshed's efforts in breeding, genotyping and generating the desired mouse models for this project; all staff at the Animal Care and Veterinary Services facilities at the University of Ottawa, who oversaw the wellbeing of all mice, without whom this work would have literally been impossible; Eddy Yakubovich for the extensive amount of time he has spent analyzing RNA-sequencing data, and explaining bioinformatics to me; Melanie Grondin for analyzing and running statistical analysis on

Incucyte® live cell imaging proliferation assays; and Emily Thompson, who has spent countless hours with me at the microtome sectioning and staining tissues. I would also like to thank all members of the Vanderhyden Lab, who have supported me every step of the way and been integral parts of my journey and success as a graduate student, challenging me to be the best version of myself. I truly couldn't have imagined being a part of a better team and going through graduate school with a better group of people.

To my friends, Doan Doan and Phillip Phi Pham, I would not have made it this far without you, thank you. I would especially like to thank my extremely supportive family- my parents, Kalpa and Tushar Vaishnav, who have given me unconditional love and continuous support over these past few years, and a special thank you to my partner, Glib Maznyi, who has unquestionably supported me through all the ups and downs of graduate studies.

Table of Contents

List of Figures

List of Tables

List of Abbreviations

Acetyltransferase P300/Cbp-associated factor (PCAF)

Adenovirus encoding for Cre recombinase (AdCre)

Analysis of variance (ANOVA)

Anti-mullerian hormone (AMH)

Antigen presenting CAFs (apCAFs)

Assisted reproductive technologies (ART)

BRCA1 (human gene)

BRCA1 (Human and mouse protein)

Brca1 (mouse gene)

BRCA1 associated Genome surveillance Complex (BASC)

BRCA1 associated RING domain protein 1 (BARD1)

BRCA1 C-terminal domain (BRCT domain)

Breast cancer susceptibility protein 1 (*BRCA1)*

Breast cancer susceptibility protein 2 (*BRCA2*)

Cancer antigen-125 (CA-125)

Cancer associated fibroblasts (CAFs)

Cell adhesion molecular (CAM)

Complimentary DNA (cDNA)

Corpus luteum (CL)

Cyclin dependent kinase (CDK)

Deoxyribonucleic acid (DNA)

Double stranded DNA breaks/ repair (DsDNA breaks/repair)

Empty adenovirus (AdEmpty)

Enhanced yellow fluorescent protein (EYFP)

Epidermal growth factor (EGF)

Epithelial ovarian cancer (EOC)

Extracellular matrix (ECM)

Fibroblast growth factor (FGF)

Follicle stimulating hormone (FSH)

Galectin 3 (Gal3)

Galectin 9 (Gal9)

Genomic DNA (gDNA)

Glycosaminoglycans (GAG)

Growth factor (GF)

Hank's balanced salt solution (HBSS)

Hematoxylin & Eosin (H&E)

Hereditary breast and ovarian cancer (HBOC)

High grade serous carcinoma (HGSC)

Homologous recombination (HR)

Hormonal replacement therapy (HRT)

Hyaluronan/ Hyaluronic acid (HA)

Inflammatory CAFs (iCAFs)

Innate lymphoid cell (ILC)

Insulin-like growth factor binding proteins (Igfbp)

Knockout (KO)

Luteinizing hormone (LH)

Lysine 320 acetylation (K320-Ac)

Lysine 373 acetylation (K373-Ac)

Lysine residues (K)

Matrix metalloproteinases (MMPs)

Microgram (µg)

Microlitre (µL)

Milligram (mg)

Millilitre (mL)

Minutes (mins)

Molecular signature database (MSigDb)

Murine ovarian fibroblasts (MOFs)

Murine ovarian surface epithelial cells (mOSE cells)

Multiplicity of infection (MOI)

Myofibroblastic CAFs (myCAFs)

Nanogram (ng)

Natural Killer cells (NK)

Neutral-buffered formalin (NBF)

Non-epithelial cancer (NEOC)

Ovarian cancer (OC)

Ovarian surface epithelium (OSE)

Partner and Localizer of BRCA2 (PALB2)

Phosphate-buffered saline (PBS)

Polyadenylated tail (PolyA tail)

Polymerase chain reaction (PCR)

Post translational modifications (PTM)

Primary ovarian insufficiency (POI)

Proteoglycans (PG)

Quantitative PCR (qPCR)

RAD50-MRE11-NBS1 complex (MRN complex)

Replication protein A (RPA)

Reverse Transcription- PCR (RT-PCR)

Ribonucleic acid (RNA)

Senescence associated- P21 associated secretory phenotype (SA-PASP)

Senescence associated secretory phenotype (SASP)

Senescence-associated β-galactosidase (SA-β-Gal)

Serine protease inhibitors (SERPIN)

Serous tubal intra-epithelial carcinoma (STIC)

Standard error of mean (SEM)

T-helper cells (Th)

Tissue inhibitors of MMPs (TIMPs)

Transforming growth factor β1 (TGF-β)

Tumor necrotic factor α (TNF-α)

Type 2 Th cells (Th2)

Ubiquitin (Ubq)

Wild type (wt)

Alpha-Smooth muscle actin (α-SMA)

Chapter 1: Introduction

1.1 Ovarian cancer: An overview

1.1.1 Ovarian cancer today

Ovarian cancer (OC) is a group of gynecological malignancies that either arise by tumorigenesis of specific cell types in the ovary or lead to tumorigenesis on the ovary. It is the fifth leading cause of cancer-related deaths in women worldwide and is the most lethal form of all gynecological malignancies. In Canada, nearly 3000 women are diagnosed with OC, and 1950 die from it, each year[1]. Diagnosis in early stages of disease, prior to metastasis is associated with a 5-year survival rate of 90%[2], however, only approximately 16% of OC patients are diagnosed with early disease[3]. Due to the lack of specific screening methods and diagnostic tests, along with few specific symptoms, most cases of OC are diagnosed at advanced stages, following metastasis and onset of severe symptoms. This causes most patients to face a dispiriting 5-year survival rate of 45%[4].

1.1.2 Classification of ovarian cancer

Depending on the cellular origins of OC, the disease is either classified as non-epithelial OC or as epithelial OC. Both, non-epithelial and epithelial OC, can be further classified into subtypes, primarily based on histopathology of the cancerous mass.

1.1.2.1 Non-epithelial ovarian cancer

Non-epithelial OC (NEOC) are rarer forms of ovarian cancer and account for only 10-15% of all cases of ovarian cancer[5]. NEOC primarily includes germ cell and sex-cord-stromal tumors. Both germ cell tumors and sex-cord-stromal tumors are true intra-ovarian cancers in that they originate and arise from cells that are native to the ovary[6]. Germ cell cancers originate from

oocytes, while sex-cord-stromal cancers originate from somatic ovarian cells such as granulosa and theca cells. Most NEOC are diagnosed at early stages, and the tumors typically remain confined to the ovary, with a 5-year survival rate of 90-100% with early diagnosis[7,8].

1.1.2.2 Epithelial ovarian cancer

Epithelial OC (EOC) accounts for the majority (90%) of all cases of OC[5] and represents diverse subtypes that are believed to be of epithelial origin. High-grade serous carcinomas (HGSC), a fast-growing, aggressive subtype of EOC, accounts for 75% of all cases of EOC, and are typically (70% of all cases) diagnosed at advanced stages of disease (stages III-IV)[9], once the disease has metastasized to the peritoneum, the inner lining of the abdominopelvic cavity. HGSC is associated with poor prognosis, high probability (70-90%) of recurrence[10], and is responsible for 50% of all OC related deaths[11]. Other EOC include low-grade serous, endometrioid, mucinous and clear-cell carcinomas, that collectively account for 25-30% of all cases of EOC[12].

1.2 The aging ovary as a pre-metastatic niche

HGSC were once thought to originate solely from transformed cells of the ovarian surface epithelium (OSE), which is the outermost layer of cells encasing the ovary[13]. In 1971 Fathalla et al. attributed the onset of EOC to incessant ovulations, suggesting that the repeated exposure of OSE cells to inflammation and minor trauma requiring wound repair may increase the risk of accumulating genetic aberrations, driving the transformation of OSE, and resulting in EOC with age[14]. However, unlike NEOC tumors, not all occurrences of EOC originate from cells native to the ovary. Recent evidence suggests that HGSC, among other EOC, such as clear cell and endometrioid carcinomas, can arise from cells that are not normally present in the ovarian tissue[6].

A growing body of research has identified serous tubal intra-epithelial carcinoma (STIC) lesions from the epithelium of the distal fallopian tube to be another source of HGSC[15–17], the most common and aggressive form of OC. STIC lesions originate in the fallopian tubes, and then migrate to the ovary, where implantation is followed with the development of a primary HGSC tumor, facilitated by the ovarian microenvironment (Figure 1). STIC lesions are identifiable as precursors to HGSC in approximately 50% of all advanced stages of disease[18]. Moreover, while endometriosis is non-neoplastic, the presence of endometrial tissue on the ovary is a known risk factor for clear cell and endometrioid EOC[19]. Additionally, the ovary has been identified as a site of frequent metastasis[20–22] from a variety of primary cancers, such as gastrointestinal, breast, endometrial/uterine, colorectal and stomach cancers[21–23]. The formation of primary and metastatic ovarian tumors from non-ovarian sources is indicative of a "fertile" ovarian microenvironment that facilitates the growth of precancerous and cancerous lesions.

The median age of onset of ovarian cancer is 63 years of age. As such, more frequently than not, ovarian cancer patients at the time of diagnosis are primarily post-menopausal women. Without any predisposition to the disease, the onset of ovarian cancer at pre-menopausal ages is uncommon[24,25]. However, the risk for OC dramatically increases around peri-menopausal ages[25] (40-45 year of age), peaking after menopause, with most patients being diagnosed between the ages of 55-64, and gradually decreases until the age of 80[26].

Pre-cancerous lesions originating from non-ovarian tissues are able to induce the formation of primary ovarian tumors, as is seen with STIC lesions and HGSC. While implantation and development of non-gynaecological metastasis to the ovary may result in secondary ovarian tumours. Taken together with increasing risk of ovarian cancer with age, this collectively suggests that the aging ovary offers an appealing pre-metastatic niche, facilitating the growth of and organ

invasion by disseminated cancer cells, leading to the formation of primary and/or secondary tumors. It is currently unclear why or how the aging ovary transforms into an appealing pre-metastatic niche.

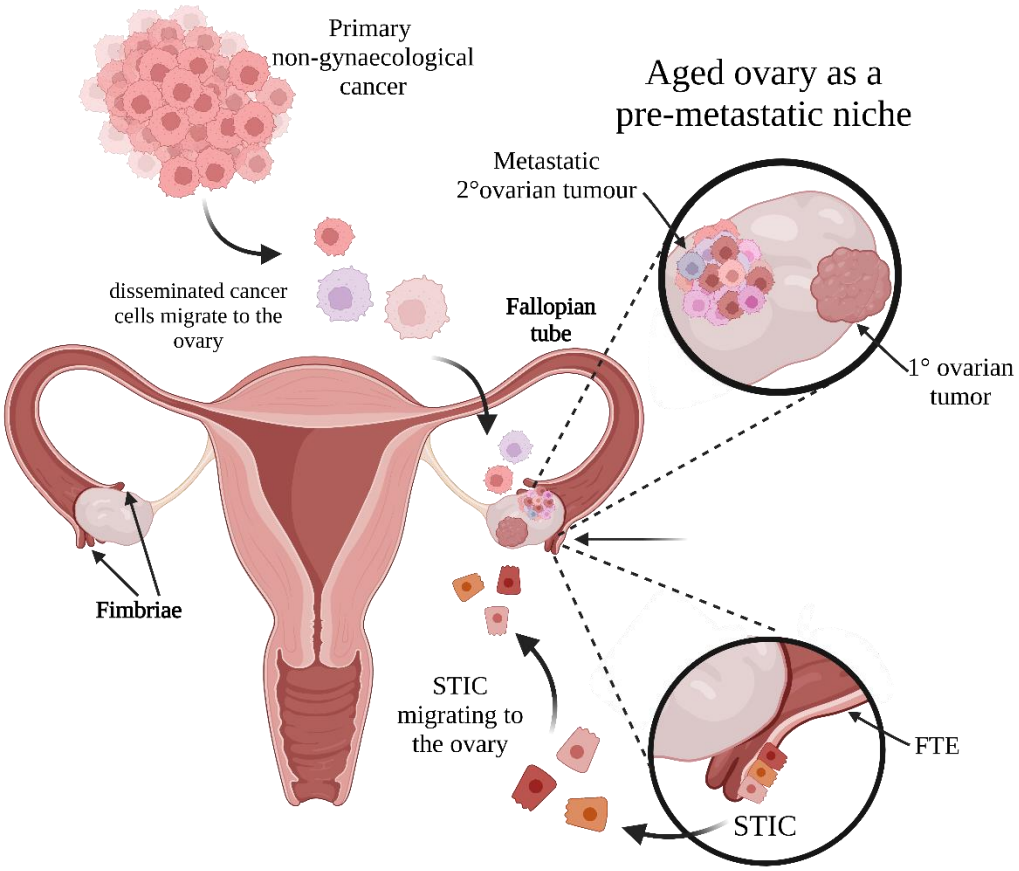

Figure 1: The aging ovary as a pre-metastatic niche. *Approximately fifty percent of all cases of high-grade serous carcinoma arise from serous tubal intraepithelial carcinoma (STIC) lesions that originate in the fallopian tube epithelium (FTE) of the fimbria and migrate to the ovary, where they implant into the aging ovary. The aging ovary functions as optimal "soil" for STIC lesion "seeds", supporting tumorigenesis. Figure created with BioRender.com.*

1.3 Symptoms and screening for ovarian cancer

According to the Ovarian Cancer Research Alliance, increased occurrence and persistence of any of the following for more than 2 weeks are considered common symptoms for ovarian

cancer: (a) bloating or abdominal distention, (b) pelvic or abdominal pain, (c) difficulty breathing or eating (feeling full quickly), and (d) urinary frequency[27]. Due to the subtle, non-specific nature of these symptoms, they are either often dismissed or easily mistaken for other more common causes and, as such, diagnosis is not made until the onset of severe symptoms, at which point disease progression is advanced. Fatigue, indigestion, back pain, constipation and menstrual abnormalities have also been found to be common symptoms among OC patients, however, these symptoms are experienced by both OC patients and healthy age-matched (no OC) women.

Ovarian cancer is only screened routinely in those at high risk of the disease (*BRCA1* or *BRCA2* mutation carriers or family history), not the general population[28,29]. Due to the lack of physical accessibility to the ovaries, screening of OC is limited to a bimanual pelvic exam, blood test for CA-125 and a transvaginal ultrasound[30]. Serum levels of CA-125, a tumor-associated antigen, have been reported to differentiate between malignant and benign tumors and to correlate with the progression of OC[31]. However, clinical evidence indicates CA-125 as a biomarker for OC has low specificity, as a variety of conditions associated with the female reproductive system, both normal and pathological, can result in elevated serum levels of CA-125, such as pregnancy, menstruation, endometriosis, benign ovarian tumors and cysts, yielding a high-false positive rate[29,32–34]. Additionally, while 90% of patients at advanced stages of OC were found to have high serum levels of CA-125, only about 50% of patients at early stages were found to have elevated serum CA-125[31], rendering blood tests for CA-125 ineffective for early detection. As such, CA-125 is not a reliable marker for OC screening. While the use of transvaginal ultrasound along with the CA-125 blood test rules out false-positive results, it cannot be used to reliably distinguish between benign and malignant tumors.

Currently, the most successful screening program aimed at early detection of OC requires major abdominal surgery, a highly invasive procedure to merely test for the presence of cancer[35]. The use of CA-125, in combination with other biomarkers, and transvaginal ultrasound to screen for OC is currently being investigated clinically; it is however not yet standard procedure.

The "silent" nature of early disease in combination with the lack of reliable screening methods results in the majority of patients being diagnosed at advanced stages of the disease. Late-stage diagnosis is associated with high recurrence rates, resistance to chemotherapy, and overall poor prognosis that results in dismal 5-year survival rates. This highlights the dire need for improved prevention for the disease. Hence, a better understanding of risk factors is required in order to develop better preventative strategies to combat the onset of disease.

1.4 Risk factors for ovarian cancer

Several risk factors collectively govern the likelihood for development of OC, and can primarily be classified into two categories, non-hereditary risk factors and hereditary risk factors. Non-hereditary risk factors include environmental factors, ovulation and age, while hereditary risk factors include genetic predisposition to the disease, all of which will be addressed here.

1.4.1 Non-hereditary risk factors

Approximately 75-80% of all cases of OC have no hereditary tendencies for the disease. Total lifetime number of ovulations and an increase in age are the primary non-hereditary risk factors for ovarian cancer. Certain environmental factors can also increase the risk for ovarian cancer, including some aspects of lifestyle, specifically the use of hormonal replacement therapy (HRT) after menopause[36]. Smoking, obesity and poor diet may play minor roles in contributing to

increased risk of OC. As for modifiable environmental factors, exposure to pesticides, herbicides and talc are believed to increase the risk of OC[37].

1.4.1.1 Ovulation as a risk factor for ovarian cancer

The total number of life-time ovulations is the primary non-hereditary risk factor for OC[38]. Decreased risk for the development of OC has been clinically observed with (5 or more years) use of oral contraceptives that function by blocking ovulation, suggesting an association between total lifetime ovulations and risk of OC onset[39–42].

Ovulation is a physiologic process that is characterized by rupture of the ovarian surface epithelium and release of a mature oocyte from a dominant follicle[43]. It is a highly inflammatory event that is initiated by a surge of luteinizing hormone (LH), and is mediated by stromal fibroblasts and immune cells[44–47]. Ovulation is the end result of folliculogenesis, which is the development of ovarian follicles through various stages to release a mature oocyte for fertilization[48]. Ovarian function (folliculogenesis) is dependent on and is tightly regulated by the timely production and release of various hormones through the hypothalamus-pituitary-ovarian axis[49]. The LH surge that is required for ovulation is produced by the anterior pituitary in response to high-frequency pulsatile release of gonadotropin-releasing hormone by the hypothalamus, which is in turn primed by the sustained release of estrogens by granulosa cells of the growing antral follicles[43,44]. Following release of the oocyte, LH and follicle stimulating hormone (FSH), released by the anterior pituitary, facilitate the transformation of the remnants of the ruptured follicle (luteinized granulosa cells and theca cells) into the corpus luteum that is then responsible for progesterone and estrogen production to support implantation and early pregnancy. Formation of the corpus luteum marks the beginning of the luteal phase, lasting between 12-14 days. Estrogen and progesterone released by the corpus luteum in turn act on the anterior pituitary to suppress the

production of LH and FSH. Dropping levels of LH and FSH in turn lead to eventual atrophy of the corpus luteum. Implantation of an embryo rescues the corpus luteum and thereby prevents the beginning of the next ovarian cycle. However, in the absence of pregnancy, the corpus luteum is degraded, marking the end of the luteal phase, which is followed by menstruation. Starting during the last few days of menstruation, the levels of FSH begin to rise, marking the start of the follicular phase, during which tertiary follicles recruited by rising FSH mature. FSH promotes proliferation of granulosa cells and induces the expression of LH receptors. As follicles continue to grow throughout the follicular phase, granulosa cells of these follicles secrete increasingly higher levels of estrogen that are necessary for the formation of a new endometrial layer, in preparation for the next ovulation[43,50]. The follicular phase comes to an end as estrogen levels peak, inducing LH production and consequent surge leading to ovulation[50]. Starting during puberty, the human ovary repeatedly goes through the above-mentioned ovarian cycle for approximately the next 30 years, with ovulation happening every 28-30 days. A typical woman will have > 360 ovulations before reaching menopause[46].

Folliculogenesis takes places in the ovarian cortex[48] (shown below in **Figure 2**), just underneath the OSE, separated by a layer of connective tissue called the tunica albuginea[13]. The central zone of the ovary is referred to as the medulla[13] and is comprised of loose connective tissue, blood and lymphatic vessels, as well as nerves[51]. The ovarian stroma includes tissue resident fibroblasts, immune cells[51] and the extracellular matrix (ECM) that is crucial for providing structural and biochemical support. Components of the stroma support all aspects of folliculogenesis and are as such indispensable for proper ovarian function. For example, mouse models of ovary specific depletion of macrophages and myeloid cells resulted in hemorrhagic

ovaries, impaired corpus luteum formation, and hence reduced progesterone production and infertility, suggesting that ovarian macrophages are crucial for proper ovarian function[52,53].

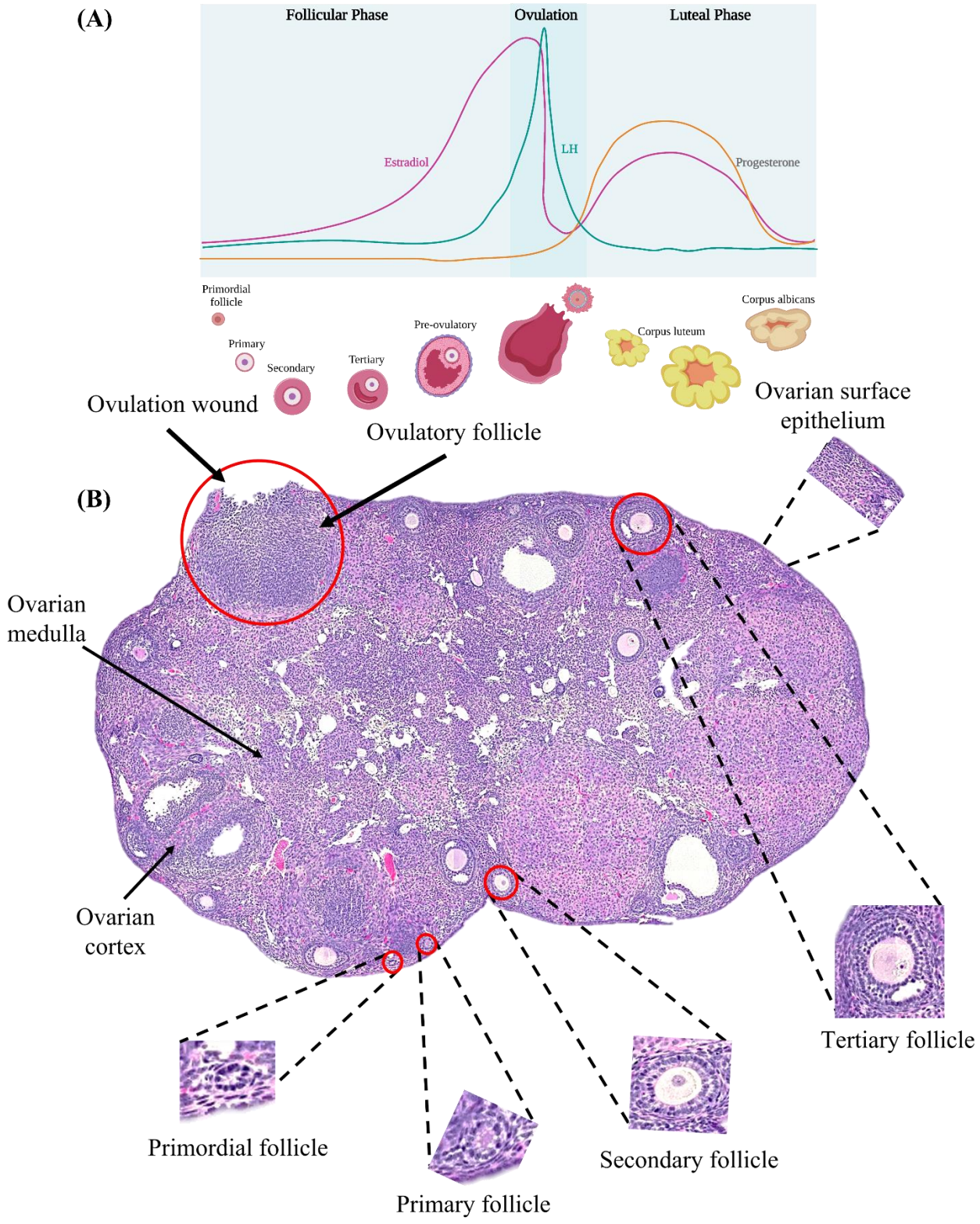

Figure 2: Hypothalamus-Pituitary-Ovarian axis dictates folliculogenesis. (A) *Relative levels of hormones during each phase of the ovarian cycle- As follicles grow during the follicular phase,*

proliferating granulosa cells release estrogen, with estrogen levels peaking right before ovulation. With levels of LH rising during the ovulatory phase, levels of estrogen sharply drop as LH spikes and induces ovulation. During the luteal phase, the corpus luteum produces estrogen and progesterone to support pregnancy. In the absence of a viable pregnancy, the corpus luteum atrophies to become a corpus albicans. ***(B)*** *Hematoxylin and eosin-stained section of a murine ovary showing follicular structure associated with different stages of follicular development and anatomical regions of the ovary: ovarian surface epithelium (OSE)- a single layer of epithelial cells that ruptures during ovulation (ovulation wound), ovarian cortex- region underlying the OSE and the site for folliculogenesis, and ovarian medulla- where dormant follicles reside. Figure 2(A) was created with BioRender.com; Hematoxylin and eosin-stained section of murine ovary in 2(B) was generated as part of a supporting study for this project.*

Each ovulatory cycle is accompanied by substantial tissue remodelling[45]. Throughout the cycle, follicles move from the rigid ovarian cortex to the softer medulla as they develop and then back to the ovarian periphery for ovulation. Follicles and other cells of the ovarian stroma secrete various matrix remodelling enzymes, such as matrix metalloproteinases (MMPs) and tissue inhibitors of MMPs (TIMPs) to soften the surrounding ECM, allowing for follicular growth and expansion[54]. As antral follicles reach pre-ovulatory stages, the ovarian ECM undergoes substantial proteoglycan degradation and remodelling that is mediated by the pre-ovulatory follicle as well as tissue resident fibroblasts and macrophages[51,55]. Furthermore, stimulation of the pre-ovulatory follicle by the LH surge induces the production of various remodelling enzymes that mediate degradation of the ECM surrounding the apical region of the follicle and facilitates weakening of the OSE layer in preparation for ovulation. The rise in LH levels has been shown to increase blood flow to the ovary, specifically to the pre-ovulatory follicle, causing it to become edematous. This increase in blood circulation close to ovulation sites has been associated with increased immune migration to the ovary, specifically basophils, macrophages, thrombocytes among other leukocytes [44,56]. The subsequent rupture of the OSE imparts substantial inflammation and requires extensive

wound healing. While the process of ovulation includes series of events distinct from that of inflammation, due to the commonalities and similarities between events associated with both- such as, vasodilation, hyperemia, edema, collagenolysis, and cell proliferation[57], as well as the ability if ovulatory events to evoke an immune response, ovulation is regarded as an inflammatory event[44,56]. This is supported by the finding that the follicular fluid released by the erupting follicle that bathes the OSE contains proteins involved in the positive regulation of immune responses, such as CCL4 and TGF-β[58]. Post-ovulatory wound healing is a collaborative effort mediated by a variety of different cell types, including the OSE cells themselves. Pro-inflammatory cytokines such as TGF-β and TNF-α, that are released in the follicular fluid, and produced by tissue resident macrophages along with other immune cells are known to activate myofibroblasts and induce the expression of α-smooth muscle actin (α-SMA), an actin isoform essential for proper wound healing. Myofibroblast activation has also been associated with increased deposition of collagen fibers and other structural proteins and remodelling of the ECM, that collectively act to facilitate the repair of ovulation induced tissue injury[59].

Throughout the reproductive period (spanning approximately 40 years), the ovaries consistently undergo cycles of extensive and dynamic tissue remodelling, persistent inflammation and wound repair, through repeated folliculogenesis and ovulation, that render the ovarian surface uneven and lead to age-associated onset of ovarian fibrosis[60–63]. While the mechanisms leading to age-associated ovarian fibrosis remain to be elucidated, it is possible that with age (and therefore, increased number of ovulatory cycles) and persistent inflammation (and consequent activation of myofibroblasts) that accompanies ovulation, the homeostasis between the synthesis and degradation of the ECM is altered, resulting in the excessive accumulation of structural ECM proteins, such as various collagens and fibronectin, consequently, resulting in age-associated

ovarian fibrosis. Pathological fibrosis, which is considered to be a response to over-exuberant wound healing response, often to repeated inflammatory injury[64,65], such as ovulation. Furthermore, consistent with this possibility is the finding that persistent myofibroblast activation has been associated with the development of pathological fibrosis and tissue stiffening[66–68].

It can therefore be hypothesized that an increase in the number of life-time ovulations poses as a risk factor for ovarian cancer through the onset of age-associated ovarian fibrosis.

1.4.1.2 Age-associated ovarian fibrosis as a risk factor for OC

Tissue fibrosis results from the excessive accumulation of ordered components of the ECM, primarily fibers of various collagens. Of note is the structure, arrangement and overall organization of collagen fibrils, for fibrosis is not simply the excessive accumulation of ECM components. As tissues age, they lose their elasticity and become increasingly stiff and rigid due to excessive accumulation of anisotropic collagen fibrils[69,70], a defining pathogenic feature of fibrosis.

The ovarian stroma is known to become fibrotic with age[60–63]. Age-associated ovarian fibrosis in the murine ovary has been shown by increased alignment and thickness of collagen fibers[61,62], which is reflective of increased tissue stiffness[71]. Increased tissue stiffness is indicative of tumor-promoting stroma and has been correlated with increased invasion of cancer cells[72–74]. In the case of breast cancer, the presence of aligned fibers of collagen III in perpendicular orientation to the tumor boundary was associated with poor prognosis and decreased disease-free survival, suggesting that the presence of pathological fibrosis not only increases risk for cancer onset but contributes to poor disease prognoses[75].

In addition to age-associated fibrosis, Briley et al. documented increased expression of genes involved in immune recruitment and production of pro-inflammatory cytokines within the aging ovary[62]. Several age-associated conditions have been associated with chronic inflammation, suggesting the highly pathogenic nature of inflammatory tissue. The presence of inflammatory cytokines and chemokines can foster tumor promoting environments and facilitate tissue invasion[76–78]. Additionally, the presence of pathological fibrosis in the lungs and liver increases the ability of metastasized cancer cells to colonize and grow in these fibrotic niches[79], and fibrotic breast and lung conditions are associated with increased pre-disposition to their respective cancers[80]. Furthermore, it has been proposed that treatment of underlying fibrosis leads to improved cancer prognosis[81–85]. Given the strong links of tissue fibrosis to tumorigenesis, the seed and soil hypothesis of metastases, along with the increased risk of ovarian cancer with age, and the fact that at least 50% of all cases of EOC can be identified to have STIC origins are all highly indicative that ovarian fibrosis is the link between ovarian aging and risk for OC.

Taken together, it is likely that age-associated ovarian fibrosis, in combination with the inflammatory microenvironment of the aging ovary, are collectively responsible for the transformation of the aging ovary into an appealing pre-metastatic niche, thereby posing a risk factor for the onset of OC. The recent findings that ovaries from post-menopausal type 2 diabetic women being treated with metformin have isotropic collagen structure, similar to that of pre-menopausal women[60] and a lower incidence of OC[86] support the association of ovarian fibrosis as a risk factor for ovarian cancer (**Figure 3**).

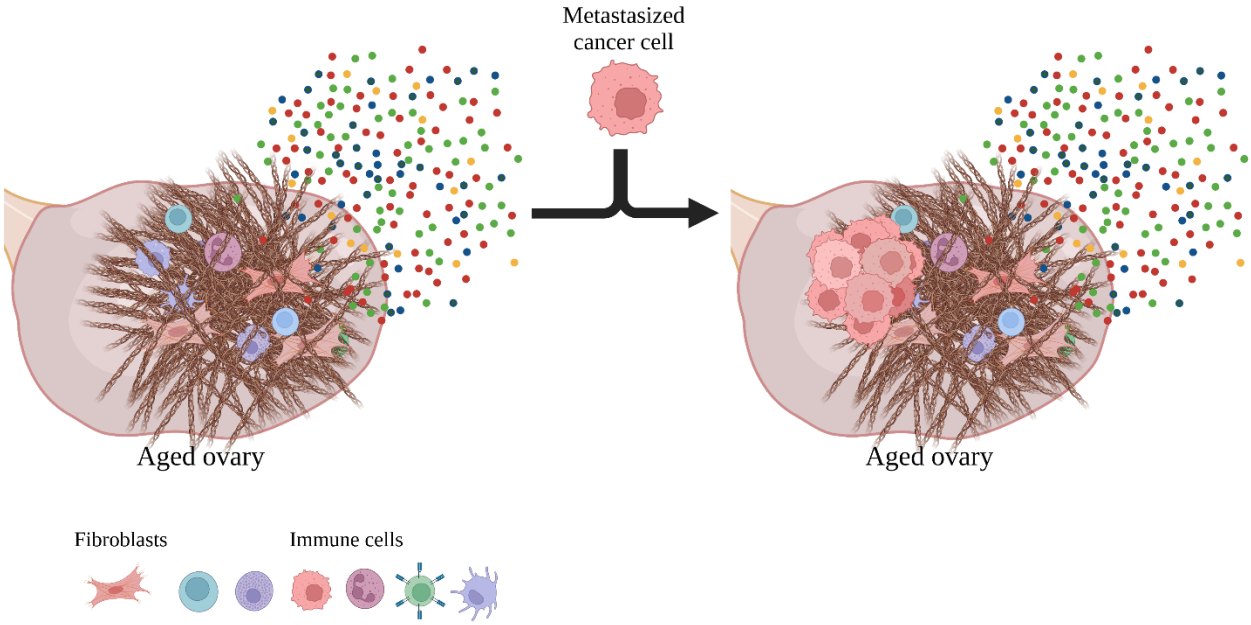

Figure 3: Model for age-associated ovarian fibrosis as a risk factor for ovarian cancer. *It is hypothesized that ordered arrangement of structural ECM protein such as collagens and fibronectin will trap a variety of immune cells that release the perfect milieu of pro-inflammatory cytokines that facilitate proliferation, dissemination, metastatic invasion and colonization by cancer cells, thereby posing a risk factor for cancer. The development of age-associated ovarian fibrosis may render the aging ovary an appealing pre-metastatic niche. Figure created using BioRender.com.*

1.4.1.3 Ovarian aging as a risk factor for ovarian fibrosis

Aging is defined as time-dependent gradual and progressive loss of physiological function and integrity through accumulation of DNA damage, oxidative stress and mitochondrial dysfunction, ultimately leading to chronic inflammation[61,87,88]. The hallmarks of aging can be classified into three categories: 1) Primary factors, which are responsible for age-associated cellular damage, such as increased production of reactive oxygen species (ROS) or DNA damage; 2) Antagonistic markers, which are responses to cellular damage, such as cellular senescence; 3) Integrative markers, the onset of which is due to age-associated damaged and directly contributes to tissue aging (example: stem-cell exhaustion and altered intercellular communication)[89,90].

Though multiple factors contribute to cellular and tissue aging, cellular senescence is considered to be a key hallmark of aging[89]. It can be defined as a protective program, a state of stable arrest of the cell cycle that is coupled with characteristic phenotypic alterations, metabolic changes, and is triggered by stressors that induce genomic instability[87,89,91]. Telomere attrition, oxidative stress, mitochondrial dysfunction, among others, threaten the integrity of the genome, and are as such considered to be primary hallmarks of aging. The onset of senescence is mediated by two key tumor suppressive pathways, p53/p21 and p16/pRb[87,89,92,93], and results in a senescence associated secretory phenotype (SASP), a hallmark feature of senescent cells.

The composition of SASP is highly variable and depends on the cell type and circumstances of senescence onset[89,91], but often includes pro-inflammatory cytokines, chemokines, interleukins, growth factors and ECM remodelling proteases[93]. While senescence associated cell cycle arrest is a powerful mechanism in preventing tumorigenesis by hindering the propagation of cells with compromised genomes, it has a multifaceted nature[89]. The induction of SASP alters the tissue microenvironment. The expression of pro-inflammatory SASP components activates and recruits a variety of adaptive and innate immune cells and results in a chronic low-level inflammation, referred to as inflammaging, that has been implicated in the pathogenesis of age-associated ailments[87,89,94,95]. Inflammaging induced by the SASP is the major extrinsic aspect of cellular senescence, however the role of SASP is far more diverse[89]. Altered expression of ECM remodelling enzymes, growth factors and structural components of the ECM in response to cellular senescence may either have positive (elimination of fibrotic niches) or negative (onset of fibrotic niches) consequences, again, dependent on the means of induction of senescence. In healthy adult tissue, a key feature of SASP is immune recruitment to eliminate senescent (damaged) cells, and consequently prevent the negative consequences of both damaged cells and SASP[89]. In the liver,

the recruitment of various immune cells to senescent cells during tumor initiation has tumor suppressing effects[96,97] and the recruitment of macrophages can limit fibrosis[98]. While the effects of SASP induction are largely positive, the recruitment of immature myeloid cells is immunosuppressive in prostate and liver cancers[99,100], and the expression of angiogenic factors stimulates tumorigenesis[101,102].

However, with age, the accumulation of damaged, senescent cells and declining immune monitoring capabilities may reduce the clearance of senescent cells, thereby resulting in persistent chronic inflammation, that is known to accelerate the process of tissue fibrosis[61,87,103,104]. Immunocompromised mice have accelerated onset of ovarian fibrosis, as compared to healthy mice[61] and the interaction between stromal fibroblasts and macrophages appear to be important in the development of aforementioned age-associated ovarian fibrosis[61], highlighting the importance of immune involvement in regulating the development of tissue fibrosis.

While wound repair is mediated by tissue-resident fibroblasts, it is also accompanied by active proliferation of tissue-specific cells. It can be speculated that over time this response is dysregulated, resulting in accumulation of senescence cells (replicative senescence) and fibrotic niches (aberrant myofibroblast activation), both of which are well-known precursors for malignancies. Single cell RNA-seq analysis has revealed the increased presence of SASP expressing fibroblasts in aged, fibrotic murine ovaries, as compared to younger ovaries[61], suggesting the presence of a pro-inflammatory ovarian microenvironment in the aging ovary, and thereby linking senescence to fibrosis and aging. Furthermore, metformin treatment prevented the formation of age-associated ovarian fibrosis, and these ovaries had fewer SASP fibroblasts, suggesting a possible positive feedback loop between presence of pathological fibrosis and expression of SASP by fibroblasts.

Organ aging is accompanied by change, perhaps none as dramatically as the ovary which is among the first organs to show signs of aging. Ovarian aging is defined as the cessation of folliculogenesis and hence, menstruation, resulting from the depletion of follicles and is accompanied morphological changes, such as an uneven ovarian surface and ovarian fibrosis[105,106]. The presence of α-SMA positive cells, indicative of myofibroblasts, in the aging murine ovary[62], links the presence of age-associated ovarian fibrosis to myofibroblast activation. Since ovarian function is heavily reliant on ovarian structure, structural abnormalities with aging are known to negatively impact ovarian function[107]. This is best exemplified by impaired ovulation, ovarian wound healing and formation of the corpus luteum with advanced reproductive age (that is accompanied by fibrosis), of the murine ovary[63]. It can therefore be speculated that at advanced ages accumulation of senescent cells in the ovary may be responsible for an inflammatory microenvironment and the development of age-associated fibrosis, that is likely to transforming the aging ovary into an appealing pre-metastatic niche.

1.4.2 Hereditary risk factors

Approximately 20-25% of all cases of OC have hereditary predisposition to the disease[3,108,109] , of which 65-75% are attributed to germline mutations in the tumor suppressor genes *BRCA1* and *BRCA2*[110], and 10-15% to Lynch syndrome[110,111]. Li-Fraumeni syndrome- an autosomal dominant condition associated with heterozygous germline mutations in the tumor suppressor gene *P53*, along with Peutz-Jeghers syndrome, and Cowden syndrome also increase the life-time risk of developing epithelial and non-epithelial subtypes of OC, however to a lesser extent[111]. Somatic or germline Mutations in DNA repair proteins such as PTEN, CHEK2, RAD51, BRIP1, BARD1, and PALB2 comprise approximately 10% of all cases of hereditary OC and are associated with a 2-4-fold increased risk of developing OC. Mutations in *P53* are the most

frequently acquired among cancer-associated mutations, with 97% of all HGSC bearing pathogenic *P53* mutations[112]. The median age of onset of OC decreases from 63 to 39.5 years among women with germline mutations in *P53* (Li-Fraumeni syndrome)[113].

1.4.2.1 Lynch syndrome

Lynch syndrome, also known as hereditary non-polyposis colorectal cancer is autosomal dominant in nature. It is characterized by germline mutations in the DNA mismatch repair genes, *MLH1*, *MSH2*, *MSH3*, *MSH6*, *PMS1* and *PMS2*, however mutations in *MLH1* and *MSH2* account for 90% of all cases of Lynch syndrome. Though individuals with Lynch syndrome have the highest risks of developing colorectal (43-48% life-time risk) and uterine cancers (40-62% life-time risk), it is associated with 8-10% life-time risk of developing OC[114].

1.4.2.2 Germline BRCA1/BRCA2 mutations

Autosomal dominant mutations in the tumor suppressor genes *BRCA1*/*BRCA2* account for the majority of cases of hereditary OC and are responsible for familial Hereditary Breast and Ovarian Cancer (HBOC) syndrome[115,116]. As compared to 1-2% life-time risk of developing OC in the general population[24,117,118], *BRCA1* mutation carriers have a life-time risk of 35-68%, while *BRCA2* mutations have a life-time risk of 10-30%[109,119]. OC is considerably more common (4x) and tends to develop at an earlier age in women with germline *BRCA1* as compared to *BRCA2* mutations[115,120]. As such, *BRCA1* mutations will be the primary focus of this work.

1.4.2.2.1 Structure and function of BRCA1

The human *BRCA1* gene maps to chromosome 17q21 and consists of 24 exons that yield a 220kD protein, consisting of 1863 amino acids[121–124]. The murine *Brca1* gene is located on chromosome 11D 65.18cM and is comprised of 25 exons that encode for a 199kDa protein

consisting of 1812 amino acids[125,126]. Murine BRCA1 is 60% identical and 72% similar to the human BRCA1 protein, with N- and C-terminals having high homology (>80%)[127,128]. The BRCA1 protein can be divided into 3 main domains, based on functionality[123] (**Figure 4**):

1) The N-terminal, encoded by exons 2-7, houses a nuclear exit site and the RING domain, that is characterized by two α-helices that coordinate 2 Zn^{+2} ions, enabling it to interact with other RING domain bearing proteins, specifically BARD1. BRCA1/BARD1 interact via their ring domains to collectively function as an E3 ubiquitin ligase.

2) Exons 11-13 encode for the majority of the BRCA1 protein, and includes 2 nuclear localization sequences (NLS), a coiled-coil domain, and a serine cluster domain (SCD) as structural features. This region encodes for binding sites for pRB, RAD50, MYC, RAD51, PALB2 and BRCA2. Proteins interacting with exons 11-13 of BRCA1 are involved in various cellular functions, such as cell cycle suppression, transcriptional regulation, and DNA repair pathways, suggesting the wide-spread involvement of BRCA1 in cellular homeostasis.

3) The C-terminal of BRCA1 (amino acids 1650-1863) contains two BRCA1 C-terminal (BRCT) domains, a conserved sequence found in many other DNA repair proteins. BRCT domains mediate interactions with various phosphorylated proteins involved in DNA repair. The BRCT domain of BRCA1 can also mediate DNA binding and interactions with non-phosphorylated proteins, such as P53. (**Figure 4**)

The majority of clinically significant mutations in BRCA1 either render the protein non-functional or with limited function and have been identified in the BRCT domain (exons 17-23), RING domain and in exons 11-13, in descending order (**shown in Figure 4**). This suggests that functions associated with these regions of BRCA1 are crucial to cellular homeostasis[123].

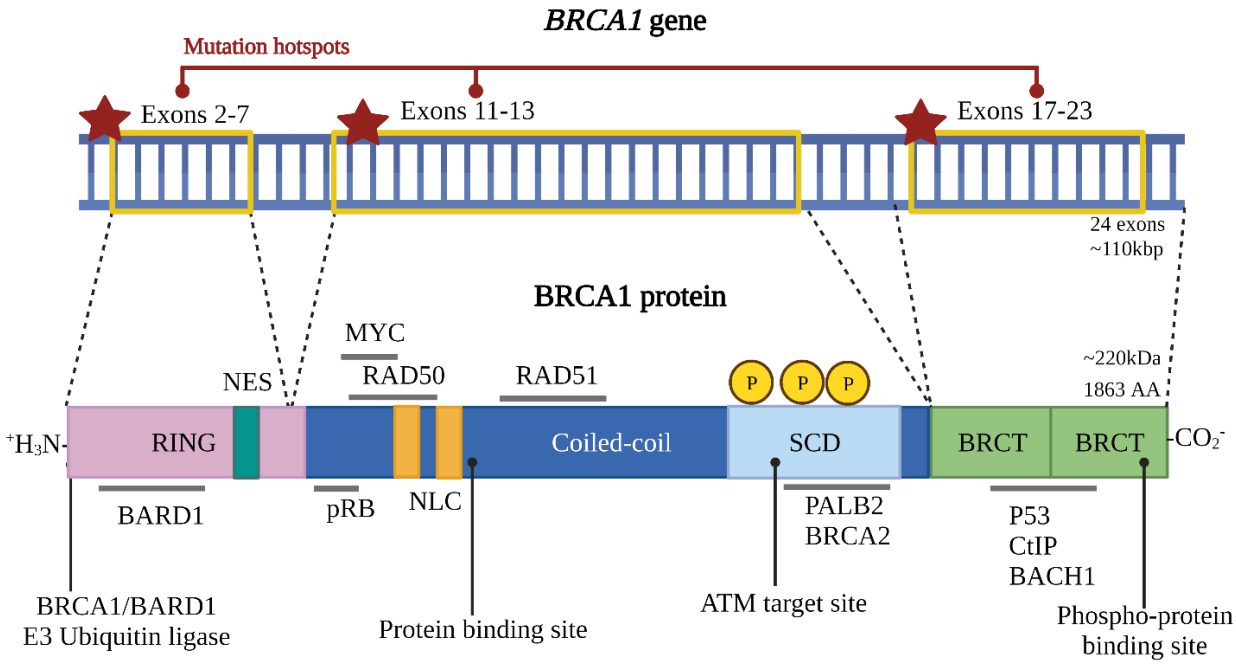

Figure 4: Brca1 encodes for an 1863 amino acid protein with diverse cellular functions. *Brca1 protein has three key domains- N-terminal RING, coiled-coil, serine cluster domain (SCD) and C-terminal BRCT, two nuclear localization and one exit signal. Mutations are most common in the BRCT domain, RING and coiled-coil/SCD domain, depicted using maroon stars. Figure created using BioRender.com.*

BRCA1 is best known for its role as a tumor suppressor. Tumor suppressor genes are those that encode for proteins that in the normal, homeostatic state function to inhibit and regulate cell proliferation to prevent tumorigenesis. While BRCA1 participates in a diverse range of cellular processes, such as regulating metabolism, antioxidant response, and autophagy, it plays a crucial role in maintaining genomic integrity through its function as: (a) a DNA damage recognition and repair protein, (b) a regulator of the cell cycle (c) an E3 ubiquitin ligase[129]. The role of BRCA1 in maintaining genomic stability will be the primary focus of this work.

(A) DNA damage recognition and repair

BRCA1 associates with various DNA repair proteins, such as MSH2, MSH6, ATM, BLM and RAD50-MRE11-NBS1 (MRN) protein complex, and DNA replication factor C to form a large protein complex referred to as BRCA1-associated genome surveillance complex (BASC) that functions to monitor and sense DNA damage[130]. BRCA1 is believed to act as a scaffolding/docking site for the components of BASC, and thereby plays an essential role in mediating the assembly of the BASC and in orchestrating the process of DNA repair [131–135] upon the sensing of DNA damage.

Different types of DNA damage trigger different DNA damage repair pathways. BRCA1 is known to participate in the repair of double stranded DNA (dsDNA) repair through homologous recombination (HR)[136–138]. DsDNA breaks typically result from errors in normal DNA replication, among other triggers such as damage by ROS, and are either repaired by non-homologous end joining (NHEJ) or by HR[139]. NHEJ is an error prone mechanism employed mostly in the G1 phase of the cell cycle prior to DNA replication[140]. While NHEJ protects the integrity of the genome by re-joining broken DNA, this process of DNA repair has high frequencies of insertions and deletions at the repaired junction[141]. Unlike NHEJ, HR is an extremely accurate pathway that repairs DNA breaks through the use a template. Due its high level of precision, it is essential in maintaining genomic stability. It is employed only after DNA replication (late S, G2 and M phases) due to its reliance on sister chromatids as a template[139,140].

Detection of dsDNA breaks recruits the assembly of the MRN complex onto broken DNA, which in turn recruits ATR/ATM to the site of damage and promotes activation via autophosphorylation. Phosphorylated ATR/ATM mediates the S139 phosphorylation of H2AX (γ-H2AX), which is a key signal in recruiting HR machinery, specifically BRCA1[138,142]. CtIP, in coordination with the MRN complex, catalyzes end resection of damaged DNA in a 5'-3' orientation, generating ssDNA that binds to replication protein A (RPA). End excision is a key

step in promoting HR and suppressing NHEJ[143]. BRCA1 is believed to facilitate end excision via interaction with CtIP, as well as by antagonizing P53 at sites of damage. The absence of BRCA1 and therefore lack of P53 inhibition promotes NHEJ[142,144] and arrest in G1 phase. The next step in HR is the loading of RAD51 onto ssDNA (RAD51 filament), which mediates strand exchange with the intact sister chromatid. BRCA1 plays an indirect, yet essential role in the formation of RAD51 filaments through its interaction with PALB2 via its coiled-coil domain. Interaction of BRCA1 with PALB2 in turn facilitates the interaction of PALB2 with BRCA2, creating the BRCA1-PALB2-BRCA2 complex, which is crucial in the formation of RAD51 filament[145]. Interaction of BRCA2 with PALB2 is crucial for its recruitment to the dsDNA break site and renders it capable of loading RAD51 onto replication protein A coated ssDNA[140,146]. Interaction of BRCA1 with PALB2 acts as a molecular switch to enable the activation of BRCA1-PALB2-BRCA2 loading complex[142,144,145]. The disruption of BRCA1 diminishes PALB2, BRCA2 and RAD51 foci at sites of DNA damage, impairing HR mediated repair of dsDNA breaks[144]. Furthermore, recent evidence suggests that interaction of BRCA1 with BARD1 through the N-terminal RING domain recruits BRCA1-PALB2 complex to sites of DNA damage, further assisting in HR.[147] Strand exchange is followed by DNA synthesis and then ligation of damaged strands, thereby repairing the dsDNA break[138,142,144,145] (**Figure 5**). Given the important role BRCA1 plays in the execution of HR, the loss of BRCA1 can impair proper HR, resulting in compromised genomic integrity.

(B) Cell cycle regulation

The cell cycle is divided into 4 phases. As cells prepare to proliferate, they firstly prepare for DNA replication in the first growth (G1) phase, which is followed by DNA synthesis in the synthesis (S) phase. Upon complete replication of the genome, cells undergo a second growth (G2)

phase to prepare for mitosis, that is followed by cell division in the mitosis (M) phase. Each phase of the cell cycle is associated with its own checkpoint criteria that must be fulfilled prior to progression into the next phase. Cyclin dependent kinases (CDKs) couple with their respective cyclins to form cyclin-CDK complexes that govern cell cycle progression and transition between phases by regulating the transcriptional activation and repression of phase specific genes.

The cyclin A-CDK2 and cyclin B-CDK1 complexes restrict HR to late S and G2 phases and drive the expression of several genes and phosphorylation of proteins required for G2/M phase DNA damage checkpoints, such as CtIP, PALB2, BRCA2[148]. The expression of *BRCA1* is regulated by the cell cycle. While barely detectable in G1, the expression of *BRCA1* steadily increases as the cell transitions from G1 to S-phase, peaks during S phase and continues to remain high throughout G2 and M phases[124], suggesting that the expression of *BRCA1* is coupled with genome replication. This highlights its function in maintaining genomic integrity throughout DNA replication. Cyclin D-CDK4/6 and cyclin E/A-CDK2 complexes, responsible for G1 progression, G1/S transition and S-phase progression, respectively[140] phosphorylate BRCA1 starting mid-G1 and continue to do so through S phase[124], likely to sense for replication mediated DNA damage. Upon DNA damage, phosphorylation of BRCA1 (via ATM/ATR kinases) negatively regulates the activity of cyclin B-CDK1 complex, that is required for G2/M transition, through the activation of CHK1 kinase[135], and interaction with CtIP and PALB2 to promote end resection and DNA repair via HR. Due to its ability to inhibit the activity of cyclin B-CDK1 complex, BRCA1 is believed to be a key component of the G2/M checkpoint that prevents pre-mature entry into the M phase in the presence of DNA damage. As such, the loss of BRCA1 function would impair the functioning of G2/M checkpoint.

(C) BRCA1/BARD1 E3 ubiquitin ligase

While BRCA1/BARD1 E3 ubiquitin ligase is one of several E3 ligases involved in DNA damage repair and cell cycle arrest, it is believed to be the most versatile in terms of its functions. It is known to mono- and poly-ubiquitinate substrates not only for proteasomal degradation, but also as a means of signalling. BRCA1-BARD1 heterodimer is known to facilitate the role of BRCA1 in recruiting appropriate protein machinery to sites of DNA damage and in regulating the cell cycle. BRCA1-BARD1 heterodimer has been shown to mono-ubiquitinate a wide range of substrates, including H2A, in vitro and in vivo and H2AX in vitro[149]. Ubiquitination of H2A is believed to regulate DNA damage response[150,151]. Additionally, BRCA1/BARD1 heterodimer regulates cell cycle progression via poly-ubiquitination of cyclin B and CDC25c, a phosphatase that is essential for the activation of the cyclin B/CDK1 complex, thereby marking them for proteasomal degradation and preventing entry into the M-phase[152]. In addition to regulating the cell cycle, E3 ligase activity mediates transcriptional regulation via mono-ubiquitination of various histone proteins to induce heterochromatin silencing and by poly-ubiquitination of transcriptional machinery such as RPB1, RPB8, TFIIE[153,154].

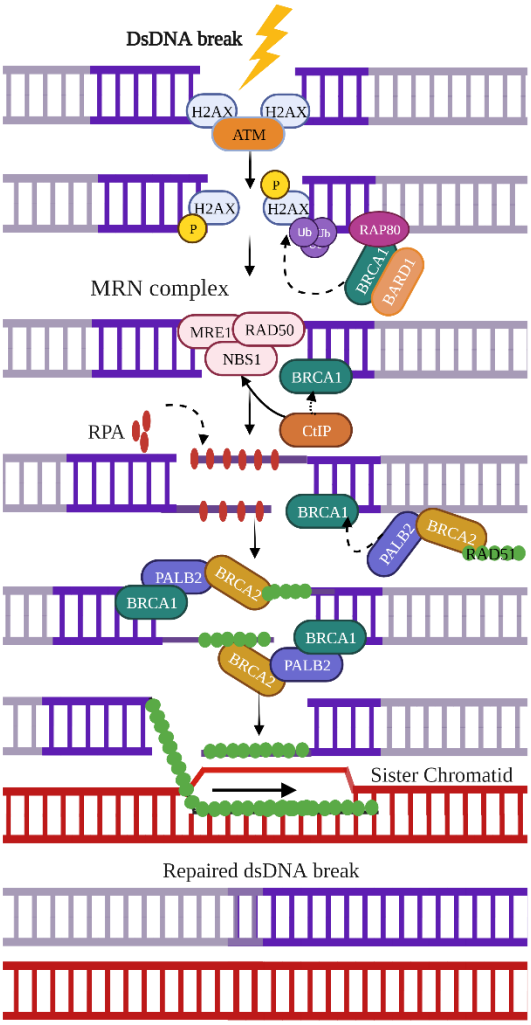

Figure 5: Brca1 protein facilitates DNA damage repair via homologous recombination. *Sites of double stranded DNA breaks flagged by S139 phosphorylation of histone H2AX (γ-H2AX) are detected by BASC, which then recruits the HR machinery, including the BRCA1-CtIP complex and the MRN complex (MRE11, RAD50, and NBS1) that collaborate to perform end resection and generate ssDNA that is stabilized by replication protein A (RPA). BRCA1-BARD1 complex recruits PALB2-BRCA2 complex to site of double stranded break, while BRCA1 indirectly facilitates displacement of RPA for the formation of RAD51 filaments by functioning as scaffolding for the PALB2-BRCA2-RAD51 complex. This is followed by strand exchange and DNA synthesis to repair the double stranded break. Figure created using BioRender.com.*

1.4.2.2.2 Germline BRCA1 mutations and hereditary ovarian cancer

HBOC syndrome, driven by mutations in the tumor suppressor genes *BRCA1* and *BRCA2*, is characterized by increased risk of male and female breast and ovarian cancer[115]. Founder *BRCA1* mutations responsible for HBOC, believed to have originated thousands of years ago, may be carried by up to 1% of the general population[155]. Both *BRCA1* and *BRCA2* mutations are more prevalent in people of Ashkenazi Jewish ancestry among other ancestries. The majority of *BRCA1* mutations are either nonsense or frameshift mutations that create insertions and deletions, often resulting in a truncated protein[156]. Germline *BRCA1* mutations are inherited in an autosomal

dominant manner, with carriers being heterozygous for an aberrant *BRCA1* allele at birth and eventual somatic loss of heterozygosity of *BRCA1*, that has been observed in hereditary cases of OC[157].

Compared to non-carriers, *BRCA1* mutations carriers have a narrower reproductive window[158], characterized by an earlier age of onset of menopause[158,159], fewer ovarian follicles and oocytes[160,161], reduced serum levels of AMH- that is reflective of a decreased ovarian reserve[162–164], reduced response to ovarian stimulation[161,164], and lower numbers of mature oocytes available for cryopreservation[165]. Collectively these features suggest the onset of primary ovarian insufficiency (POI)[161,164], defined as a premature (before the age 40) decline in ovarian function[166–168]. In the case of *BRCA1* mutation carriers, follicle depletion that is believed to result in POI, has been shown to be caused by an inadequate initial pool of primordial follicles, and pathologic destruction of follicles due to impaired dsDNA repair pathways[163,166].

In a preliminary study in the Vanderhyden lab, natural ovarian aging in non-mutation carriers was accompanied by the development of age-associated ovarian fibrosis that becomes evident during or after menopause, whereas *BRCA1* mutations carriers tended to develop fibrosis at pre-menopausal ages (**Table 1**; Curtis McCloskey, unpublished data). Such accelerated onset of ovarian fibrosis in combination with increased incidence of POI among *BRCA1* mutation carriers collectively suggests the possibility of premature ovarian aging in *BRCA1* mutation carriers. In support of this, *Brca1* null mice (*Brca1*$^{\Delta 11/\Delta 11}$; *Trp53*$^{+/-}$) displayed signs of systemic premature aging, characterized by reduced life-span (6-12 months), early onset of kyphosis and osteoporosis, substantial muscle atrophy, reduced adipose tissue, dermal thickness, and decreased wound healing as well as hair regeneration capacity, suggesting progressive decline of functions of multi-organ systems, as compared to *Brca1*$^{+/+}$; *Trp53*$^{+/-}$ mice[169]. Given the role of BRCA1 as a DNA

repair protein, mutations that render the protein non-functional impair the efficiency of DNA repair, a characteristic that has been identified to play a central role in human ovarian aging[163]. Furthermore, targeted mutations in DNA repair related genes in mice have also exhibited signs of pre-mature systemic aging, highlighting the importance of DNA damage repair in aging and in determining life-span[170–172]. Since cancer is well known to be a disease of age[173–177], decrease in the median age of onset of OC from 63 to 42 years for *BRCA1* mutation carriers, suggests an association between *BRCA1* mutations, and accelerated ovarian aging.

While impaired ovarian function with advanced age is attributed to declining quality and quantity of oocytes, it is likely that aging somatic cells in the ovary may be responsible for the concomitant age-associated changes in ovarian structure. Ovarian fibroblasts residing in the stroma normally regulate the structure of the ovarian extracellular matrix to facilitate ovarian function. Though the mechanisms underlying age-associated ovarian fibrosis remain unknown, it is possible that aging ovarian fibroblasts may drive the development of ovarian fibrosis with persistent activation.

Impaired DNA damage response due to somatic loss of heterozygosity of *BRCA1* is known to compromise the integrity of the genome, which, in ovarian epithelial cells is believed enhance the likelihood of malignant transformation of epithelial cells to promote carcinogenesis, and in oocytes may result in POI, which, in combination with early onset of ovarian fibrosis encompasses functional and structural changes associated with ovarian aging. Though the underlying cause for accelerated ovarian fibrosis observed in *BRCA1* mutation carriers is currently unknown, human dermal fibroblasts with *BRCA1* epimutation overexpressed genes encoding for structural and enzymatic components of the ECM and display characteristics of activated myofibroblasts that are primarily implicated with fibrotic matrix deposition and organ fibrosis.

Group	Case no.	Age	BRCA status	Other risk factors	Fibrosis (0 = no, 1 = yes)	Total fibrotic ovaries by group
Pre-menopausal	19	45	wt	no	0	**1/3 (33%)**
	20	42	wt	no	0	
	21	41	wt	no	1	
	22	42	wt	Lynch Syndrome	1	**2/3 (66%)**
	23	43	wt	Family History	1	
	24	43	wt	Lynch Syndrome	0	
	25	35	BRCA+	no	1	**3/5 (60%)**
	26	45	BRCA1+	no	1	
	27	38	BRCA2+	no	0	
	28	36	BRCA1+	no	0	
	29	35	BRCA2+	no	1	
Post-menopausal	30	68	wt	no	1	**5/6 (83%)**
	31	82	wt	no	0	
	32	66	wt	no	1	
	33	63	wt	no	1	
	34	63	wt	no	1	
	35	71	wt	no	1	
	36	75	BRCA+	no	0	**6/7 (86%)**
	37	63	BRCA+	no	1	
	38	68	BRCA2+	no	1	
	39	71	BRCA2+	no	1	
	40	61	BRCA+	no	1	
	41	67	BRCA2+	no	1	
	42	63	BRCA2+	no	1	

Table 1: BRCA1 mutation carriers (BRCA+) tend to have fibrotic ovaries at premenopausal age. *Unpublished data from the Vanderhyden Lab (Curtis McCloskey, unpublished).*

1.5 Rationale, Hypothesis and Aims

1.5.1 Rationale

Evidence from the current literature suggests that age-associated ovarian fibrosis, in combination with the inflammatory microenvironment of the aging ovary, are collectively responsible for the transformation of the ovary into an appealing pre-metastatic niche, thereby contributing to the risk for the onset of OC. The acceleration in the onset of fibrosis at pre-menopausal ages for BRCA1 mutation carriers seen in our preliminary study, and the known earlier onset of OC in these women offer a possible mechanism for the association between aging and cancer risk. It can therefore be hypothesized that *BRCA1* mutations may contribute to the risk

for OC through the development of premature ovarian aging, that is characterized by an accelerated onset of ovarian fibrosis and an inflammatory microenvironment.

Tissue fibrosis is defined as excessive accumulation of ordered components of the ECM, such as collagens and fibronectin fibers. The presence of activated fibroblasts in the aging, fibrotic murine ovary suggests involvement of fibroblasts in the development of age-associated ovarian fibrosis. Stromal fibroblasts play a central role in the synthesis, degradation and remodelling of the ECM to facilitate ovarian function and mediate wound healing. Activated myofibroblasts play an indispensable role in mediating wound healing and are characterized by the expression of α-SMA and are known to secrete structural components of the ECM, specifically collagen fibers. It is therefore possible that *BRCA1* mutations in ovarian fibroblasts may enhance their activation in response to pre-existing inflammatory conditions present in the ovary, resulting in the accelerated development of fibrosis. There is evidence suggesting *BRCA1* mutations promote fibroblast activation as mutation carriers have more frequent ovarian stromal hyperplasia, as compared to non-carriers[178]. Another study showed that human dermal fibroblasts carrying *BRCA1* epimutations have increased expression of markers of activated fibroblasts, such as *ACTA2*, *FAP*, *TNC*, and also displayed differential expression of ECM-related genes, compared to wild type dermal fibroblasts[179]. Collectively, this evidence suggests that loss of *BRCA1* function in fibroblasts may result in fibroblast hyperactivity, contributing to accelerated onset of ovarian fibrosis.

1.5.2 Hypothesis

We hypothesize that loss of *Brca1* expression in murine ovarian fibroblasts (MOFs) accelerates the onset of ovarian fibrosis through fibroblast hyperactivation.

1.5.3 Objectives and Aims

As such, we outlined three objectives to study the effect of *Brca1* deficiency in ovarian fibroblasts.

1. Establishment of viable cultures of primary murine ovarian fibroblasts through optimization of isolation technique and culture conditions.
2. Characterize TGF-β mediated activation of primary murine ovarian fibroblasts.
3. Characterize the effects of *Brca1* deficiency in primary murine ovarian fibroblasts.

Chapter 2: Methods and Materials

2.1 Experimental animals

Brca1$^{LoxP/LoxP}$ EYFP [FVB;129-*Brca1*^{tm2Brm}EYFP] conditional knockout mice, bearing LoxP sites in introns 4 and 13 of the *Brca1* gene, were generated by breeding *Brca1*^{tm1Brn} mice to B6.129X1-Gt(ROSA)26Sor$^{tm1(EYFP)Cos}$/J mice. The resulting mice bear a LoxP-flanked STOP sequence followed by the Enhanced Yellow Fluorescent Protein (EYFP) gene and its associated polyA tail (**Figure 6**). *Brca1*$^{LoxP/LoxP}$ EYFP were intercrossed with FVB/N mice to generate *Brca1*$^{LoxP/wt}$ EYFP mice (**Figure 7**). All experiments described were performed according to the *Guidelines for the Care and Use of Animals* established by the Canadian Council on Animal Care using protocols approved by the University of Ottawa Animal Care Committee.

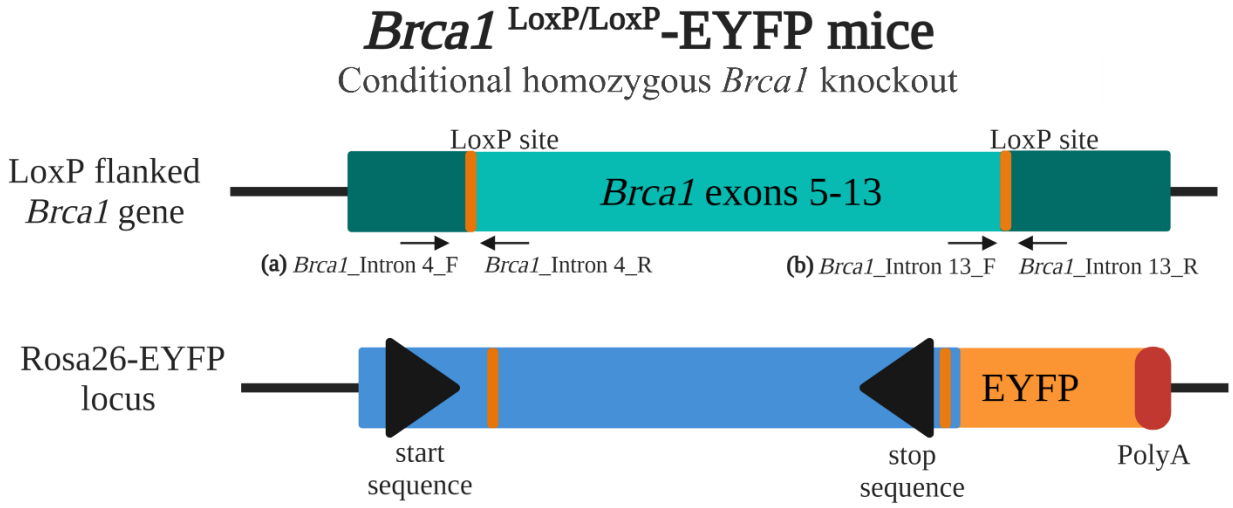

Figure 6: Genomic modification in conditional homozygous Brca1 knockout (Brca1$^{LoxP/LoxP}$ EYFP) mice*. These mice bear LoxP sites in introns 4 and 13 of the Brca1 gene, on both alleles. The Rosa26 locus is modified by the insertion of the enhanced yellow fluorescent protein (EYFP) gene and a bovine growth hormone polyadenylated sequence (polyA tail). The EYFP gene is preceded by a LoxP flanked stop sequence. Vertical orange bands indicate LoxP sites, triangles indicate start and stop sequences; Red oval indicates polyA tail. Small black arrows (a) and (b) indicate primers for Brca1_intron4_F&R (forward and reverse) and Brca1_intron13_F&R that*

were used to detect the presence of LoxP sites in the Brca1 gene. Figure created using BioRender.com.

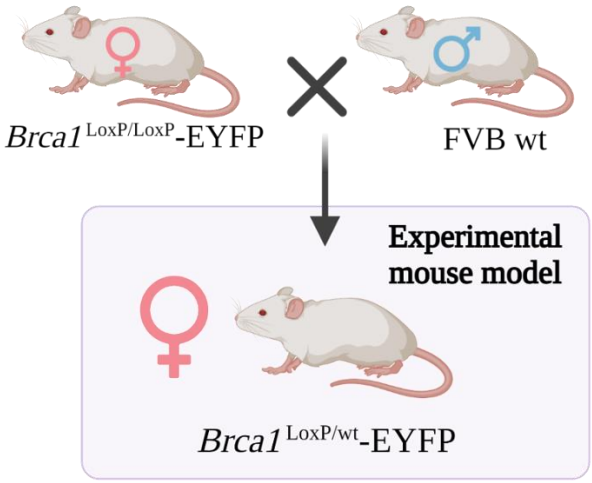

Figure 7: Brca1$^{LoxP/LoxP}$ EYFP mice were used to generate Brca1$^{LoxP/wt}$ EYFP mice with conditional heterozygous expression of Brca1. *Breeding scheme used to create Brca1$^{LoxP/wt}$-EYFP mice. Female Brca1$^{LoxP/LoxP}$ EYFP mice were crossed with male wild type FVB/N mice to create female Brca1$^{LoxP/wt}$-EYFP mice. Animals were genotyped to ensure the presence of LoxP sites on just one allele of Brca1. Figure created using BioRender.com.*

2.2 Genomic DNA extraction

Ear punches from mice were incubated in the DNA extraction solution, consisting of Tissue prep solution mixture (4:1 ratio of Sigma E7526-24ML and T3073-30ML) for 10-15 minutes (mins) at room temperature (RT), and then incubated at 95°C for 3 mins. 50 µL of neutralization solution B (50µL per reaction; Sigma N3910-24ML) was added to the enzymatic mixture and vortexed briefly to mix. Extracted genomic DNA (gDNA) was then used for genotyping.

2.3 Genotyping

Genomic DNA extracted from ear punches, collected at weaning, was subjected to polymerase chain reactions (PCR) to identify the mice as wild type or LoxP flanked (floxed).

Primers were obtained from Invitrogen as lyophilized powder and were resuspended in TE buffer (1nM EDTA (pH 8.0), 10mM Tris-Cl (pH 8.0), H_2O) at 100 µM to create the stock. Working solutions were prepared at 10 µM. Each PCR reaction was prepared using mqH_2O to have a final volume of 10 µL, with 1x concentration of Extract-N-Amp (stock at 2x; Sigma XNAT2R), 0.40-0.5 µM of each primer (stock at 10 µM) in the reaction, and 2 µL of gDNA. All PCR amplifications were carried out in a Bio-Rad T100^{TM} thermal cycler and PCR samples were separated on 1.2-1.5% agarose gels in Tris acetate-EDTA (TAE buffer) for 45 mins at 110 volts.

Floxed sequence was detected using primers *Brca1*_intron4_F and *Brca1*_intron4_R, or *Brca1*_intron13F and *Brca1*_intron13_R in introns 4 and 13, respectively (**Table 3**). Amplification using intron4_F&R primers yields 461bp and 391bp amplicons for floxed and wild type (wt) sequences, respectively. Amplification using primers for intron13_F&R yielded 562bp and 492bp amplicons for floxed and wt sequence, respectively. Heterozygous animals yielded both 461bp and 391bp amplicons (intron 4) and 563bp and 492bp (intron 13). PCR reactions were performed as described above and conducted as indicated in **Table 4**. Finished PCR products were stored at 4°C, and then separated using gel electrophoresis as indicated above.

Genotyping primer pair	Detection of	Primer sequence (5'- 3')	Amplicon size (bp)
***Brca1*_intron4_ F&R**	LoxP site in intron 4	F: TATCACCACTGAATCTCTACCG R: GACCTCAAACTCTGAGATCCAC	Floxed: 461 wt: 391
***Brca1*_intron13 _F&R**	LoxP site in intron 13	F: TATTCTTACTTCGTGGCACATC R: TCCATAGCATCTCCTTCTAAAC	Floxed: 562 wt: 492
***Brca1*_intron4_ F&R and *Brca1*_intron13 _F&R**	Recombination of *Brca1*	F: TATCACCACTGAATCTCTACCG R: TCCATAGCATCTCCTTCTAAAC	600
***Brca1*_exon11_ F&R**	wt *Brca1*	F: ATCAGTAGTAGAAATCCAAGCCCACC R: TGCCTCTCCCAGCATTGTTAG	592

***Table 2: List of primers for genotyping experimental animals**. All primers were reconstituted in TE buffer (1mM EDTA + 10mM Tris-Cl in mqH_2O) to be at 10µM for PCR.*

PCR amplification steps	*Brca1*_intron4_F&R *Brca1*_intron13_F&R	*Brca1*_intron4_F & *Brca1*_intron13_R *Brca1*_exon11_F&R
Step 1: Initial denaturation	94°C for 5 mins	94°C for 3 mins
Step 2: Denaturation	94°C for 30 sec	94°C for 30 sec
Step 3: Annealing	60°C for 30 sec	56°C for 30 sec
Step 4: Extension	72°C for 60 sec	72°C for 30 sec
# of cycles (steps 2-4)	30	30
Denaturation	NA	NA
Annealing	NA	NA
Extension	NA	NA
# of cycles (steps 6-8)	NA	NA
Final extension	72°C for 10 mins	72°C for 10 mins
Store	4°C ∞	4°C ∞

Table 3: PCR conditions used for genotyping using primers from Table 3. *All PCRs for genotyping were performed using the Bio-Rad T100™ thermal cycler, separated on 1.2-1.5% agarose gels (1% SafeRed) for 45 mins at 110 volts.*

2.4 Primary murine ovarian fibroblast (MOF) isolation and culture

Brca1$^{LoxP/LoxP}$ EYFP or *Brca1*$^{LoxP/wt}$ EYFP mice (between ages of 6-10 weeks) were euthanized via CO_2 asphyxiation and dissected to collect both ovaries. Seven to ten mice were used for each isolation experiment. Freshly collected ovaries were stored in cold phosphate-buffered saline (PBS; Gibco™; #14190-144) on ice during collection. Using a stereomicroscope (Leica WILD M3C), any remaining adipose tissue, as well as the ovarian bursa were removed. Each ovary was then washed with cold sterile PBS to remove any exogenous non-ovarian tissue. Using 26- and 27-gauge needles, under a stereo microscope, each ovary was punctured to release the contents of growing follicles, such as oocytes and granulosa cells. While this method ensures the removal of larger follicles, it is unlikely to remove the smaller primordial follicles. Ovaries were punctured until no visible granulosa cells layers were released when they were patted flat

using a blunt surgical probe, to ensure the elimination of as many granulosa cells as possible. Ovarian tissue was rinsed with fresh sterile PBS several times during the process of removing granulosa cells to minimize granulosa cell contamination. Next, the remaining ovarian tissue was transferred to enzymatic cocktail I [8mg/mL collagenase III (StemCell technologies; #07423) and 1500 kunitz units DNase I (Qiagen; #79256) in Hank's balanced salt solution (HBSS, Gibco^{TM};14170-112); 1mL enzymatic cocktail I for 2 ovaries] and minced using sterile dissection scissors to aid the digestion of the ECM proteins that trap tissue resident fibroblasts and hold the tissue together. Ovarian tissue was incubated in enzymatic cocktail I at 37°C for 15 mins on a rotary shaker. To avoid the formation of clumps and promote proper digestion, the enzymatic cocktail mixture was gently mixed every 5 mins. Following incubation in enzymatic cocktail I, tissue was centrifuged at 0.4g for 5 mins and resuspended in enzymatic cocktail II [1500 kunitz units DNase I in 0.25% Trypsin (Gibco^{TM}; #25200-056); 1mL enzymatic cocktail II for 2 ovaries] to further promote the breakdown of connective tissue proteins. Following a 10-minute incubation at 37°C on a rotary shaker, trypsin was inactivated by the addition of warm MOF media [filtered 1xDMEM (Corning; #10-013-CV) containing 10% FBS, 1% PenStrep (Gibco^{TM}; # 15140-122) and 4 ng/mL of FGF (R&D system; #3139-FB)]. Inactive enzymatic-tissue mixture was passed through a 40 µm nylon mesh cell strainer (ThermoFisher Scientific; #22363547) to remove any oocytes and tissue debris. Filtered cell suspension was then centrifuged at 0.4g for 5 mins and resuspended in 1mL of warm MOF media. Cell suspension was immediately plated onto a pre-warmed fibronectin coated T25 flask. MOFs were passaged 7-10 days later, upon reaching confluence. MOFs were cultured in MOF media at 37 °C in hypoxic conditions (5% O_2, 5% CO_2) on fibronectin coated tissue culture plates to mimic their native environment (fibronectin to stimulate ECM structure and hypoxic conditions to stimulate relatively lower blood oxygen levels

in the ovary), in order to minimize transition shock from in vivo to in vitro growth conditions and promote cell survival and growth.

2.5 Fibronectin coated plates.

In order to best mimic the native environment of fibroblasts, all tissue culture flasks and plates were coated with fibronectin to facilitate growth. Human plasma fibronectin (Sigma-Aldrich; #F0895-1MG) was diluted in 1x serum-free Hank's Balanced Salt Solution (HBSS; Gibco^{TM}, #14170-112) at 20µg/mL. Tissue culture plates were coated with human plasma fibronectin at a concentration of 2µg/cm^2 and kept at RT in a biosafety cabinet (to maintain sterile conditions) for an hour. Excess fibronectin was removed by rinsing the plates with sterile PBS. Plates were allowed to dry for 2-3h at RT in a biosafety cabinet. Dried plates were sealed and stored at 4°C until use. Coverslips used for immunofluorescence were coated with fibronectin using the same protocol.

2.6 Transduction of cells with adenovirus

Primary *Brca1*$^{LoxP/LoxP}$ EYFP or *Brca1*$^{LoxP/wt}$ EYFP MOFs were either transduced with recombinant adenovirus expressing cre recombinase, Ad5CMVCre (AdCre; Vector Development Laboratory) or recombinant empty adenovirus, Ad5CMVEmpty (AdEmpty; Vector Development Laboratory) or no virus (control) at passage 1 (p1), to create *Brca1* (-/- or -/wt) deficient MOFs (**Figure 8**). MOFs at confluence were washed with PBS and detached using 0.05% trypsin (Gibco^{TM}; #25300-054). Freshly detached cells were centrifuged at 0.4g for 5 mins at RT, resuspended in 2ml of warm serum starved MOF media (filtered 1xDMEM containing 1% PenStrep) and counted using Cell Countess® II (Life technologies; #AMQAX1000). Double the number of MOFs were transduced with AdCre than with AdEmpty to account for substantially reduced cell count following *Brca1* KO induced cytotoxicity. Three hundred thousand cells (for

no virus control and AdEmpty treatment), and six hundred thousand cells (for AdCre treatment) were incubated in poly-L-lysine (PLL at 1µg/mL; Sigma Aldrich; #P9155) for 15 mins at RT prior to exposure to adenovirus. Cells were coated with PLL, a positively charged molecule to promote electrostatic interactions with the negatively charged surface of adenoviruses, thereby increasing the efficiency of virus transduction. MOFs were transduced with either AdCre or AdEmpty in suspension at 50 multiplicity of infection (MOI) for 3.5-4 hours at 37°C in 5% O_2 and 5% CO_2. Transduced and control cells were then plated on fibronectin coated 6-well plates. Four hours later, adenovirus containing media was gently removed once MOFs had attached and was replaced with warm MOF media. Cells were then allowed to recover from transduction for 14 days at 37°C in 5% O_2 and CO_2.

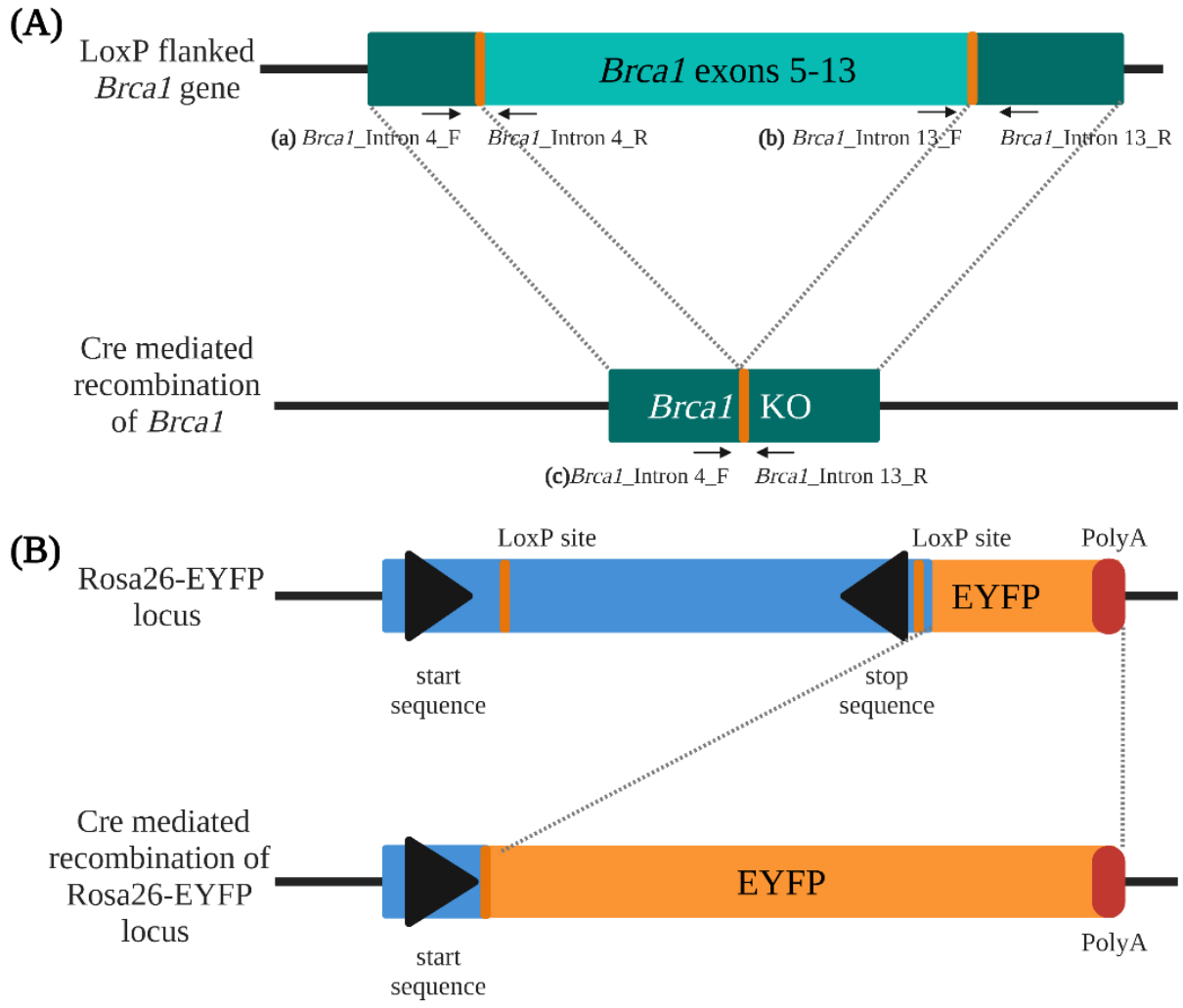

Figure 8: Expression of cre recombinase creates Brca1 knockout that is coupled with EYFP expression. *Transduction of adenoviral cre recombinase leads to the excision of nucleotides enclosed by LoxP sites, that is* ***(A)*** *exons 5-13 of Brca1 and* ***(B)*** *stop sequence in the Rosa26-EYFP locus, creating either a homozygous or heterozygous Brca1 knockout and expression of EYFP. Vertical orange bands indicate LoxP sites, triangles indicate start and stop sequences; Red oval indicates polyA tail. Small black arrows (a), (b) and (c) indicate sites of amplification for primers; Primers labelled as (c) Brca1_intron4_F & Brca1_intron13_R were used to detect cre mediated recombination of Brca1. Lack of Brca1 recombination would not support amplification using this set of primers, as introns 4 and introns 13 are spatially separated in the wild type Brca1 sequence. Figure created using BioRender.com.*

2.7 Detection of recombination at LoxP sites

Genomic DNA was either extracted from MOFs (isolated from *Brca1*$^{LoxP/LoxP}$ EYFP or *Brca1*$^{LoxP/wt}$ EYFP mice) in culture, as described above in section 2.2, to detect cre mediated excision of exons 5-13 of *Brca1*, henceforth referred to as *Brca1* KO. When recombination has occurred, introns 4 and 13 are in close proximity to one another, allowing primers intron4_F and intron13_R to detect the amplification of a 600bp amplicon (**Figure 8A**). However, when recombination has not taken place, introns 4 and 13 are spatially separated, preventing amplification using these primers. Additionally, primers *Brca1*_exon11_F and *Brca1*_exon11_R, which produce a 592bp amplicon, were used to detect the presence of wt *Brca1*. PCR reactions were prepared, performed (**Table 3**), and separated using gel electrophoresis, as described in section 2.3.

2.8 TGF-β treatment

MOFs and NIH3T3 cells were treated with TGF-β at 10ng/mL (R&D systems; #240-B) for 48h. Cells were washed with 1xPBS and flash frozen. RNA was collected as described in section 2.12.

2.8.1 TGF-β treatment of MOFs

MOFs were plated at 3.0 x 10^5 cells/well and serum starved for 48h. Control (wt), AdCre and AdEmpty MOFs were serum starved for 12h and then treated with TGF-β, 14 days after infection. Cells were treated with TGF-β in serum-free medium for 48h at 37°C under hypoxic conditions.

2.8.2 TGF-β treatment of NIH3T3 cells

NIH3T3 cells were plated at 3.0 x 10^5 cells/well 36h prior to treatment. At 12h prior to treatment, conditioned media was replaced with NIH3T3 starving media [1xDMEM + 2.5% newborn calf serum]. Cells were treated with TGF-β in NIH3T3 starving media for 48h at 37°C under normoxic conditions.

2.9 Immunofluorescence

Control and transduced (AdEmpty and AdCre) MOFs were plated at a seeding density of 3 x 10^5 control and AdEmpty cells and 6 x 10^5 AdCre cells/well (per 2mL media) on fibronectin coated coverslips. Double the number of MOFs were transduced with AdCre than with AdEmpty to account for substantially reduced cell count following Brca1 KO induced cytotoxicity. Day 14 after infection, conditioned media was removed from wt, AdEmpty and AdCre treated *Brca1*$^{LoxP/LoxP}$, and *Brca1*$^{LoxP/wt}$ MOFs and cells were then washed with PBS. MOFs were fixed using 4% paraformaldehyde for 20 mins at RT, then permeabilized and blocked using 0.2% Triton x-100 (15 mins) and 10% goat serum (1h). Permeabilized and blocked cells were incubated with primary antibodies for either 1h at RT or overnight at 4°C. Primary antibodies were diluted in 10% goat serum at the following concentrations: rabbit anti-vimentin (Abcam; ab45939; used at 1 µg/mL), mouse anti-pan-keratin (Abcam; ab8068; used at 1 µg/mL), rabbit anti-inhibin (Biorbyt; orb157692; used 1:100), mouse anti-α smooth muscle actin (Invitrogen; #14-9760-82; used at 1 µg/mL). Following three 5-minute washes with PBS, cells were stained with either anti-mouse or anti-rabbit secondary antibodies (diluted in 10% goat serum) for 1h at RT, at the following concentrations: Alexa Fluor™ 647 Donkey anti-mouse (ThermoFisher Scientific; #A-31571), at 1:1000; Alexa Fluor™ 488 donkey anti-mouse (ThermoFisher Scientific; # A-21202) at 0.2 µg/mL; Alexa Fluor™ 594 goat anti-rabbit (ThermoFisher Scientific; A-11012) at 1:1000; Alexa Flour™ 647 goat anti-

rabbit (ThermoFisher Scientific; A-21244). Nuclei were then stained using Hoechst (1:250) in PBS, followed by three 5-minute washes with PBS to remove excess secondary antibodies. Cell-containing coverslips were mounted onto Superfrost plus microscope slides (ThermoFisher Scientific; #12-550-15), using either Immu-Mount™ (ThermoFisher) or ProLong™ diamond antifade mountant with DAPI (ThermoFisher Scientific; #P36971). Images were acquired using Axioskop2 MOT fluorescence microscope.

2.10 Apoptosis assay

RealTime-Glo™ Apoptosis Assay (Promega; JA1000) was used to measure apoptosis in control, AdEmpty and AdCre treated *Brca1*$^{LoxP/LoxP}$ and *Brca1*$^{LoxP/wt}$ MOFs over a span of 14 days, starting 3.5 hours after exposure to virus. 10,000 MOFs (control and AdEmpty) and 12,000 MOFs (AdCre) were plated and transduced in flat, clear bottom 96 well ImageLock plates (Sartorius, #4379). Apoptosis assay kit components were added to the cell culture media at 1x concentration, as per the manufacturer's protocol at the end of virus infection (4h). Luminescence produced by functional luciferase, upon the binding of Annexin V fusion proteins to phosphatidylserine on the outer leaflet of the plasma membrane during early apoptosis, was measured every 24 hours using Biotek cytation 5 imaging reader at a gain of 100, 150 and 200. Raw data was normalized using mean of negative control (no cells with kit). Mean luminescence was compared by statistical analysis using Quadratic mixed effect regression performed using R-studio.

2.11 EYFP monitoring

EYFP expression by the Rosa26 locus was used to track *Brca1* deletion (**Figure 8B**), as well as to ensure that the cell population prior to RNA/DNA/protein extraction comprised of *Brca1* negative cells (i.e., EYFP positive cells). EYFP expression was

monitored in AdEmpty and AdCre treated *Brca1*$^{LoxP/LoxP}$ and *Brca1*$^{LoxP/wt}$ MOFs for 14 days, starting at 48h. Fluorescence was detected using excitation and emission spectra of 500nm and 539nm, respectively, using a Biotek cytation 5 imaging reader.

2.12 Incucyte® live-cell analysis

The Incucyte® live-cell analysis system was used to measure the rate of proliferation of control, TGF-β treated, AdEmpty and AdCre MOFs in MOF media and under serum starved conditions, for 112 hours (4.6 days). MOFs were plated at a seeding density of 10,000 cells/well (2mL media) for control, AdEmpty and TGF-β treatments and at 12,000 cells/well for AdCre treated MOFs in either MOF media, or in starving media. Cells were allowed to grow under normoxic conditions at 37°C and 5% CO_2 in the Incucyte® live-cell analysis system and cell confluence was measured every 2 hours. Mean confluence was compared by statistical analysis using non-linear regression analysis performed using R-studio.

2.13 RNA, gDNA and protein extraction

Depending on the experimental design, time frame and cell type, RNA, gDNA and protein were collected at different time points (control and TGF-β treated MOFs and NIH3T3 cells: 48h; control, AdEmpty and AdCre: 14 days). RNA, gDNA and protein were extracted using Allprep DNA/RNA/protein mini kit (Qiagen; # 80004) as per the manufacturer's protocol. Extracted RNA was used for RNA-sequencing and to synthesize cDNA using iScript™ Reverse Transcription Supermix, as per manufacturer's protocol (Bio-rad; #1708841). A Bio-Rad T100™ thermal cycler was used to perform reverse transcription and cDNA was then used for quantitative polymerase chain reaction and PCR arrays as described below. Extracted gDNA was used to confirm cre-mediated recombination of *Brca1*, as described in section 2.7.

2.14 Quantitative polymerase chain reaction (qPCR)

Changes in mRNA expression of *Brca1* and of key genes involved in TGF-β mediated fibroblast activation were accessed using qPCR, after TGF-β and AdEmpty and AdCre treatment of MOFs. All primers used for qPCR were designed and validated using pooled cDNA from MOFs, by the Vanderhyden lab. Extensive screening for specificity and efficiency of amplification during validation ensured reliable results. Samples for qPCR were prepared using SsoAdvanced Universal SYBR® green (Bio-Rad, #1725274), as per the manufacturer's protocol. *Gapdh*, *Hrpt1* and *Act-β* were used as housekeeping genes to normalize raw data collected using an ABI 5700 Fast Real-Time PCR system. Data was analyzed using the delta-delta-CT (ΔΔCT) method to compare gene expression in all samples relative to a control (control MOFs/NIH3T3 cells for TGF-β treatments and AdEmpty treated MOFs for the effects of *Brca1* deletion). Depending on the analysis, either two-way ANOVA, three-way ANOVA or students T-test was performed, using GraphPad Prism 9. A list of the primers used is shown in **Table 4**.

Target gene	Annealing temperature	Sequence (5'-3')	Amplicon size (bp)
Brca1	59°C	F: GAAGCGGGGAGAATGGACTC R: CTCTCAAATCGTCCCTCTGTCA	139
Col1a1	59°C	F: CAGTCGCTTCACCTACAGCA R: CGGGAGGTCTTGGTGGTTTT	99
Col1a2	59°C	F: TGGTGTTCGTGGTTCTCAGG R: AAAGTCATAGCCACCTCCGC	100
Col4a1	59°C	F: CGGCTATTCCTTCGTGATGC R: GATGGCGTGGGCTTCTTGA	207
Col7a1	60°C	F: GAACATCACATCGCACAGCC R: CGGTCACCTCATAGTCCGTG	176
Postn	60°C	F: GAAGTGATCCACGGAGAGCC R: GCAGGTGTGTCTGTAATGATTCG	116

Act-β	60°C	F: CCTTCCTTCTTGGGTATGGA R: ACGGATGTCAACGTCACACT	81
Gapdh	59°C	F: ACAACTTTGGCATTGTGGAA R: GATGCAGGGATGATGTTCTG	133
Hrpt1	60°C	F: AGGACCTCTCGAAGTGTTGG R: CGTGATTCAAATCCCTGAAG	115

Table 4: List of validated qPCR primers. *All primers were designed using the NCBI primer design tool, reconstituted in TE buffer and validated using pooled cDNA from MOFs. Three housekeeping genes, Act-β, Gapdh and Hrpt1 were used to normalize qPCR data.*

2.15 RT^2 profiler PCR array

A fibrosis PCR array (Qiagen; #330231) was performed to determine the effects of *Brca1* KO on the expression of genes involved in fibrosis. MOFs were plated at 3.0 x 10^5 (AdEmpty) and 6.0 x 10^5 cells (AdCre) and transduced as described in section 2.6. RNA was extracted 14 days post-transduction using AllPrep DNA/RNA/Protein mini kit (Qiagen). RT^2 first strand kit (Qiagen; #330404) was used to synthesize cDNA, as per the manufacturer's protocol. Master mixes for each sample were prepared using diluted cDNA and RT^2 SYBR® green ROX qPCR master mix (Qiagen; #330539), as per the manufacturer's protocol. The array was run in triplicate (n=3). An ABI 5700 Fast Real-Time PCR system was used to perform thermal cycling, as well as collect raw data, which was normalized to a set of housekeeping genes specific to the array. Relative quantification method ($2^{-\Delta\Delta Ct}$) was used to determine changes in gene expression, relative to AdEmpty treated MOFs. An unpaired student's T test was performed using Microsoft Excel.

2.16 RNA sequencing

As previously described, MOFs isolated on three independent occasions were each transduced with AdEmpty or AdCre to create *Brca1* KO (n=3). RNA was extracted 2 weeks after transduction (AllPrep DNA/RNA/Protein minikit, Qiagen) and quantified using a Nanodrop

Spectrophotometer ND-100 (Nanodrop Technologies Inc.). RNA integrity was assessed using a Bioanalyzer (Agilent technologies). Each sample containing at least 500ng of RNA was submitted to Genome Québec to be sequenced on a NovaSeq6000 sequencer. RNA-seq data was aligned using Kallisto and differential expression analysis was performed using DESeq2 (R Project)[180]. Genesets were either acquired from MSigDb or adapted from literature or custom designed and scored using Singscore (R Project), which applies a scoring method proposed by Foroutan et al. (2018)[181] and Bhuva et al. (2020)[182], to generate a gene module score using rank-based statistics to analyze each sample's gene expression profile and scores the expression activities of genesets at a single-sample level. As such, the gene module score for a given geneset is a rank-based average of all genes within that geneset. Geneset acquired from MSigDb: "G2/M DNA damage checkpoint" (Figure 20A), "DNA double strand break repair" (Figure 20B), "DNA double strand break response" (Figure 20C), "Inhibition of replication initiation via Rb-E2f1" (Figure 21A), "Cellular protein ubiquitination" (Figure 22A) and "Cellular E3 ubiquitin ligase function" (Figure 22B). Gene lists for "Senescence core genes" (Figure 23), "Senescence effector genes" (Figure 25) and "SASP signature" (Figure 29A) were acquired from Landry et al. 2022[61]. Datasets generated by Knight and colleagues 2006[183] and Sturmlechner and colleagues 2022[184] were used to custom build the following gene list: "Genes regulated (activated and repressed) by Trp53-Ac" (Figure 27B) and "Senescence-associated p21 activated secretory phenotype (SA-PASP)" (Figure 29B), respectively. Gene lists "Trp53 SASP" and "NFκB SASP" were acquired from Lopes-Paciencia et al 2019[185]. Gene list "Markers of apCAFs" was custom built using Friedman et al. 2020[186]. Genes differentially expressed in *Brca1* KO MOFs, as compared to AdEmpty (wt) MOFs with Log2 fold change >1 for upregulation and Log2FC<-1 for downregulation were the only ones

considered biologically relevant (Figure 18). Normal student's T-test was used for all statistical analyses (R Project). Genes with p-value> 0.05 were not considered in this study.

2.17 Acidic senescence associated-β-galactosidase activity staining

To access cellular senescence in *Brca1* KO in MOFs, AdCre and AdEmpty treated *Brca1*$^{LoxP/wt}$-EYFP MOFs were stained using the senescence associated β-galactosidase activity assay (SA-β-Gal stain). Sixteen days post-transduction AdCre and AdEmpty treated MOFs were washed with PBS and fixed with 0.5% glutaraldehyde in PBS (ThermoFisher Scientific, #BP2548-1) for 15 mins at RT. Fixed MOFs were rinsed and stored at 4°C overnight in PBS. The following day, cells were washed with 1mM $MgCl_2$ in PBS at pH5.5 for 10 mins, twice, at RT. Next, cells were incubated in pre-heated (37 °C) X-gal staining solution, comprised of 1X KC (composition in **Table 6**) and 1X X-Gal solution (Bioshop, #XGA001) in $MgCl_2$ (pH 5.5) at 37°C, in the dark for 35-45 minutes. X-gal is a chromogenic substrate for β-galactosidase, thus the interaction of X-gal with β-galactosidase renders the senescent cells detectable by a cyan pigment. The cells were then washed with 100mM Tris at pH 8.0 for 1 min at RT three times to stop the reaction. Cells were imaged in 100mM Tris, using an EVOS^{TM} core AMEX-1200 transmitted-light inverted imaging system (Invitrogen; #12-563-649).

SA-β-gal staining solutions	Components	Storage conditions/ Important details
X-gal staining solution	5% 20X KC solution, 2.5% 40X X-gal solution in 1mM magnesium (pH 5.5)	Made fresh, 15 mins prior to use. First, KC solution is added to 1mM magnesium chloride solution, followed by x-gal solution. Staining solution was heated at 37°C in the dark for 10 mins and filtered with 0.2 µm filter prior to use.
20X KC solution	100mM Potassium Ferricyanide, 100mM Potassium Ferrocyanide trihydrate, in 1x PBS	RT, in the dark
40X X-gal solution	1mg/mL x-gal in N,N-Dimethylformamide	-20°C, in the dark

Table 5: List of solutions used for SA-β-Gal Staining. *X-Gal staining solution was prepared immediately before use, while 20X KC and 40X X-Gal stocks were prepared ahead of time. All reagents (unless otherwise stated) were purchased from ThermoFisher Scientific.*

Chapter 3: Results

3.1 MOF isolation technique yields cultures that have little to no epithelial cell contamination.

In order to confirm the identity of isolated cells as fibroblasts and to check for potential contamination from other ovarian cell types (epithelial and granulosa cells primarily), MOF cultures were co-stained to detect the presence of vimentin, a type III intermediate filament, that is expressed in cells of mesenchymal origin, such as fibroblasts; Keratin, a type I/II intermediate filament abundantly present in cells of epithelial origin; and inhibin α, a protein secreted by granulosa cells. Immunofluorescence revealed MOFs in cultures to be abundantly expressing vimentin, and little to no keratin (**Figure 9A**), confirming their mesenchymal origin, and indicating minimal epithelial contamination. Little to no inhibin α was detected using immunofluorescence (**Figure 9B**) in MOF cultures.

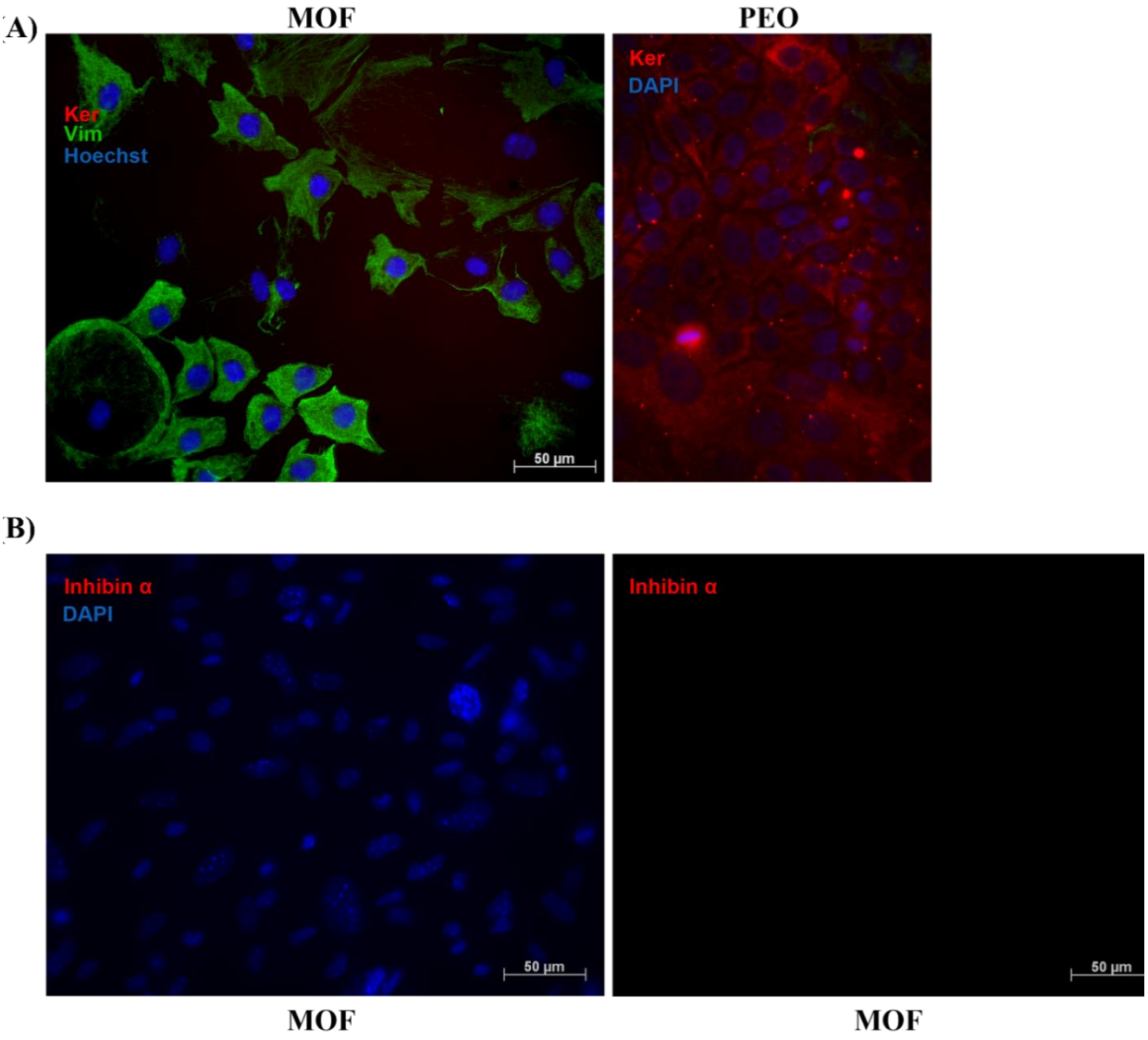

Figure 9: Immunofluorescence and RNA-seq reveal that MOF isolation technique yields cultures that are enriched in fibroblasts, have minimal epithelial or granulosa cell contamination. ***(A)*** *Cells in culture stain positively for vimentin (green) but show little to no cytokeratin staining (red). PEO1 cells were used as a positive control for cytokeratin staining.* ***(B)*** *MOF cultures show no inhibin staining, using immunofluorescence. Immunofluorescence was performed on freshly isolated MOFs as described in sections 2.9. Nuclei are visualized in blue, either using DAPI or Hoechst. Images were taken at 20x using an Axioskop2 MOT fluorescence microscope.*

3.2 TGF-β mediated activation of MOFs is associated with typical gene expression of markers of myofibroblasts.

NIH3T3 cells (embryonic fibroblasts from NIH/Swiss mice were used to establish controls for TGF-β mediated activation of myofibroblasts. Activation of myofibroblasts is associated with increased expression of *Acta2*, which encodes for α-smooth muscle actin, an isoform of actin that is essential to mediate wound healing, as well as cell adhesion molecules and ECM proteins, particularly collagen fibers, and enzymes required for their synthesis and assembly[187]. Markers of TGF-β mediated myofibroblast activation were identified using RNA-sequencing data from Yeung et al. (2013) that highlighted transcriptomic changes associated with TGF-β treated telomerase-immortalized normal ovarian fibroblasts (NOF151-hTERT)[188]. Using qPCR, we assessed differential gene expression among control and TGF-β treated NIH3T3 fibroblasts and MOFs. TGF-β treatment of NIH3T3 significantly upregulated mRNA expression of *Acta2* and *Col7a1* and significantly decreased the expression of *Postn*, and *Col1a2* (**Figures 10A-D**). While TGF-β treatment of MOFs significantly increased mRNA expression of *Acta2* and *Col7a1* (**Figures 10A, B**), it did not alter the expression of *Postn* or *Col1a2* (**Figure 10C, D**). Observed changes in the expression of the latter two genes were unexpected as both periostin (*Postn*) and collagen 1 (*Col1a2*) are known to be upregulated with TGF-β treatment in fibroblasts[187]; however, the significant increase in expression of *Acta2* and *Col7a1* is suggestive of TGF-β mediated activation of MOFs.

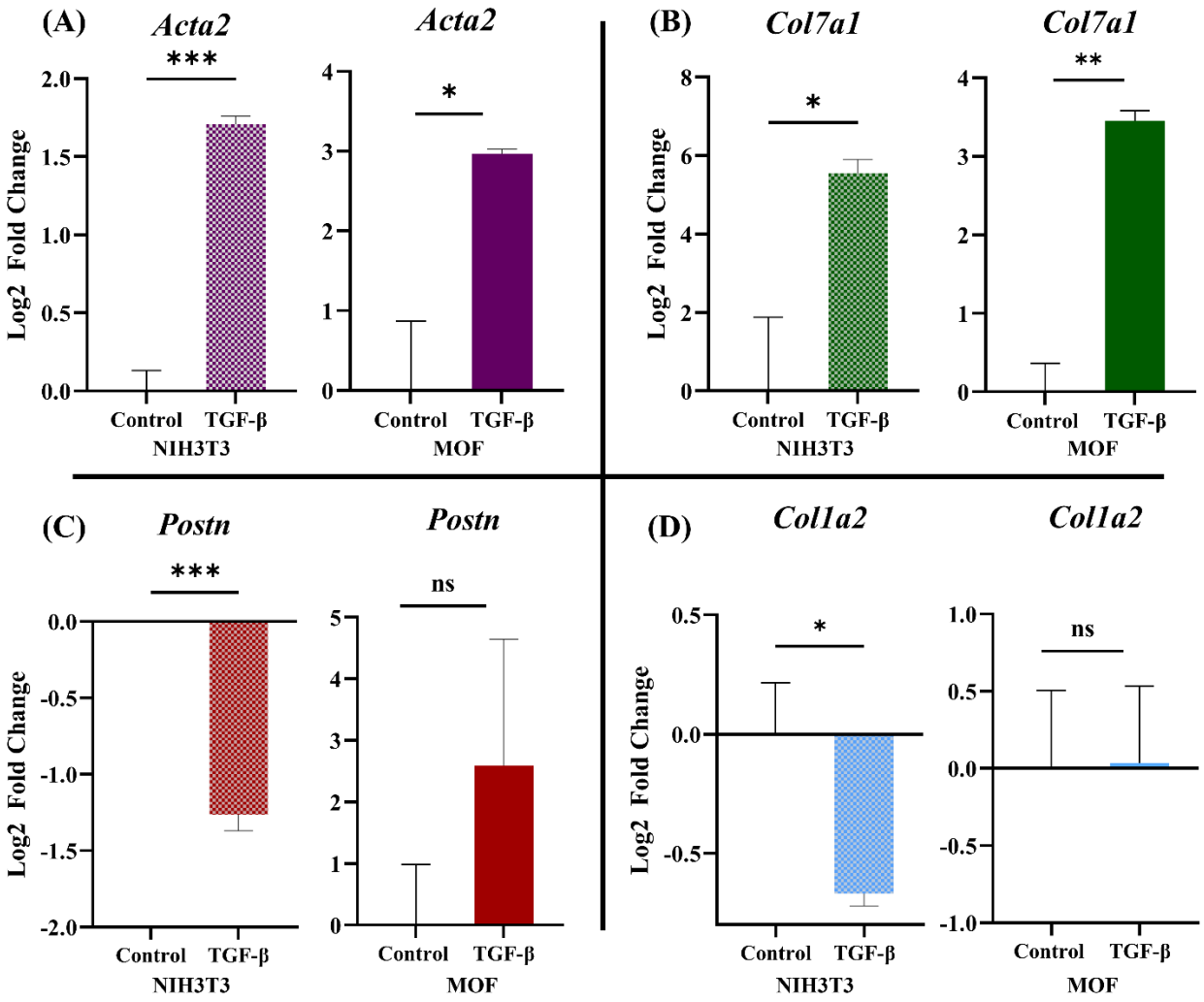

Figure 10: Markers of activated fibroblasts are expressed upon TGF-β treatment of MOFs. *NIH3T3 fibroblasts and MOFs were treated with TGF-β at 10ng/mL for 48h in 37°C at 5% CO_2 under normoxic and hypoxic conditions, respectively. In both types of fibroblasts TGF-β induced upregulation of* ***(A)*** *Acta2* and **(B)** *Col7a1, however, had differential effects on the expression of Postn and Col1a2. The expression of both* ***(C)*** *Postn and* ***(D)*** *Col1a2 was downregulated in NIH3T3 fibroblasts and was unaltered in MOFs in response to TGF-β. MOFs were isolated as described in section 2.4. Both, MOFs and NIH3T3 fibroblasts were treated with TGF-β as described in sections 2.8.1 and 2.8.2, respectively. RNA was assessed using qPCR analysis and results are presented as Log2 fold change (Relative fold change). ABI 5700 Fast Real-Time PCR system was used to perform thermal cycling. Gene expression was normalized using housekeeping genes Act-β, Gapdh and Hrpt1, analyzed using the relative quantification ($2^{-\Delta\Delta Ct}$) method and is presented as log2 fold change. Experiment was performed in triplicate (n=3); Error bars indicate*

*standard error of mean (SEM). Unpaired T-test was applied using GraphPad Prism, * = p < 0.05; ** = p < 0.01; ***= p< 0.001; ns= not significant.*

3.3 Loss of *Brca1* expression reduces cell survival and changes morphology.

3.3.1 Adenoviral Cre mediated loss of *Brca1* in MOFs is coupled with EYFP expression.

EYFP expression, through the Rosa26 locus, was tracked as a reporter of cells in which cre mediated recombination of *Brca1* likely occurred, and apoptosis was measured to monitor recovery of MOFs from adenoviral transduction. EYFP expression was detected in AdCre infected MOFs (called AdCre MOFs hereon) at 48 hours post-infection, but not in AdEmpty MOFs (**Figure 11A**), thereby confirming the expression and subsequent activity of adenoviral cre recombinase. Prior to 48 hours, EYFP was undetectable in both, AdCre and AdEmpty MOFs. Consistent with 48h post-infection, EYFP expression was detected in AdCre MOFs at 144h (6 days) post-infection, but not in AdEmpty MOFs (**Figure 11B**), suggesting successful cre mediated recombination of *Brca1* in MOFs.

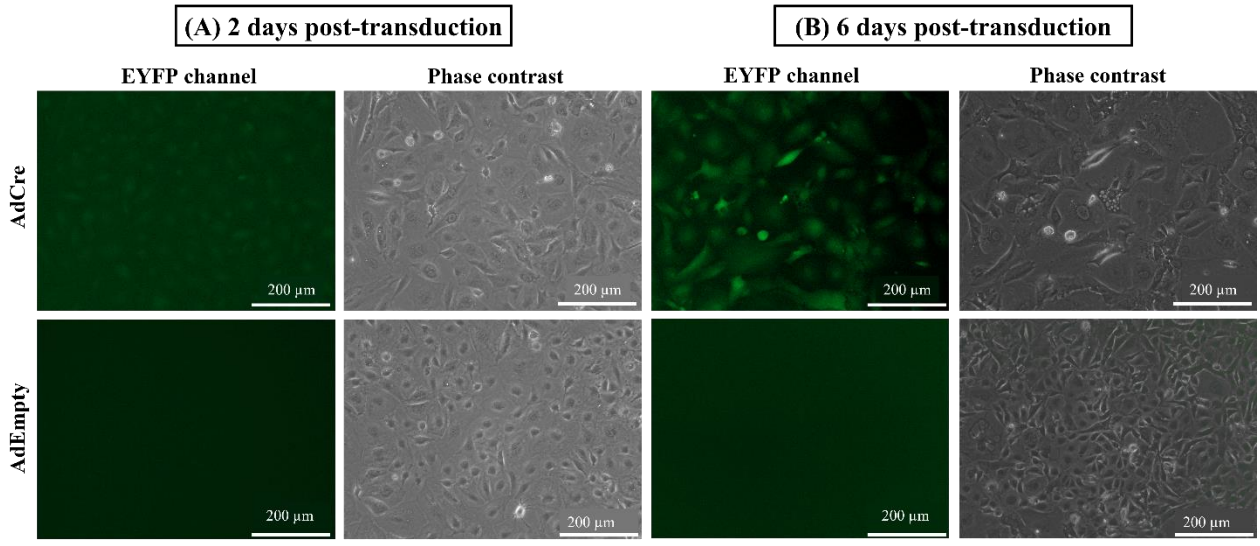

Figure 11: AdCre mediated deletion of Brca1 is coupled with EYFP expression. (A) *EYFP expression is first detected in AdCre, but not AdEmpty MOFs 2 days (48h) post-infection. At this time, both AdCre and AdEmpty MOFs display wt morphology;* ***(B)*** *EYFP expression is enhanced*

in AdCre MOFs 6 days (144h) post-transduction, while EYFP remains undetected in AdEmpty MOFs; AdCre MOFs display altered morphology while AdEmpty MOFs retain their wt morphology. MOFs were isolated and transduced with adenovirus as described in sections 2.4 and 2.6, and were cultured in MOF media, at 37°C in 5% O_2. Biotek cytation 5 imaging reader was used to visualize EYFP and capture images at 10x.

3.3.2 Adenoviral cre mediated recombination successfully creates *Brca1* KO

Day 14 post-transduction, mRNA and gDNA were extracted from *Brca1* KO MOFs to confirm *Brca1* KO. Recombination of *Brca1* as well as wildtype *Brca1* products were detected in gDNA collected from AdCre infected MOFs, with the latter to a much lower extent (**Figure 12A**). Only wildtype *Brca1* was detected in gDNA from AdEmpty MOFs (**Figure 12A**). QPCR analysis revealed a significant decrease in the mRNA expression of *Brca1* with AdCre transduction, compared to AdEmpty infected MOFs (**Figure 12B**), suggesting a successful *Brca1* KO in most cells.

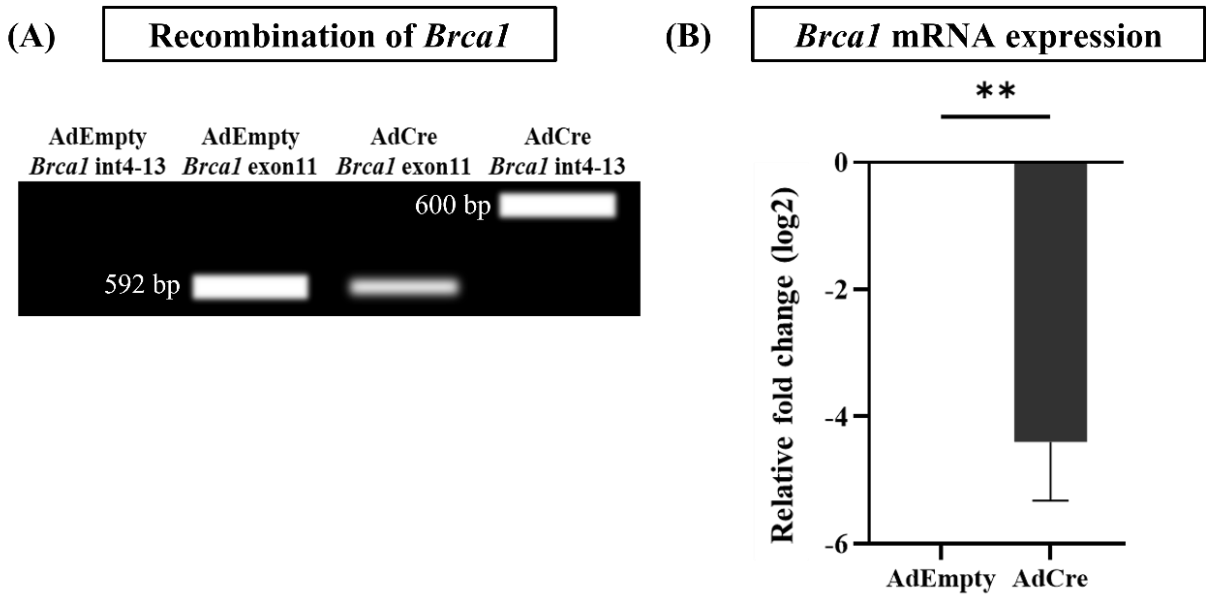

Figure 12: Transduction of MOFs with AdCre successfully created Brca1 KO. *MOFs in culture were collected at day 14 for gDNA and RNA extraction to check for genomic recombination and relative mRNA expression of Brca1.* ***(A)*** *PCR using gDNA from AdCre MOFs produced two*

amplicons, a 592bp product from wt Brca1 (primer set targets exon 11), and a 600bp product from cre-mediated recombination of Brca1 (primer set targets intron4-13 junction), while PCR using gDNA from AdEmpty MOFs resulted in amplification of a 592bp wt product but not a 600bp recombination product. ***(B)*** *QPCR revealed significantly decreased mRNA expression of Brca1 in AdCre MOFs as compared to AdEmpty MOFs. MOFs were isolated and transduced with adenovirus as described in sections 2.4 and 2.6. RNA and gDNA were extracted as described in 2.16. Brca1_intron4_F and Brca1_intron13_R were used to check for recombination of Brca1 and Brca1_exon 11_F&R was used to detect wt Brca1. PCR reactions were prepared as described in section 2.4 and performed as outlined in Table 3 using the BioRad TM100 thermal cycler. 1.5% agarose gel in TAE was used to separate PCR products, which were then visualized using UV spectra. ABI 5700 Fast Real-Time PCR system was used to perform thermal cycling. Raw data normalized using housekeeping genes Act-β, Gapdh and Hrpt1, analyzed using the relative quantification (2-ΔΔCt) method and presented as Log2 fold change (Log2FC; relative fold change). Experiment was performed in triplicate (n=3); Error bars indicate standard error of mean (SEM). Unpaired student's T-test was applied using GraphPad Prism; **= p-value < 0.01.*

3.3.3 Sudden loss of *Brca1* is cytotoxic and leads to cell death via apoptosis.

Using a luminescence-based apoptosis assay, a significant increase in apoptosis was observed in *Brca1* KO MOFs compared to AdEmpty MOFs from days 2-6 post transduction, after which no significant differences were observed between the two groups, suggesting that the sudden loss of BRCA1 function induces apoptosis in MOFs (**Figure 13**). For both, *Brca1* KO and AdEmpty MOFs, apoptosis was found to peak at 48 hours, and then decreased gradually, reaching a plateau at day 14, suggesting recovery from virus transduction (**Figure 13**).

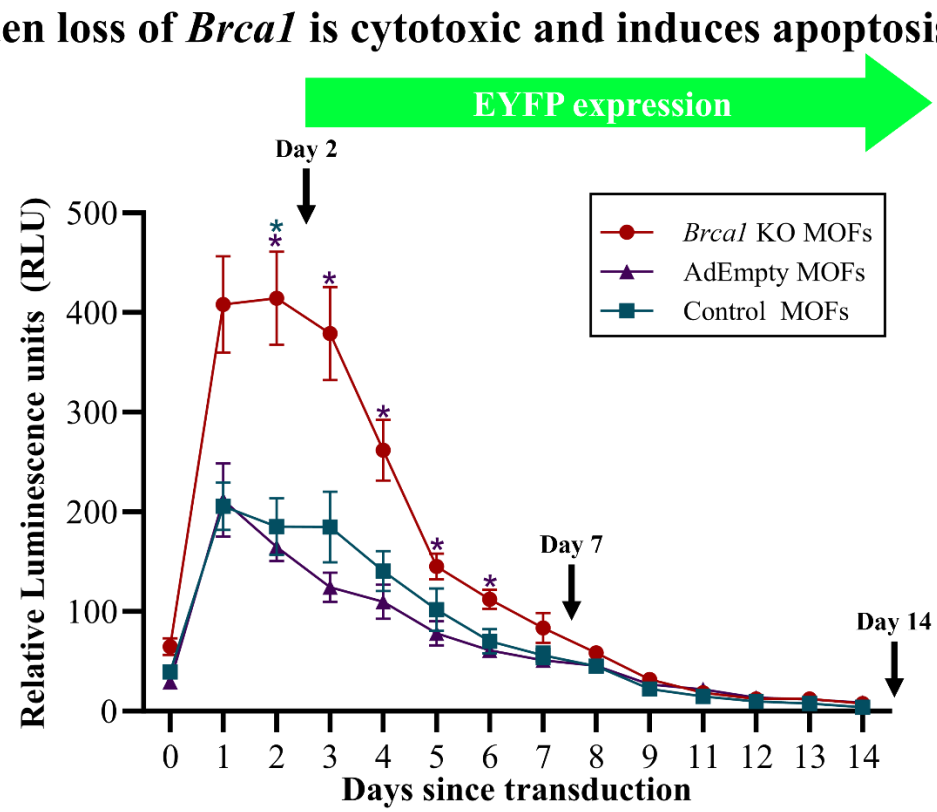

Figure 13: Sudden loss of Brca1 induces apoptosis in MOFs. *At all time points, apoptosis was recorded to be highest in AdCre MOFs, as compared to AdEmpty or control MOFs. Apoptosis in all groups gradually decreased with time, tapering off at approximately day 14 post-transduction, indicating recovery from virus transduction. MOFs were isolated and transduced with adenovirus as described in sections 2.4 and 2.6. Cell death was measured using RealTime-Glo™ Apoptosis Assay, starting at the end of virus transduction up until day 14. Biotek Cytation 5 imaging reader was used to measure luminescence every 24h, with timepoint 0h representing 4h post-transduction. Experiment was performed in triplicate (n=3). Error bars indicate SEM. Two-way ANOVA was applied using GraphPad Prism. *= p-value < 0.05.*

3.3.4 MOFs surviving initial loss of *Brca1* adopt a flattened morphology.

AdCre transduced MOFs in culture at day 14 expressed EYFP (**Figure 14**) and had adopted a unique morphology characterized by enlarged, flattened cytoplasm, while AdEmpty MOFs had retained their wildtype morphology post-transduction (**Figures 11A-B, 14**). This suggests that

cells that were able to withstand the sudden loss of *Brca1* survived but adopted a unique enlarged and flattened morphology over a span of 14 days.

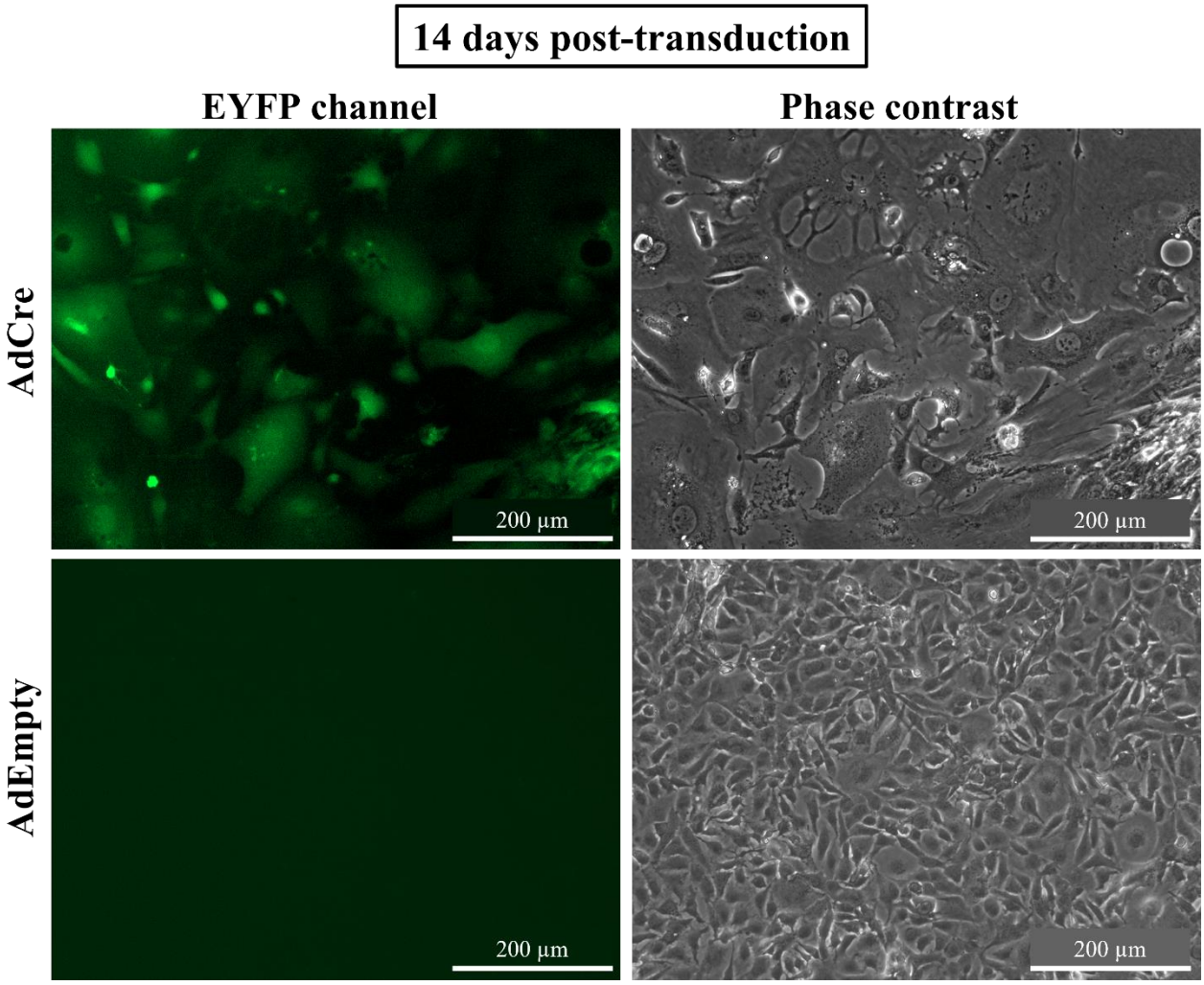

Figure 14: Brca1 KO MOFs display unique enlarged and flattened morphology. *14 days (336h) post-transduction AdCre MOFs strongly express EYFP and display a unique flattened morphology, while AdEmpty MOFs retain their wt morphology and do not express EYFP. MOFs were cultured in MOF media, at 37°C in 5% O_2. Biotek cytation 5 imaging reader was used to visualize EYFP and capture images at 10x.*

3.4 Loss of *Brca1* in MOFs does not result in transcriptional activation of markers of fibrosis.

3.4.1 *Brca1* KO in MOFs downregulates genes involved in TGF-β signalling.

Given the hypothesis that loss of BRCA1 may be associated with the development of fibrosis, a fibrosis PCR array was used to compare the differential expression of various pro-fibrotic genes and members of the TGF-β signalling pathway in AdEmpty (wt *Brca1*$^{LoxP/LoxP}$) and AdCre MOFs (*Brca1*$^{\Delta 5\text{-}13}$, i.e., *Brca1* KO). *Brca1* KO in MOFs did not significantly upregulate any pro-fibrotic markers, however, the mRNA expression of several components of TGF-β signalling, such as *Smad4*, *Smad6*, *Tgfbr1*, *Cebpb*, *Jun*, *Myc*, and *Stat6* was significantly decreased (**Figure 15**; highlighted in blue).

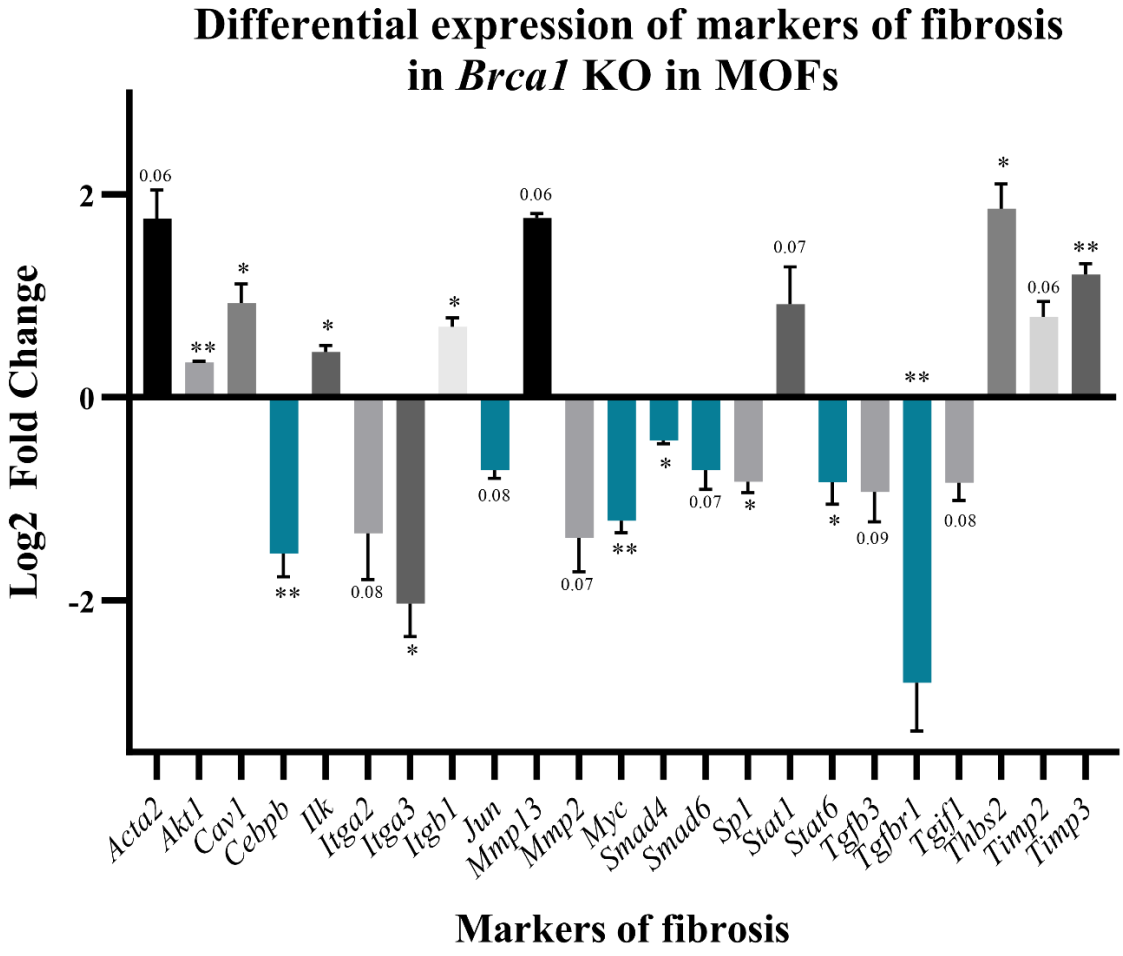

Figure 15: Brca1 KO in MOFs results in downregulation of transcripts for several TGF-β signalling components. *Genes significantly up and down regulated with loss of Brca1 were identified using the RT2 profiler fibrosis PCR array. Adenovirus transduction and RNA extraction were performed as described in sections 2.6 and 2.13. ABI 5700 Fast Real-Time PCR system was used to perform thermal cycling for RT2-profiler fibrosis PCR array. Raw data was normalized to a set of housekeeping genes and analyzed using the relative quantification method ($2^{-\Delta\Delta Ct}$) and is presented as log2 fold change (Relative fold change) in Brca1 KO MOFs as compared to AdEmpty MOFs. Experiment was performed in triplicate (n=3). Error bars indicate SEM. Unpaired T-test was applied using MS-Excel; * = p-value < 0.05; ** = p-value < 0.01; p-values > 0.05 are indicated in figures.*

3.4.2 *Timp3* and *Mmp13* appears to be upregulated with *Brca1* KO in MOFs.

The mRNA expression of *Acta2* appears to be upregulated, however this did not quite reach statistical significance (**Figure 16A**). Additionally, mRNA expression of structural extracellular matrix proteins that are known to be upregulated with fibroblast activation and in fibrotic niches, such as *Col1a2* and *Col3a1* (**Figure 16B, C**) were unaltered in *Brca1* KO MOFs. However, two matrix remodelling enzymes, *Timp3* and *Mmp13* (p-value= 0.06) were found to be upregulated with *Brca1* loss in MOFs (**Figures 16D, E**). These changes in gene expression were confirmed using RNA-sequencing which showed that expression of *Acta2*, *Timp3* and *Mmp13* was significantly upregulated, and the expression of *Col1a1* and *Col3a1* was unaffected (**Figure 16F**). Collectively, these findings suggest that the loss of *Brca1* in MOFs may result in fibroblast activation, however this might be independent of TGF-β signalling.

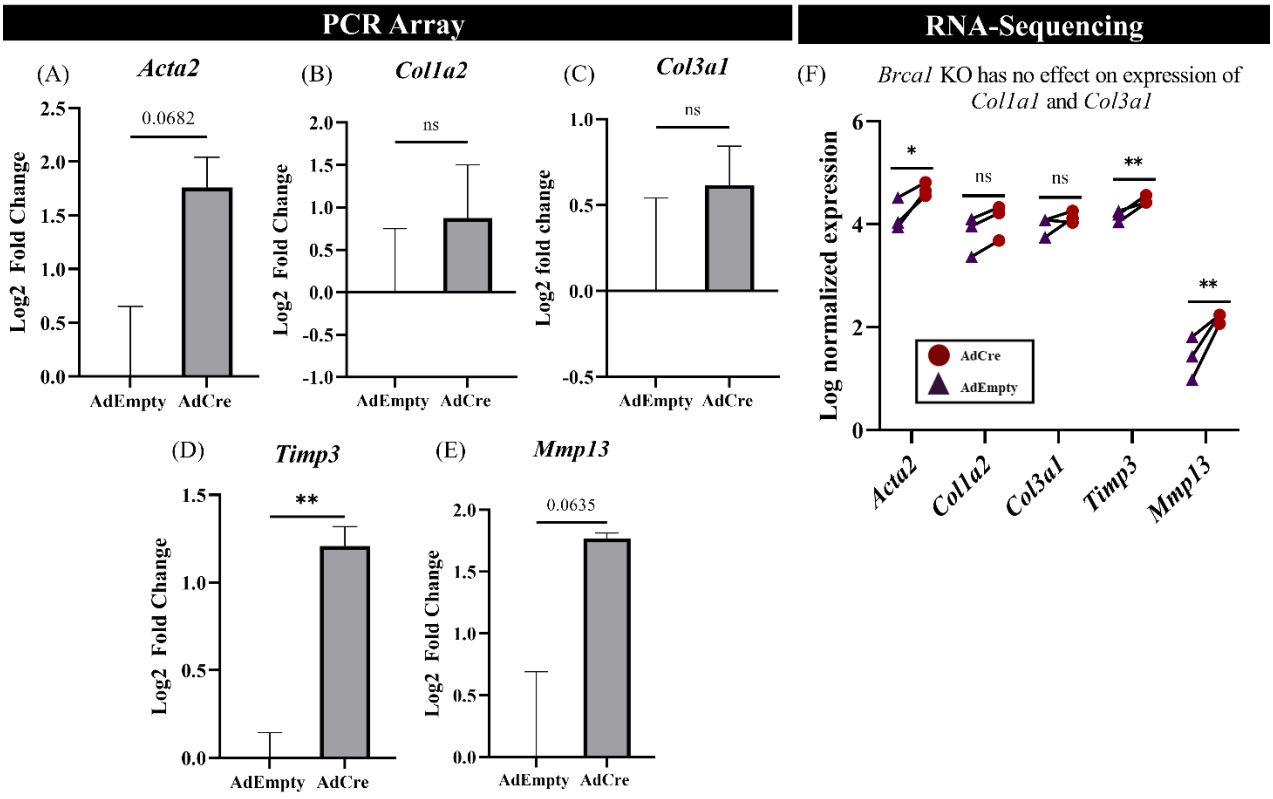

Figure 16: Loss of Brca1 induced myofibroblast activation of MOFs. *RT2- profiler PCR array indicates that Brca1 KO in MOFs appears to* ***(A)*** *upregulate Acta2 (p=0.068),* ***(B, C)*** *has no effect on the expression of Col1a2 and Col3a1, key structural components of the ECM, but does* ***(D)*** *significantly upregulate matrix remodelling enzyme, Timp3 and* ***(E)*** *trends towards upregulation of Mmp13 (p=0.064).* ***(F)*** *Differential expression of these ECM associated genes was confirmed using RNA-seq. Adenovirus transduction and RNA extraction were performed as described in sections 2.6 and 2.13. ABI 5700 Fast Real-Time PCR system was used to perform thermal cycling for RT2-profiler fibrosis PCR array. Raw data was normalized to a set of housekeeping genes and analyzed using the relative quantification method ($2^{-\Delta\Delta Ct}$) and is presented as log2 fold change (Relative fold change). RNA-seq data was analyzed using DESeq2 (R project) to access differential expression of genes (A), which is presented as Log2FC in Brca1 KO MOFs as compared to AdEmpty MOFs. Experiment was performed in triplicate (n=3). Error bars indicate SEM. Differential gene expression from RNA-sequencing is shown as log normalized expression between AdCre and AdEmpty (F). Unpaired T-test was either applied using GraphPad Prism (A-E) or performed in R (F); * = p-value < 0.05; ** = p-value < 0.01; ns= not significant.*

3.5 Loss of *Brca1* in MOFs is associated with myofibroblast activation and alterations in ECM homeostasis and immune regulation.

3.5.1 *Brca1* KO increases genome organization & immune regulation pathways in MOFs.

RNA-seq was used to assess global transcriptomic changes associated with the loss of *Brca1* in MOFs; Transduction of MOFs with AdCre decreased the mRNA expression of *Brca1*, relative to that of AdEmpty MOFs, thereby confirming *Brca1* KO and indicating that the observed transcriptomic effects are likely due to loss of *Brca1* (**Figure 17A**). However, in contradiction to immunofluorescence staining, RNA-seq revealed the expression of *Inha*, a gene encoding for the alpha subunit of inhibin, a marker of granulosa cells (**Figure 17B**), indicating the presence of granulosa cells in MOFs cultures. Suggesting that while our isolation technique avoids epithelial cell contamination, it does not yield cultures free of granulosa cells. As such, MOF cultures contain at least two types of ovarian cells, stromal fibroblasts and granulosa cells. Gene Ontology pathways from GSEA revealed significant increases in processes and pathways involving genomic reorganization, assembly, and disassembly of the organizational units of the genome, as well as processes mediating immune regulation, and revealed a significant decrease in the processing of non-coding mRNA (**Figure 17C**). Given the known role of BRCA1 in DNA repair and maintenance of genomic integrity, the upregulation of pathways involved in genome reorganization and chromatin assembly/disassembly with loss of BRCA1 function consolidates the role of BRCA1 as an essential player in the maintenance of genomic integrity in MOFs.

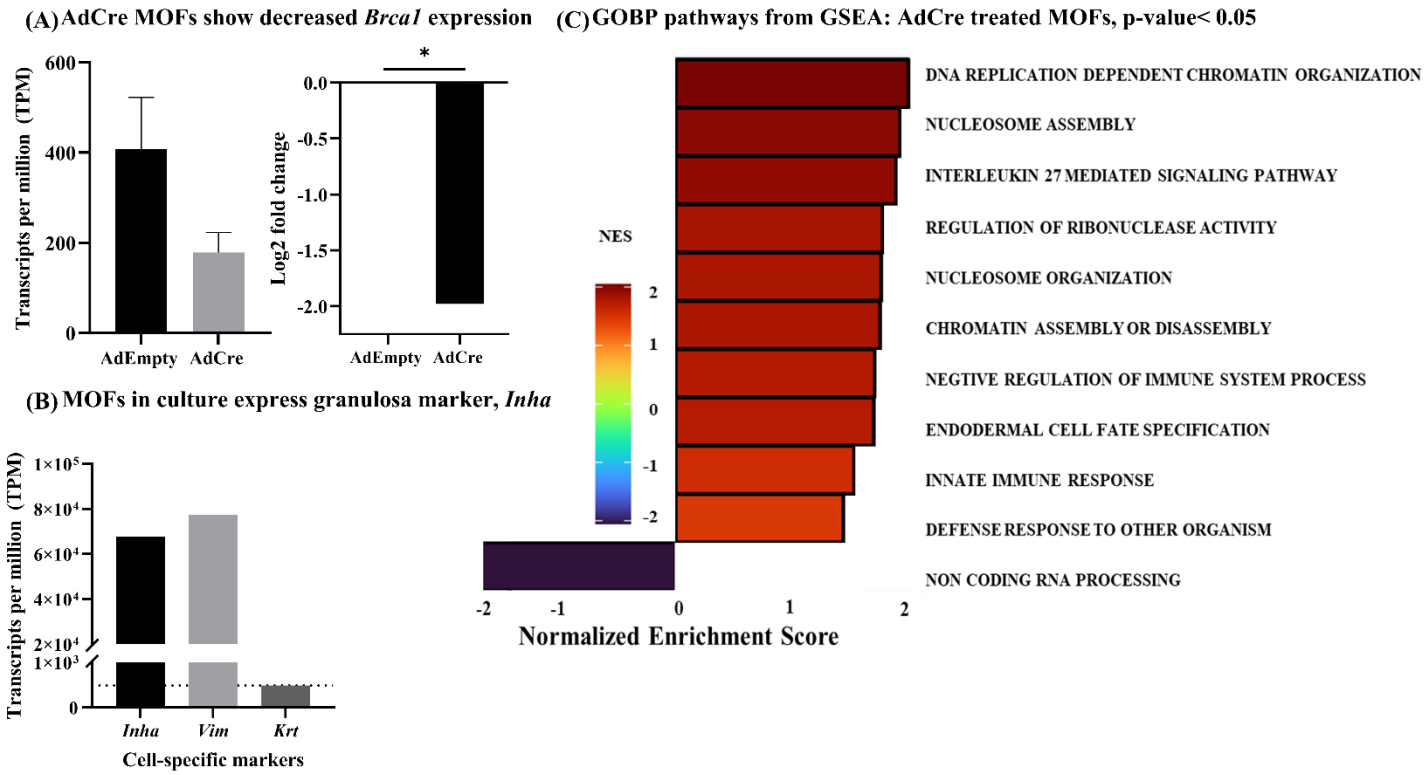

Figure 17: Gene ontology pathways identify genome organization and immune regulation pathways to be most significantly upregulated with loss of Brca1 in MOFs. *Relative abundance of Brca1 mRNA in each group is shown as* ***(A)*** *transcripts per million (TPM) and log2 fold change. AdCre treatment significantly decreased Brca1 mRNA expression relative to AdEmpty treated cells, confirming Brca1 KO in MOFs.* ***(B)*** *The mRNA expression of Inha, a gene encoding for the alpha subunit of inhibin, a marker of granulosa cells was expressed by MOFs, while relative expression of keratin mRNAs (marker of epithelial cells) was relatively low. mRNA expression is presented as TPM.* ***(C)*** *Gene Ontology (GO) pathways from GSEA reveal increased reorganization of genome, along with pathways involved in mediating immune responses, while the processing of non-coding RNA was downregulated. Adenovirus transduction and RNA extraction were performed as described in sections 2.6 and 2.13; RNA was sequenced on a NovaSeq 6000 sequencer by Genome Quebec; RNA-seq data was aligned and analyzed as described in section 2.16; RNA-seq data was analyzed using DESeq2 (R project) to access differential expression of genes (A), which is presented as Log2FC in Brca1 KO MOFs as compared to AdEmpty MOFs. Experiment was performed in triplicate (n=3). Error bars indicate SEM. Unpaired student's T-test was performed using R;*= p-value < 0.05.*

3.5.2 *Brca1* KO is likely associated with altered homeostasis of the ECM.

Since fibrosis is ordered arrangement of structural proteins of the ECM, genes that encode for proteins required for the homeostatic organization of the ECM are of particular importance. Volcano plot showing differential gene expression of AdCre MOFs, as compared to AdEmpty MOFs revealed significantly decreased expression of *Dcn*, *Adamts9*, and *Igfbp5* (highlighted in amber; **Figure 18**). These genes encode for proteins that are necessary in maintaining the structure of the ECM, and Igfbp5 is also involved in the regulation of cell proliferation. The gene product of *Dcn*, decorin is especially important for matrix organization. Additionally, the mRNA expression of *H2-Aa*, a gene encoding for one of the MHC-II complex subunits, was upregulated with loss of *Brca1* (highlighted in purple; **Figure 18**), suggesting altered immune modulation and communication in *Brca1* KO MOFs. Log2 fold change threshold for biologically relevant differences in gene expression is defined by dashed blue line (Log2 fold change=1) and lie on either side of dashed blue line, and represent differentially expressed genes with log2 fold change greater and less than 1, for upregulation and downregulation, respectively.

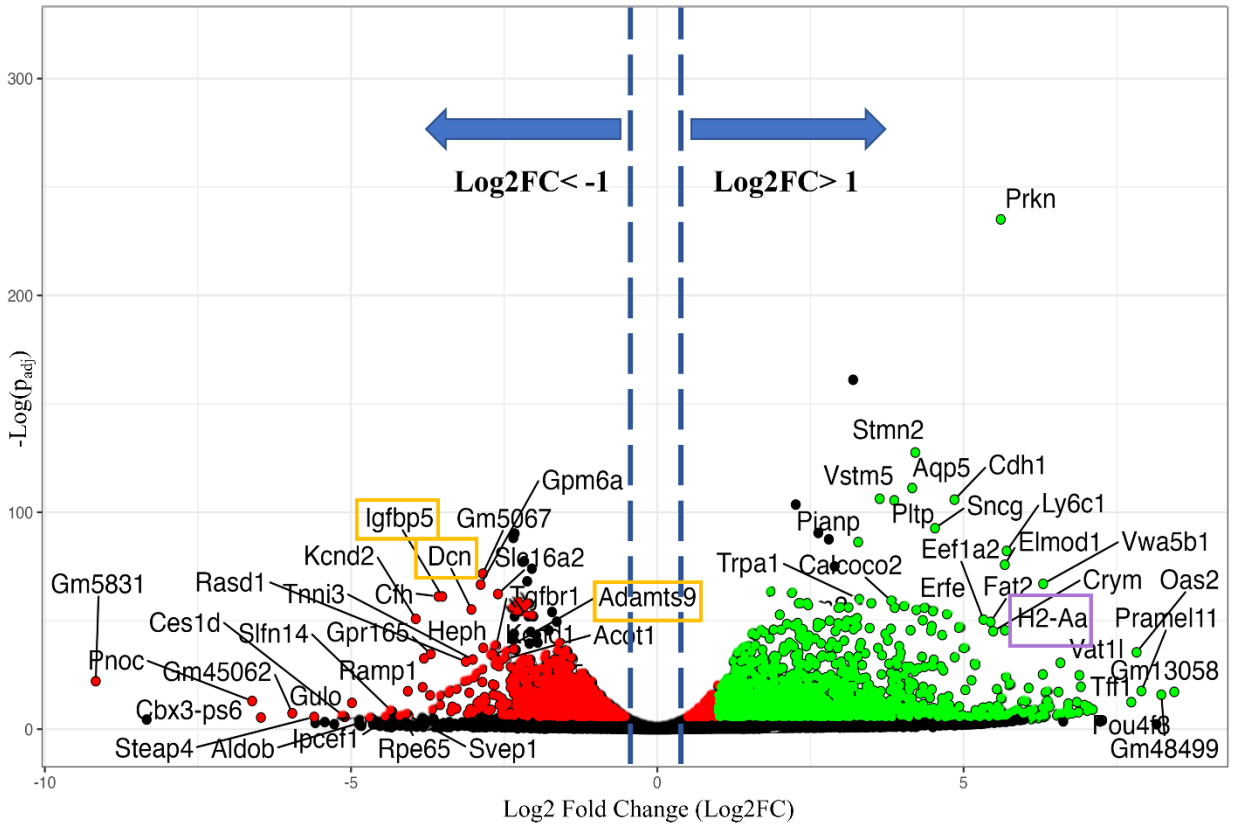

Figure 18: Volcano plot showing significant differential gene expression between AdCre and AdEmpty MOFs. *RNA-seq revealed decreased expression (to the left) of various regulatory components of the ECM, namely Igfbp5, Dcn and Adamts9 (highlighted in amber) and upregulated (to the right) MHC-II component H2-Aa (highlighted in purple). X-axis represents Log2 Fold Change (Log2FC), and Y-axis represents -Log(p_{adj}). RNA-seq data was analyzed using DESeq2 (R project) to access differential expression of genes. Differentially expressed genes (DEGs) enclosed by dashed blue lines represent increases < Log2FC of 1, and decreases > Log2FC of -1, and were not taken into account.*

3.5.3 *Brca1* KO induces myofibroblast activation of MOFs.

Brca1 KO MOFs significantly upregulated the expression of *Acta2*, *MyoD1*, a critical transcription for differentiation of myofibroblasts and genes encoding the structural components of the ECM, such as *Col11a1*, *Col18a1*, *Col8a1*, *Col14a1*, *Col4a1*, *Col2a1* and *Eln* (log2FC > 1.5; p-value < 0.05), relative to AdEmpty MOFs (**Figure 19A**), suggesting that loss of *Brca1* in MOFs mimics myofibroblast activation. Immunofluorescence revealed the formation of α-smooth muscle actin (α-SMA; encoded by *Acta2*) stress

fibers in *Brca1* KO MOFs, but not AdEmpty MOFs (**Figure 19B**), further confirming MOF activation. However, no significant changes in the mRNA expression of *Dpp4* or *Fap*, key markers associated with fibrosis, were observed with *Brca1* loss. Myofibroblast activation and consequent increased synthesis of ECM proteins along with decreased expression of genes encoding for organizational glycoproteins (*Dcn*) and remodelling enzymes (*Mmp13, Timp3, Adamts9*) (**Figures 16, and 18**) when taken together suggests the possibility that *Brca1* loss may result in dysregulated homeostasis of the ECM.

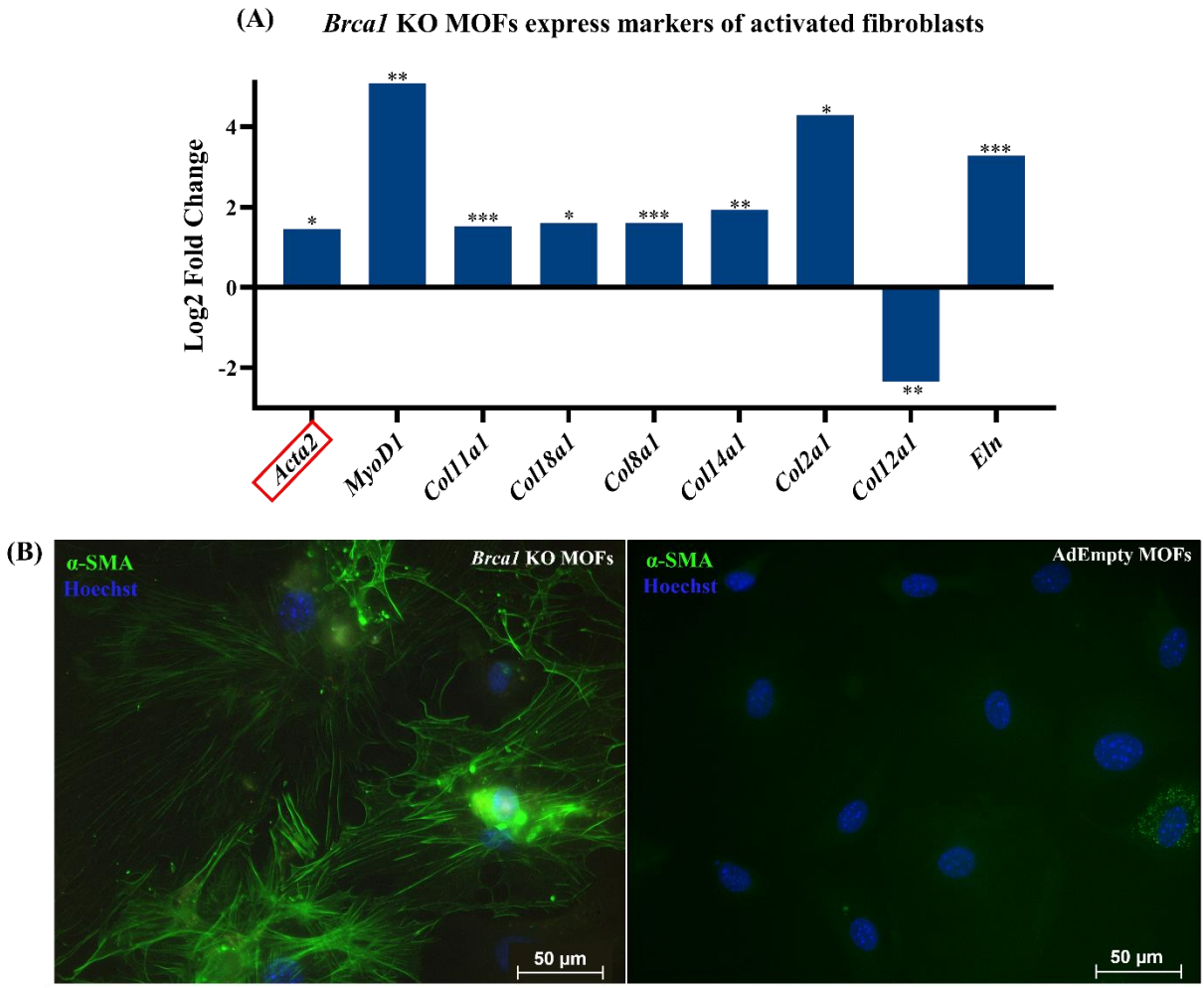

Figure 19: Deletion of Brca1 in MOFs induces myofibroblast activation. (A) *Brca1 KO MOFs upregulate Acta2, a known marker of myofibroblasts (activated fibroblasts), along with Col11a1, Col18a1, Col8a1, Col14a1, Col2a1, Eln and downregulated Col12a1.* ***(B)*** *α-SMA stress fibers in Brca1 KO MOFs. Immunofluorescence was performed on Brca1 KO MOFs 14 days post-AdCre*

*transduction. Nuclei are visualized in blue, using Hoechst. Images were taken at 20x using Axioskop2 MOT fluorescence microscope. RNA-seq data was analyzed using DESeq2 (R project) to access differential expression of genes, which is presented as Log2FC in Brca1 KO MOFs as compared to AdEmpty MOFs. Experiment was performed in triplicate (n=3). Unpaired student's T-test was performed using R; * = p-value < 0.05; ** = p-value ≤ 0.01; ***= p-value ≤ 0.001.*

3.6 *Brca1* KO MOFs exhibit impaired dsDNA damage repair, G2/M DNA damage checkpoint, and ubiquitination, that likely impedes cell cycle progression.

3.6.1 *Brca1* function is required for proper dsDNA repair and for the G2/M checkpoint.

The role of BRCA1 in maintaining genomic integrity and in orchestrating DNA repair pathways has been previously established, with *Brca1* mutant cells exhibiting impaired dsDNA repair. As such we sought to assess the consequences of loss of BRCA1 on dsDNA repair processes in MOFs. Data was compared to established gene sets from MSigDb associated with various DNA repair processes. Consistent to literature findings, the loss of *Brca1* significantly impaired the overall average gene expression (gene module score) of proteins required for the G2/M DNA damage checkpoint (**Figure 20A**), which acts to prevent cell cycle progression and allows cells to repair any DNA damage from genome replication, prior to mitosis. Additionally, the gene expression profile of *Brca1* KO MOFs revealed impaired dsDNA break repair and cellular response to dsDNA damage (**Figures 20B, C**). Collectively, these results suggest impaired dsDNA damage repair in MOFs, thereby indicating that, as in other cell types, BRCA1 in MOFs functions as a key mediator in the assembly and function of DNA repair complexes, as well as in DNA damage surveillance.

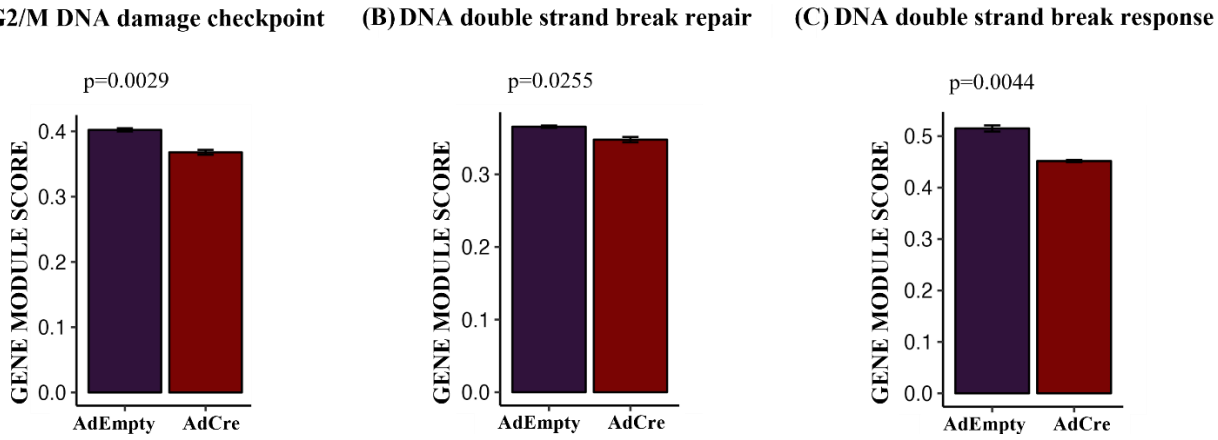

Figure 20: Loss of Brca1 function impairs expression of DNA damage checkpoints, DNA damage repair pathways. *Brca1 KO decreased the expression of genes involved in* ***(A)*** *G2/M DNA damage checkpoint regulation, as well as* ***(B)*** *double stranded DNA break repair pathways and* ***(C)*** *cellular response to dsDNA damage. RNA-seq data was analyzed using DESeq2 (R project) to access differential expression of genes, which is presented as gene module score. Experiment was performed in triplicate (n=3); All genesets were acquired from MSigDb and scored as described in section 2.15; Error bars indicate SEM; Unpaired student's T-test was applied using R.*

3.6.2 Impaired dsDNA damage repair likely halts the cell cycle to promote DNA repair.

Members of the E2f family of transcription factors control the transcription of genes involved in DNA replication and cell cycle progression into the next phase, making them critical regulators of the cell cycle[189]. Transcriptional activity of E2f is regulated by pRb. As such, when E2f is a part of the pRb-E2f complex, initiation of DNA replication is inhibited. Hyperphosphorylation of pRb by the cyclinD-CDK4/6 complex promotes release of E2f, rendering it transcriptionally active, enabling DNA replication and cell cycle progression. *Brca1* KO MOFs were found to have increased expression of genes involved in inhibition of DNA replication mediated via the pRb-E2f complex (**Figure 21A**), suggesting inhibition of cell cycle progression.

This was found to be consistent with decreased expression of *Pold1* and *Pold4*, both of which encode for subunits of replicative DNA polymerase δ, as well as increased expression of *Polk*, which encodes for DNA polymerase κ, a specialized error-prone polymerase that is equipped to bypass dsDNA damage to continue strand extension (highlighted in green; **Figure 21B**). Additionally, the expression of genes encoding for DNA repair proteins *Xrcc2*, *Rad51c* and *Gadd45a* was also significantly decreased with *Brca1* KO (highlighted in purple; **Figure 21B**). Loss of function mutations in *Xrcc2* and *Rad51c* are associated with increased genomic instability and have been identified in various cancers[190]. *Gadd45a* encodes for a nucleotide excision repair protein that is essential in mediating cellular stress responses. As such, these data suggest the possibility that BRCA1 may be responsible for the transcriptional regulation of various DNA repair proteins. It is however unclear whether *Brca1* does so directly or indirectly via intracellular signal transduction. Nonetheless reduced expression of DNA repair proteins, and replication machinery, as well as increased expression of translesion synthesis polymerases suggests reduced DNA repair efficiency and accumulation of dsDNA damage, which are associated with cell cycle arrest.

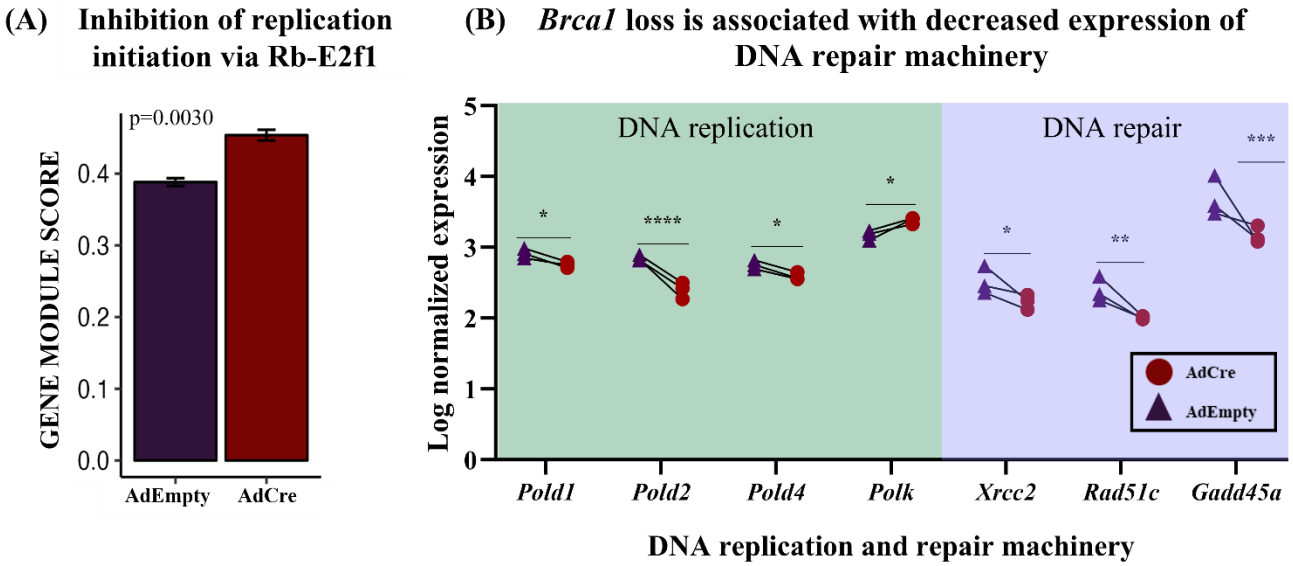

Figure 21: Brca1 likely functions as an important transcriptional regulator for DNA repair machinery. *Loss of Brca1 in MOFs* ***(A)*** *increased expression of genes encoding proteins that inhibit initiation of replication (mediated by Rb1-E2f1 complex), relative to AdEmpty infected cells.* ***(B)*** *Genes encoding for components of DNA repair machinery were downregulated (highlighted in red box), while genes encoding for translesion synthesis, DNA replication machinery (highlighted in green box) were upregulated in Brca1 KO in MOFs. RNA-seq data was analyzed using DESeq2 (R project) to access differential expression of genes, which is presented as gene module score (A) and as log normalized expression in Brca1 KO MOFs as compared to AdEmpty MOFs (B). Experiment was performed in triplicate (n=3). Geneset (A) was acquired from MSigDb and scored as described in section 2.16. All differentially expressed genes exceed log2FC≥0.55. Unpaired student's T-test was applied using R.*= p-value <0.05; **= p-value ≤ 0.01; ***= p-value ≤ 0.001; ****= p-value < 0.0001.*

3.6.3 BRCA1/BARD1 E3 ubiquitin ligase function appears to regulate cellular ubiquitination.

Apart from its role as an integral orchestrator of DNA damage surveillance and repair, BRCA1 interacts with BARD1 via its RING domain to enzymatically function as an E3 ubiquitin (Ubq) ligase that is known to mediate various aspects of DNA damage surveillance and repair, cell-cycle regulation and transcriptional regulation of cellular pathways through ubiquitination of a myriad of substrates[191]. Given that the loss of *Brca1* impaired DNA repair pathways and the G2/M checkpoint in MOFs, we sought to access whether the E3 ubiquitination function of *Brca1* too was impaired. The expression of several cellular E3 Ubq conjugating enzymes was decreased with loss of *Brca1* which led to a decreased module score for gene sets associated with cellular protein ubiquitination and ubiquitin ligase function (**Figure 22A, B**). It is possible that impaired E3 Ubiquitin ligase activity of BRCA1/BARD1 may partly contribute to impaired DNA repair pathways and cell cycle checkpoint.

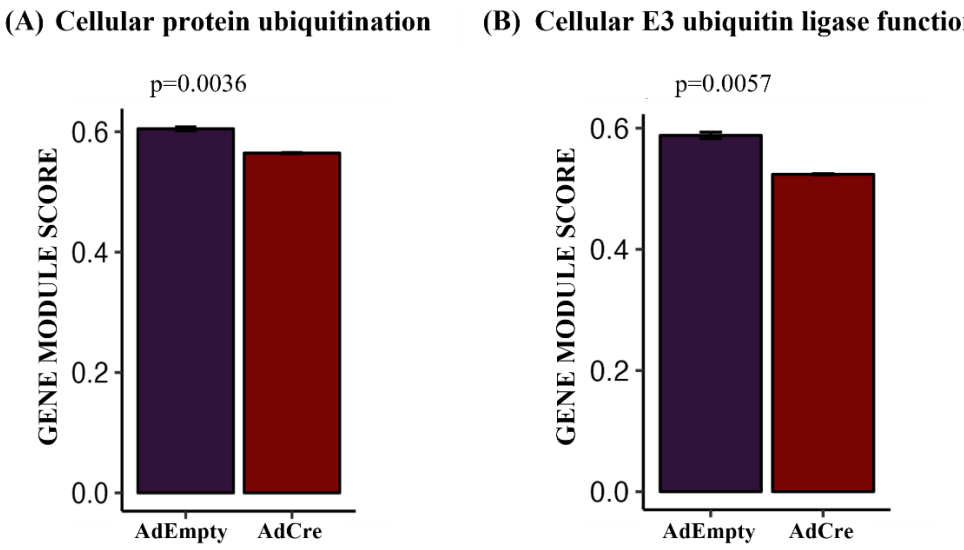

Figure 22: **Deletion of *Brca1* decreases the expression of cellular E3 ubiquitin ligases.** *Brca1 KO MOFs exhibit reductions in* ***(A)*** *global cellular ubiquitination and* ***(B)*** *E3 ubiquitin ligase functionality, which represents the final step in protein ubiquitination whereby E3 ubiquitin ligases (such as* Brca1/Bard1 *complex) transfer ubiquitin to target proteins. RNA-seq data was analyzed using DESeq2 (R project) to access differential expression of genes, which is presented as gene module score. Experiment was performed in triplicate (n=3). Both gene sets were acquired from MSigDb and scored as described in section 2.16; Error bars indicate SEM; Unpaired student's T-test was applied using R.*

3.7 The loss of *Brca1* in MOFs is associated with reduced proliferation and induction of cellular senescence.

3.7.1 Loss of *Brca1* is likely associated with increased expression of core senescence initiators.

Next, we sought to determine if loss of BRCA1 function and subsequent impairment of DNA repair pathways and DNA damage checkpoints lead to disruption of genes associated with cell cycle arrest. The gene module score of senescence core genes was significantly upregulated with loss of *Brca1* expression (**Figure 23A**). *Brca1* KO MOFs significantly increased the expression of three core senescence initiators: *Cdkn1a* (p21; log2FC=1.00), *Cdkn2a* (p16;

log2FC=1.83) and Tnfrsf10b (TRAIL2; log2FC=0.88), identifying them as core genes, which are responsible for the initiation of cellular senescence following the loss of *Brca1* in MOFs (**Figure 23B**). Cell cycle arrest and as well as enlarged and flattened cellular morphology are primary indicators of cellular senescence[192].

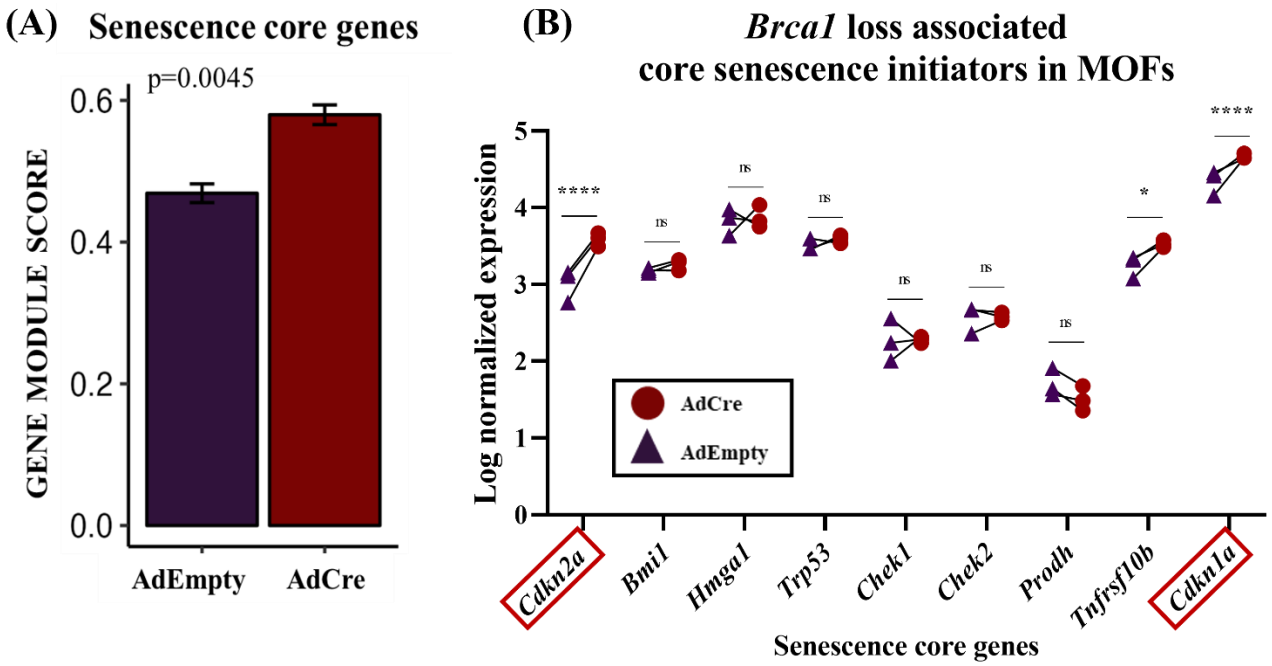

Figure 23: Brca1 KO MOFs upregulate mRNA expression of core senescence initiators cellular senescence. ***(A)*** *Gene module score of core senescence initiators was significantly upregulated in Brca1 KO MOFs.* ***(B)*** *The expression of core senescence genes- Cdkn1a, Cdkn2a and Tnfrsf10b was significantly upregulated by Brca1 KO MOFs. RNA-seq data was analyzed using DESeq2 (R project) to access differential expression of genes, which is presented as gene module score (A) and log normalized expression in Brca1 KO MOFs as compared to AdEmpty MOFs (B). Experiment was performed in triplicate (n=3). List of core senescence genes was adopted from Landry et al. 2022 and scored as described in 2.16. Error bars indicate SEM. Unpaired student's T-test was applied. *= p-value <0.05; **= p-value ≤ 0.01; ***= p-value ≤ 0.001; ****= p-value < 0.0001. Cdkn1a, and Cdkn2a meet Log2FC threshold defined in Figure 18, while Tnfrsf10b does not (Log2FC= 0.88).*

3.7.2 Loss of *Brca1* in MOFs inhibits cell cycle progression & alters cellular morphology.

Since cellular senescence is a stress response that elicits a permanent arrest in cell cycle progression and triggers profound phenotypic changes, we accessed the expression of genes associated with cell cycle progression and arrest, in *Brca1* KO and wt (AdEmpty) MOFs and visualized the accompanying change in morphology. Our findings revealed that the loss of *Brca1* in MOFs is associated with decreased expression of *Pold2* and *E2f5*, both of which genes associated with DNA replication and cell cycle progression (**Figure 24A**; highlighted in green), as well as increased expression of genes encoding for inhibitors of the cell cycle, specifically, *Cdkn1a*, *Cdkn2a*, which encode inhibitors of cyclin dependent kinases, p21 and p16, respectively; *Rb1* encodes for pRb, an inhibitor of E2F family of cell cycle progression transcription factors (**Figure 24A**; highlighted in red). The decrease in the expression of cell cycle promoting genes and concurrent increase in the expression of inhibitors of cell cycle progression may collectively be indicative of cell cycle arrest. *Brca1* KO MOFs were observed to adopt an enlarged, flattened morphology that is characteristic of senescent cells. *Brca1* KO (EYFP+) MOFs (**Figure 24B**; top) show enlarged and flattened morphology, as compared AdEmpty MOFs (auto-fluorescent; **Figure 24B**; bottom) that retain their wt morphology. Vimentin (intermediate cytoskeletal filament) staining of MOFs also shows spread out, flatted cellular morphology (**Figure 24B**).

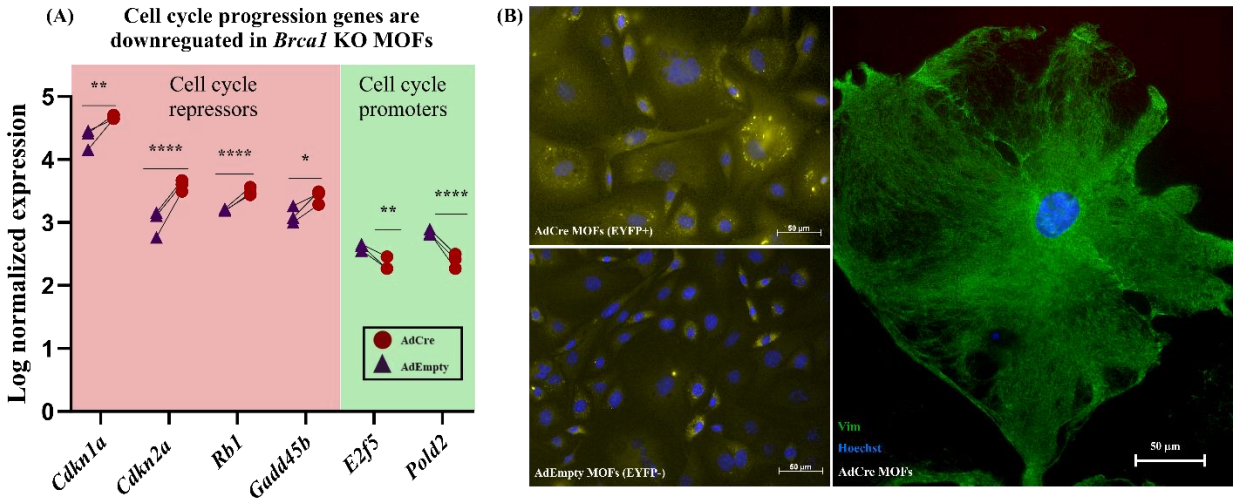

Figure 24: Brca1 KO MOFs increase the expression of negative cell cycle regulators and develop senescence-like morphology. *Loss of Brca1 expression in MOFs led to* ***(A)*** *a concurrent increase in expression of inhibitors of cell cycle (highlighted in blue) and a decrease in the expression of genes required for cell cycle progression (highlighted in green). All genes meet the Log2FC threshold defined in Figure 19.* ***(B)*** *Loss of Brca1 expression also led to the development of senescence-like cell morphology, characterized by increased cell size, enlarged flatten cytoplasm, and abnormal nuclei. AdEmpty MOFs retain their wt fibroblast morphology and do not express EYFP. Immunofluorescence was performed on AdCre MOFs using vimentin to visualize cytoplasmic structure and nuclei were stained using Hoechst. MOFs exhibit auto-fluorescence and as such can be visualized without any staining when excited using wavelength of 488nm (as is the case for AdEmpty MOFs in (B)). RNA-seq data was analyzed using DESeq2 (R project) to access differential expression of genes, which is presented as log normalized expression in Brca1 KO MOFs as compared to AdEmpty MOFs. Experiment was performed in triplicate (n=3); Unpaired student's T-test was applied using R; *= p-value <0.05; **= p-value ≤ 0.01; ***= p-value ≤ 0.001; ****= p-value < 0.0001. All images in B were captured at 40x using Axioskop 2 MOT fluorescence microscope.*

3.7.3 Senescence effector signature of *Brca1* KO MOFs is characterized by upregulation of *Map2k6* and downregulation of *Tgfb1i1*.

Upon initiation of senescence (by core genes), the induction of cellular senescence is then mediated by senescence effector genes, which not only enable cells to acquire senescence but are also responsible for the senescence associated secretory phenotype (SASP), a hallmark feature of cellular senescence. Using a pre-established list of senescence effector genes outlined in Landry et al 2022, we accessed differential expression of various senescence effector genes in *Brca1* KO MOFs. The senescence effector gene signature of *Brca1* KO MOFs was characterized by decreased expression of *Brf1*, and *Map2k6* and increased expression of *Tgfb1i1* (highlighted in purple; **Figure 25**).

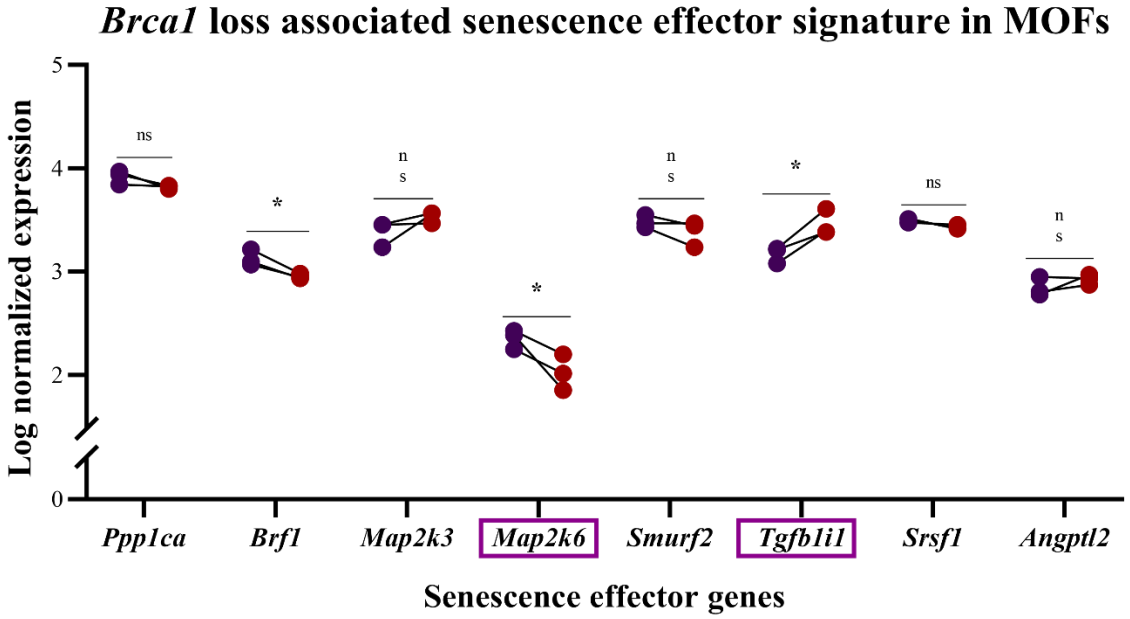

Figure 25: Brca1 KO MOFs exhibit differential expression of senescence effector genes Map2k6 and Tgfb1i1. *Gene signature of senescence effectors is characterized by downregulation of Map2k6 and upregulation of Tgfb1i1. Experiment was performed in triplicate (n=3); Senescence effector gene set was adopted from Landry et al. 2022); RNA-seq data was analyzed*

*using DESeq2 (R project) to access differential expression of genes, which is presented as log normalized expression in Brca1 KO MOFs as compared to AdEmpty MOFs. Map2k6 and Tgfb1i1 meet the Log2FC threshold defined in Figure 18, while Brf1 does not. Unpaired student's T-test was applied using R; *= p-value <0.05; **= p-value ≤ 0.01; ***= p-value ≤ 0.001; ****= p-value < 0.0001.*

3.7.4 Loss of *Brca1* in MOFs reduces cell proliferation.

To determine whether the changes in expression of genes associated with the cell cycle reflect the predicated inhibition of cell proliferation, the confluence of cells over time was determined. We observed significantly reduced proliferation of *Brca1* KO (AdCre) MOFs, as compared to wt (AdEmpty) MOFs (**Figure 26**). This data is consistent with findings from RNA-seq showing transcriptional activation of CDK inhibitors and repression of cell cycle enhancers (**Figure 24**), suggesting the possibility that the loss of *Brca1* resulted in inhibition of the cell cycle in MOFs.

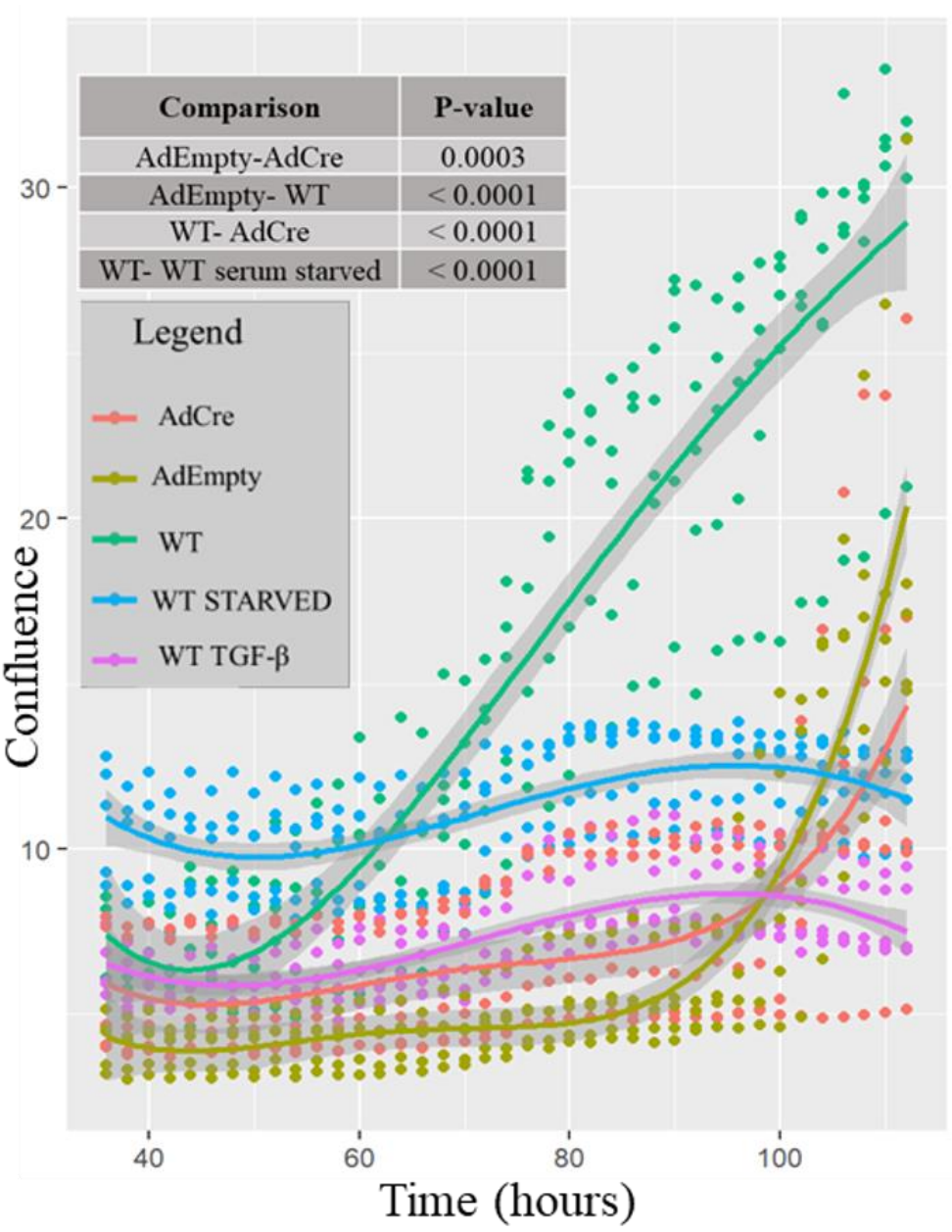

Figure 26: Loss of Brca1 limits proliferation of MOFs. *Confluency was measured for 4.5 days using Incucyte® live-cell analysis to determine the growth rate of MOFs under each condition, which was defined as a function of time and is represented by condition specific solid lines. Loss of Brca1, adenovirus transduction, serum starvation and TGF-β treatment reduced proliferation of MOFs. Non-linear regression analysis was performed using R-studio.*

3.7.5 *Brca1*$^{+/-}$ KO MOFs exhibit senescence-associated β-galactosidase activity.

Acidic β-galactosidase activity is a defining feature of senescence and distinguishes senescent cells from quiescent cells and those in temporary cell cycle arrest. To determine whether MOFs become senescent upon loss of BRCA1, as predicted by the RNA-seq data, MOFs were stained for senescence-associated β-galactosidase (SA-β-Gal) activity. *Brca1*$^{LoxP/wt}$-EYFP MOFs transduced with AdCre (*Brca1*$^{-/+}$ MOFs) stained positively (cyan) for SA-β-Gal activity 14 days post-transduction, while AdEmpty transduced *Brca1*$^{LoxP/wt}$-EYFP MOFs showed minimal to no SA-β-Gal staining **(Figure 27A**), confirming cellular senescence occurs in response to (heterozygous) loss of *Brca1* in MOFs and ruling out the possibility of virus transduction inducing senescence. Cellular senescence is a stress response that has been attributed to acetylation of lysine 320 of p53, which promotes cell survival under stressful cellular conditions through transcriptional activation of genes associated with cell cycle arrest, and repression of genes associated with apoptosis. Consistent with the presence of SA-β-Gal staining, *Brca1* KO MOFs showed increased expression of genes activated by acetylation of lysine 320 on p53, namely, *Cdkn1a*, *Cdkn2a*, *Fosl* and *Tnfrsf21* and showed decreased expression of those repressed, such as, *Mki67*, *Btg2*, *Sema4d*, *Casp6*, *Casp2* and *Cap9* (**Figure 27B**). Given the increased expression of CDK inhibitors, p21 and p16 that are encoded by *Cdkn1a* and *Cdkn2a*, respectively, we sought to access the expression of various other CDK inhibitors. We observed significantly increased expression of two other CDK inhibitor encoding genes, namely, *Cdkn1c* and *Cdkn2b*, which encode for p57 and p15 (**Figure 27C**). Upregulation of CDK inhibitors, and positive SA-β-gal staining in combination with flattened, enlarged morphology and reduced proliferation of *Brca1* KO MOFs suggests the induction of cellular senescence and cell cycle arrest.

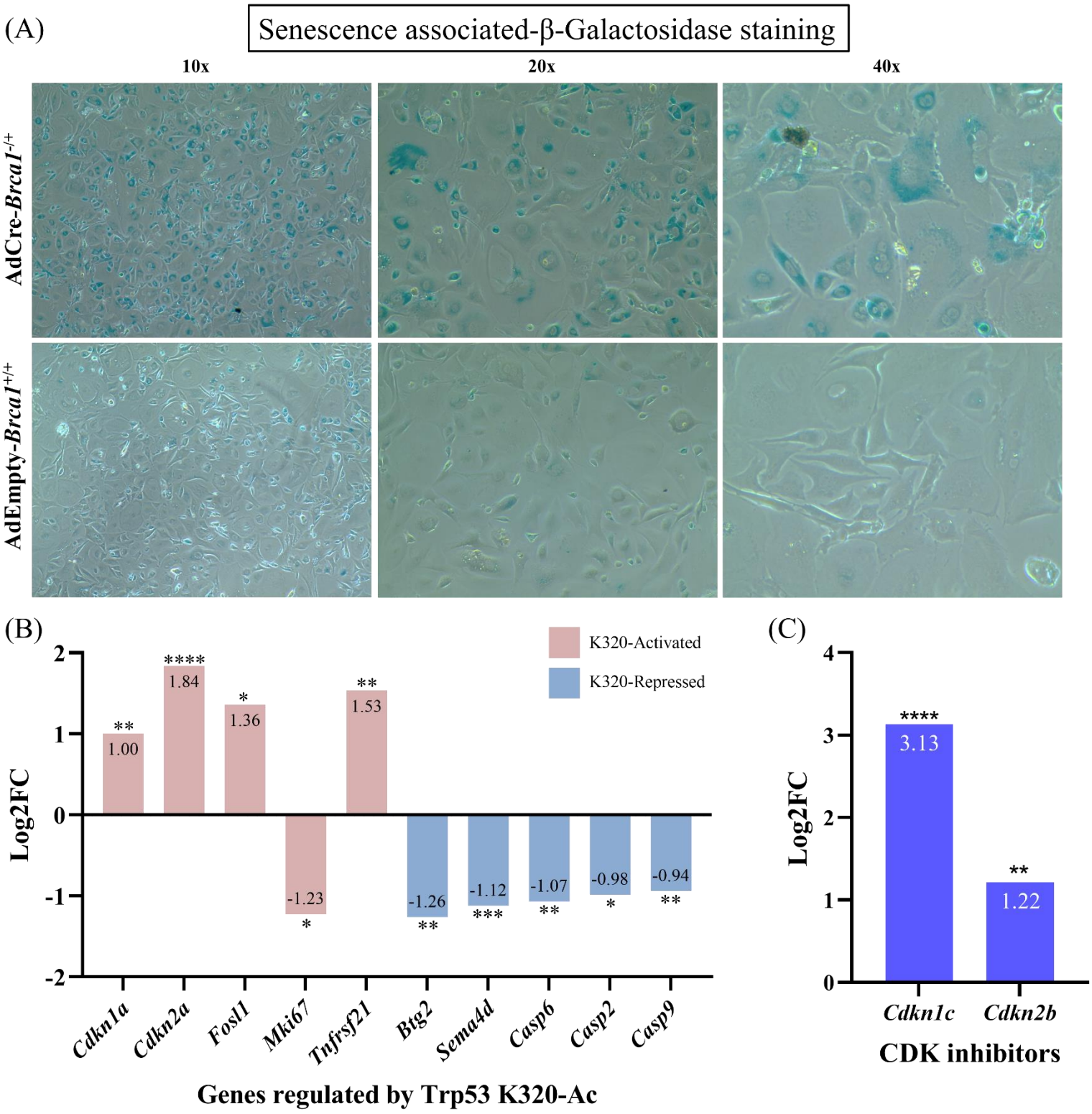

Figure 27: Heterozygous loss of Brca1 renders MOFs senescent. (A) *Brca1*$^{-/+}$ *(AdCre) MOFs (top panel), but not Brca1*$^{LoxP/wt}$ *EYFP (AdEmpty) MOFs (bottom panel) stain positively for acidic*

senescence associated-β-galactosidase (SA-β-Gal) activity. ***(B)****Brca1*$^{-/-}$*MOFs upregulate genes activated by pro-survival p53 K320-Ac and downregulate those that repressed by the same. p53 K320-Ac activated genes are shown pink and those repressed in blue.* ***(C)****Brca1 KO MOFs upregulate CDK inhibitors Cdkn1c and Cdkn2b. Images w ere captured at 10, 20 and 40x using EVOS*^{TM} *core AMEX-1200 transmitted-light inverted imaging system. RNA-seq data was analyzed using DESeq2 (R project) to access differential expression of genes, which is presented as Log2FC in Brca1 KO MOFs as compared to AdEmpty MOFs. Experiment was performed in triplicate (n=3). Datasets generated by Knight and colleagues 2006*[183] *were used to custom build gene list used in figure (B). Log2FC for all genes meets the threshold described in figure 18. Statistical significance of differentially expressed genes was accessed using an unpaired student's T-test, which was applied using R. * = p-value < 0.05; ** = p-value ≤ 0.01; ***= p-value ≤ 0.001; ****= p-value < 0.0001.*

3.8 SASP of *Brca1* KO MOFs is rich in adhesion molecules, matrix remodelling enzymes, and immunomodulatory molecules that may facilitate the formation of an immunosuppressive niche.

3.8.1 *Brca1* KO induced SASP is rich in adhesion molecules and ECM enzymes.

The SASP is a dynamic phenomenon that varies in composition, and with time as well as is biased by cell type and mode of senescence induction. Traditionally, SASP is composed of inflammatory cytokines, growth factors, modulators of the ECM, and angiogenic factors. However, composition of SASP is governed by the activity of Trp53, which can either positively regulate NFκB activity to produce a strongly inflammatory SASP (referred to as NFκB SASP), or negatively regulate it to induce a unique non-inflammatory SASP (referred to as Trp53 SASP) that is rich in growth factors and modulators of the ECM[185]. Additionally, p21 is also known to contribute to the secretory phenotype of senescent cells (referred to as SA- p21 activated secretory phenotype), SA-PASP, and is independent to SASP that is regulated by Trp53 and NFκB[184]. While NFκB- and Trp53- mediated SASP exist in a mutually exclusive manner, SA-PASP may co-exist with either

type of SASP. RNA-seq identified the SASP signature of *Brca1* KO induced senescence in MOFs to be enriched in adhesion molecules, matrix remodelling enzymes, their inhibitors, growth factors and immunomodulatory molecules (**Figures 28A-B**). We observed significantly increased gene module score for SASP regulated by p53 but did not observe any significant changes in the gene module score among AdEmpty and *Brca1* KO MOFs for SASP mediated by NFκB (**Figure 28C**). Consistently, we did not observe any significant increased in the expression of genes encoding for pro-inflammatory cytokines Il-6 and Il-1α, that are associated with NFκB SASP (**Figure 28D**). These data suggest that the secretory phenotype of senescent *Brca1* KO MOFs is due to the activation of SASP regulator p53 and p21, while NFκB does not appear to contribute to the SASP of *Brca1* KO MOFs.

Closer assessment of the secretome of *Brca1* KO MOFs, revealed significant increases in the expression of diverse components of the ECM, such as cell adhesion molecules (CAMs) (**Figure 29A**), including structural proteins (**Figure 19A**), remodelling enzymes (**Figure 29B**), potent mitogens (**Figure 29C**) as well as numerous components associated with increased stiffness of the ECM, such as cross-linking enzymes, glycosaminoglycans, and various enzymatic and non-enzymatic components required for the synthesis of collagen and elastic fibers, which are known constituents of fibrotic niches (**Figure 30**). This suggests that loss of *Brca1* in ovarian fibroblasts may lead to dysregulation in the composition and structure of the surrounding extracellular matrix. It is however unclear if the observed changes in gene expression are due to the direct consequences of loss of *Brca1* or to indirect effectors (senescence or myofibroblast activation).

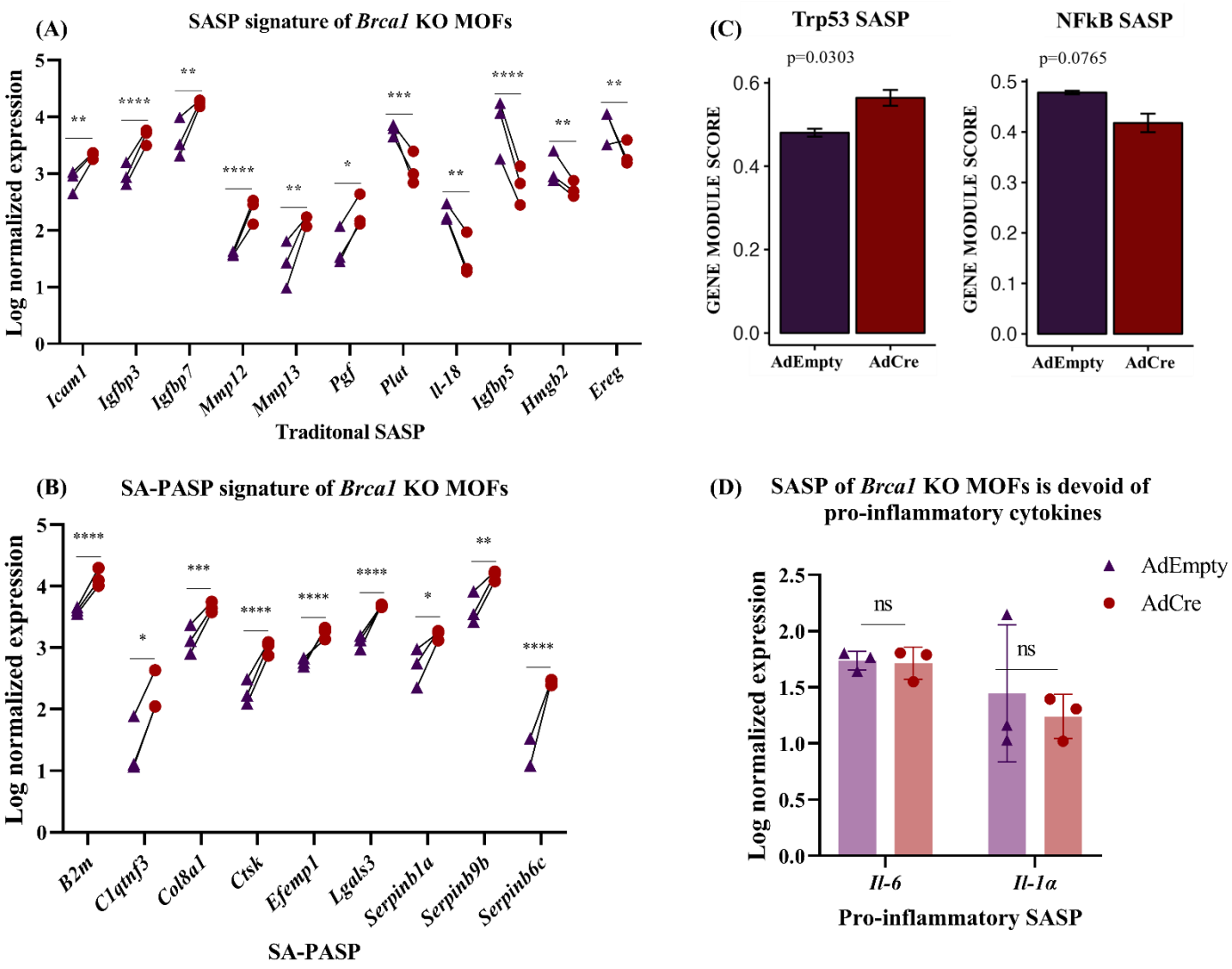

Figure 28: SASP of Brca1 KO MOFs is enriched with components of the ECM and appears to be driven by p53 and p21. (A) *SASP of Brca1 KO MOFs is enriched in cell adhesion molecules and matrix remodelling components.* ***(B)*** *Senescence dependent p21 activated secretory phenotype (SA-PASP) of Brca1 KO MOFs is enriched in components of the ECM including, membrane glycoproteins, protease inhibitors and immunomodulatory molecules.* ***(C)*** *Overall SASP expression prolife of Brca1 KO MOFs is aligned with that driven by p53 but not NFκ-B. RNA-seq data was analyzed using DESeq2 (R project) to access differential expression of genes, which is presented as log normalized expression in Brca1 KO MOFs as compared to AdEmpty MOFs (A, B, D) and as gene module score (C). Experiment was performed in triplicate (n=3). Error bars indicate SEM; Custom gene set for "traditional SASP" (A) was adapted from Landry et al. (2022)[61]; SA-PASP gene list (B) was custom designed using datasets generated by Sturmlechner and colleagues*

(2022)[184]*; Trp53 and NFκ-B SASP genesets (C) were adapted from Lopes-Paciencia et al. 2019*[185]*, and scored as described in section 2.16. All genes in (A and B) meet the log2FC threshold described in figure 18. Statistical significance of differentially expressed genes was accessed using an unpaired student's T-test, which was applied using R. * = p-value < 0.05; ** = p-value ≤ 0.01; ***= p-value ≤ 0.001; ****= p-value < 0.0001.*

Reactome of *Brca1* KO MOFs is enriched with diverse components of the extracellular matrix

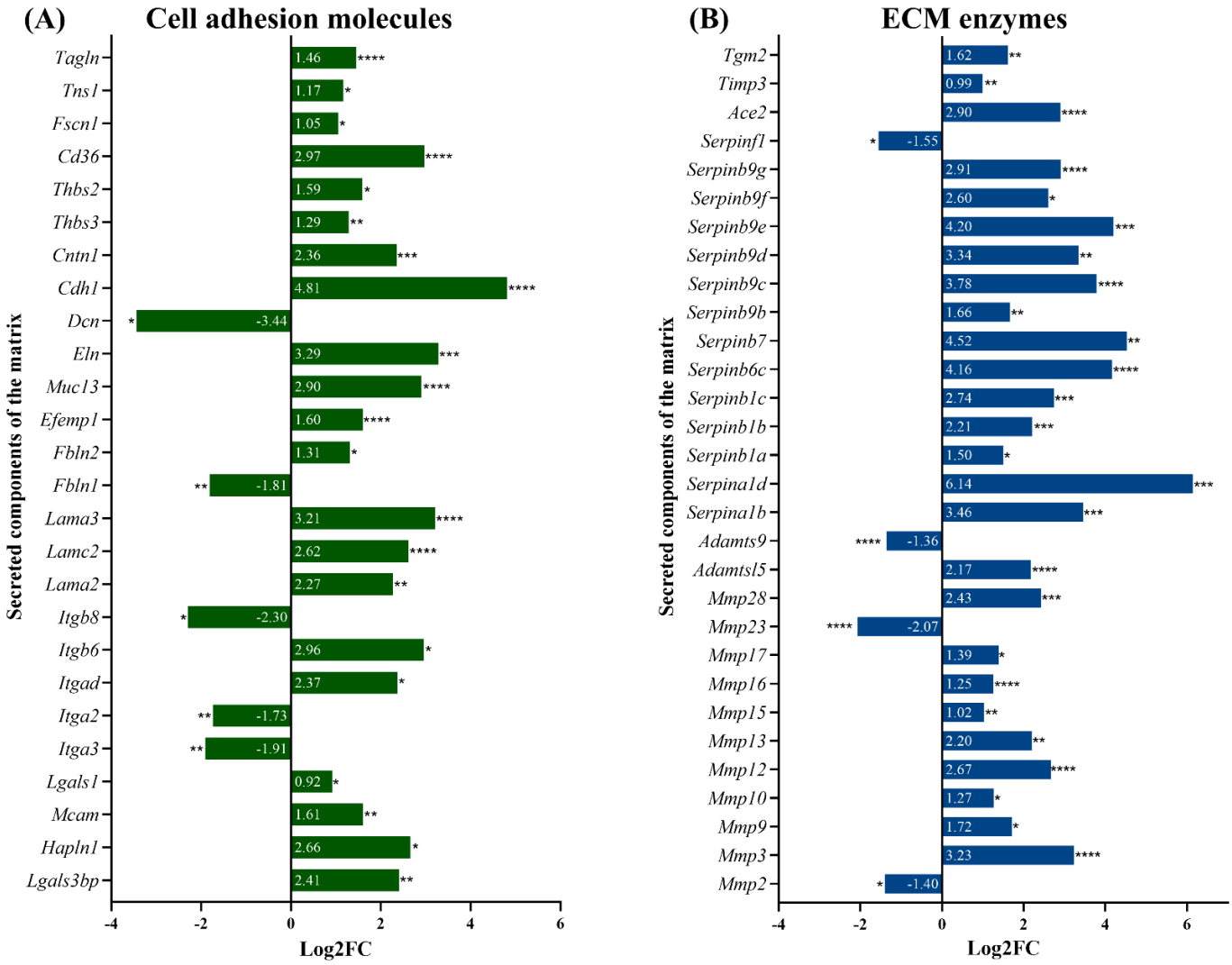

Figure 29: Brca1 KO MOFs enhances expression of ECM components. *Loss of Brca1 in MOFs results in upregulation of genes encoding for many secreted molecules/components of the ECM, including* ***(A)*** *numerous cell adhesion molecules and structural proteins, and* ***(B)*** *matrix remodelling and crosslinking enzymes, families of protease inhibitors, as well as* ***(C)*** *potent mitogenic molecules. RNA-seq data was analyzed using DESeq2 (R project) to access differential expression of genes, which is presented as Log2FC in Brca1 KO MOFs as compared to AdEmpty MOFs (A-C) and as log normalized expression in Brca1 KO MOFs as compared to AdEmpty MOFs (C). Error bars (C) indicate SEM. Experiment was performed in triplicate (n=3). Log2FC for all genes meets the threshold described in figure 18. Statistical significance of differentially expressed genes was accessed using an unpaired student's T-test, which was applied using R. * = p-value < 0.05; ** = p-value ≤ 0.01; ***= p-value ≤ 0.001; ****= p-value < 0.0001.*

Brca1 KO MOFs upregulate secreted components associated with increased stiffness of the extracellular matrix

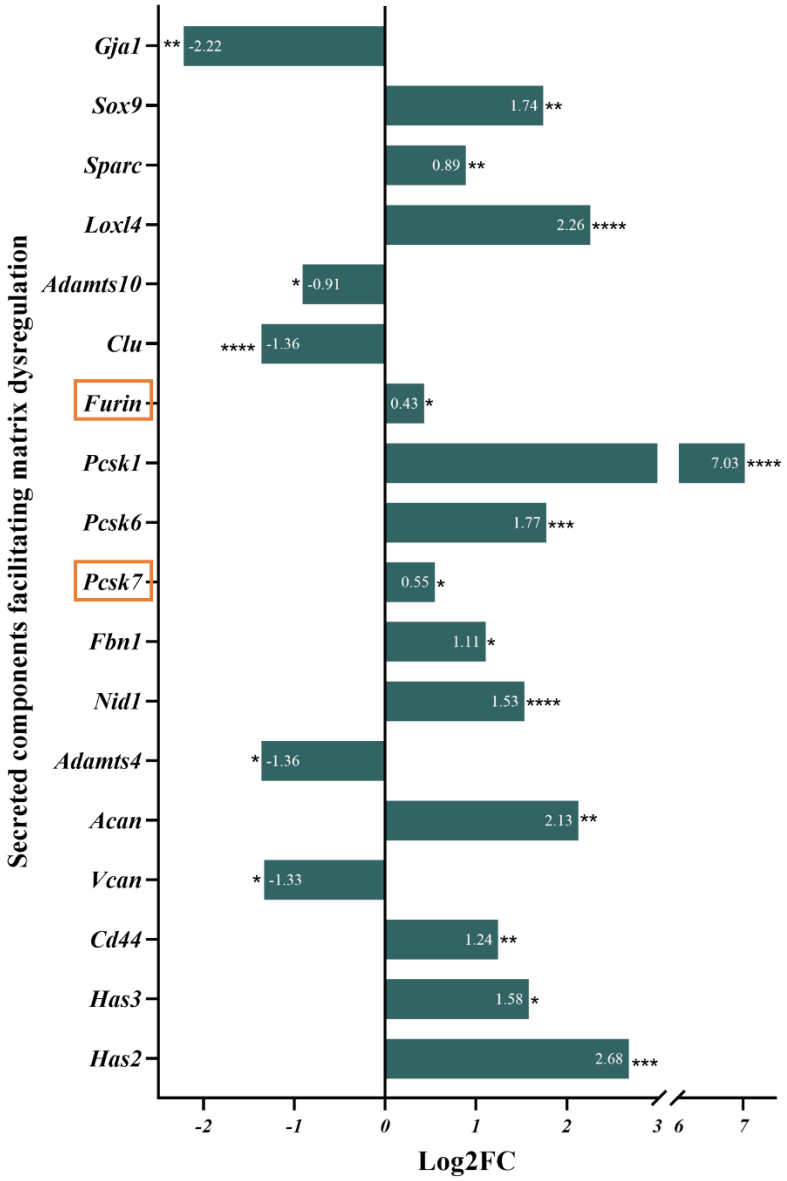

Figure 30: Brca1 KO MOFs enhances expression of ECM components. *Loss of Brca1 in MOFs results in upregulation of genes encoding for various enzymatic and non-enzymatic secreted components of the extracellular matrix that are associated with increased stiffness of the ECM and fibrotic niches, including proteins required for the synthesis of collagen and elastic fibers, which are known constituents of fibrotic niches. Experiment was performed in triplicate (n=3); RNA-seq data was analyzed using DESeq2 (R project) to access differential expression of genes, which is presented as Log2FC in Brca1 KO MOFs as compared to AdEmpty MOFs. All genes other than*

*ones highlighted in orange meet the log2FC threshold described in figure 18; Statistical significance of differentially expressed genes was accessed using an unpaired student's T-test, which was applied using R; * = p-value < 0.05; ** = p-value ≤ 0.01; ***= p-value ≤ 0.001; ****= p-value < 0.0001.*

3.8.2 *Brca1* KO upregulates expression of immune modulators.

Given that inflammation and immune regulation are key features of the SASP, we sought to access the expression of immune modulators in *Brca1* KO MOFs. Transcriptomic analyses revealed significant increases in the expression of various true and decoy death receptors, chemokines, interleukins, and their cell surface receptors (**Figure 31**) that are largely associated with the anti-inflammatory type II immune response (highlighted in purple), that is known to facilitate wound healing and tissue repair through resolution of inflammation and dampens adaptive immune responses[193–195]. Though it is unclear if the observed increases in gene expression of immunomodulatory molecules is due to the development of senescence or due to the direct loss of *Brca1*, it is evident that increased expression of anti-inflammatory molecules impart *Brca1*-deficient MOFs the ability to communicate with the immune, allowing them to modulate immune responses.

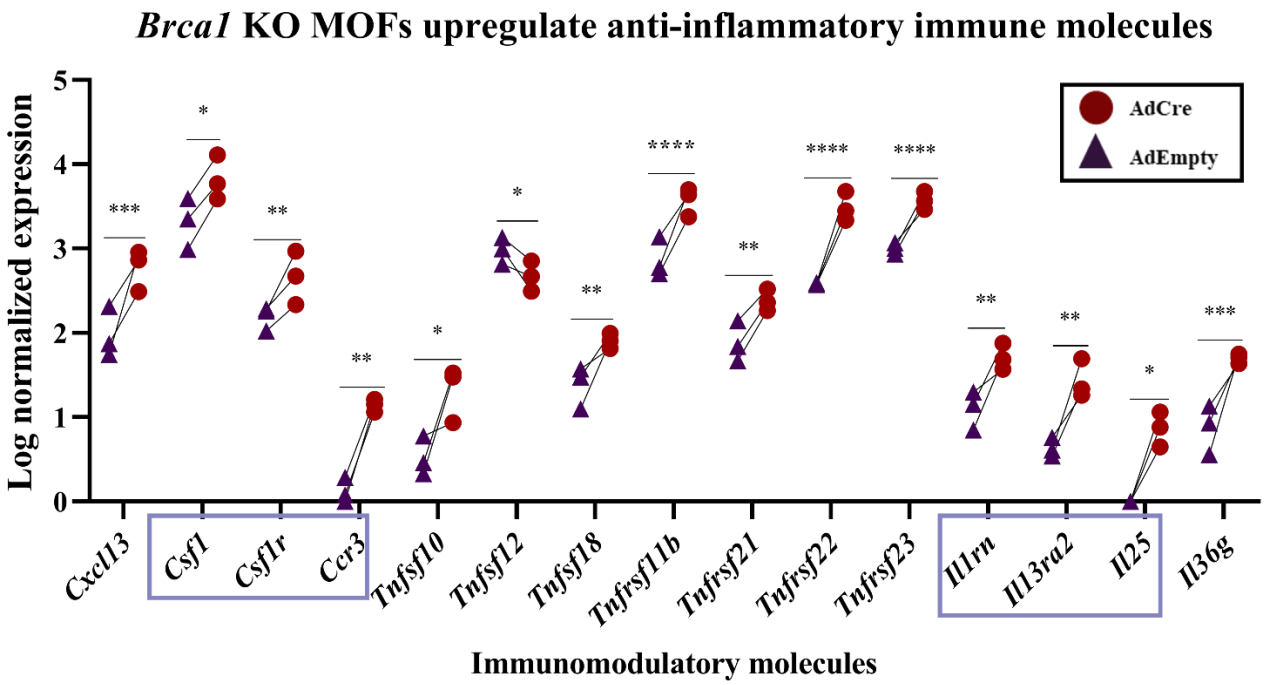

Figure 31: Loss of Brca1 in MOFs is associated with increased expression of anti-inflammatory immune modulators. *The expression of genes encoding for immunomodulatory molecules such as cytokines, chemokines, true and decoy death receptors, interleukins, and receptors was enhanced in MOFs after deletion of Brca1. Genes encoding for immune modulators associated with type II immune response are highlighted in purple. RNA-seq data was analyzed using DESeq2 (R project) to access differential expression of genes, which is presented as log normalized expression in Brca1 KO MOFs as compared to AdEmpty MOFs. Experiment was performed in triplicate (n=3). All differentially expressed genes meet the threshold described in figure 18; Unpaired student's T-test was applied using R; * = p-value < 0.05; ** = p-value ≤ 0.01; ***= p-value ≤ 0.001; ****= p-value <0.0001.*

3.8.3 *Brca1* KO MOFs may mimic antigen presenting cancer associated fibroblasts.

Since *Brca1* KO MOFs upregulated various anti-inflammatory cytokines and interleukins, we sought to access the expression of other immune modulatory molecules. Interestingly, the gene expression of several components of the major histocompatibility complex (MHC) I and II, as well as that of markers of antigen-presenting cancer associated fibroblasts (apCAFs), such as *Ly6c1* and *Lgals3* among others, was found to be significantly upregulated in *Brca1* KO MOFs (**Figure 32A,**

B). Increased expression of components of MHC-I and II, especially in combination with the upregulation of anti-inflammatory immune modulators, provides *Brca1* KO MOFs an additional means of communicating with the immune system, specifically CD4+, CD8+ T and NK cells. Dysregulation of the ECM via increased expression and secretion of CAMs, matrix proteins, remodelling components, in combination with apCAF-mimicking ability of *Brca1* KO MOFs might further suggest that loss of *Brca1* function in MOFs could contribute to the formation of an immunosuppressive niche in the murine ovary, rendering it an appealing pre-metastatic niche.

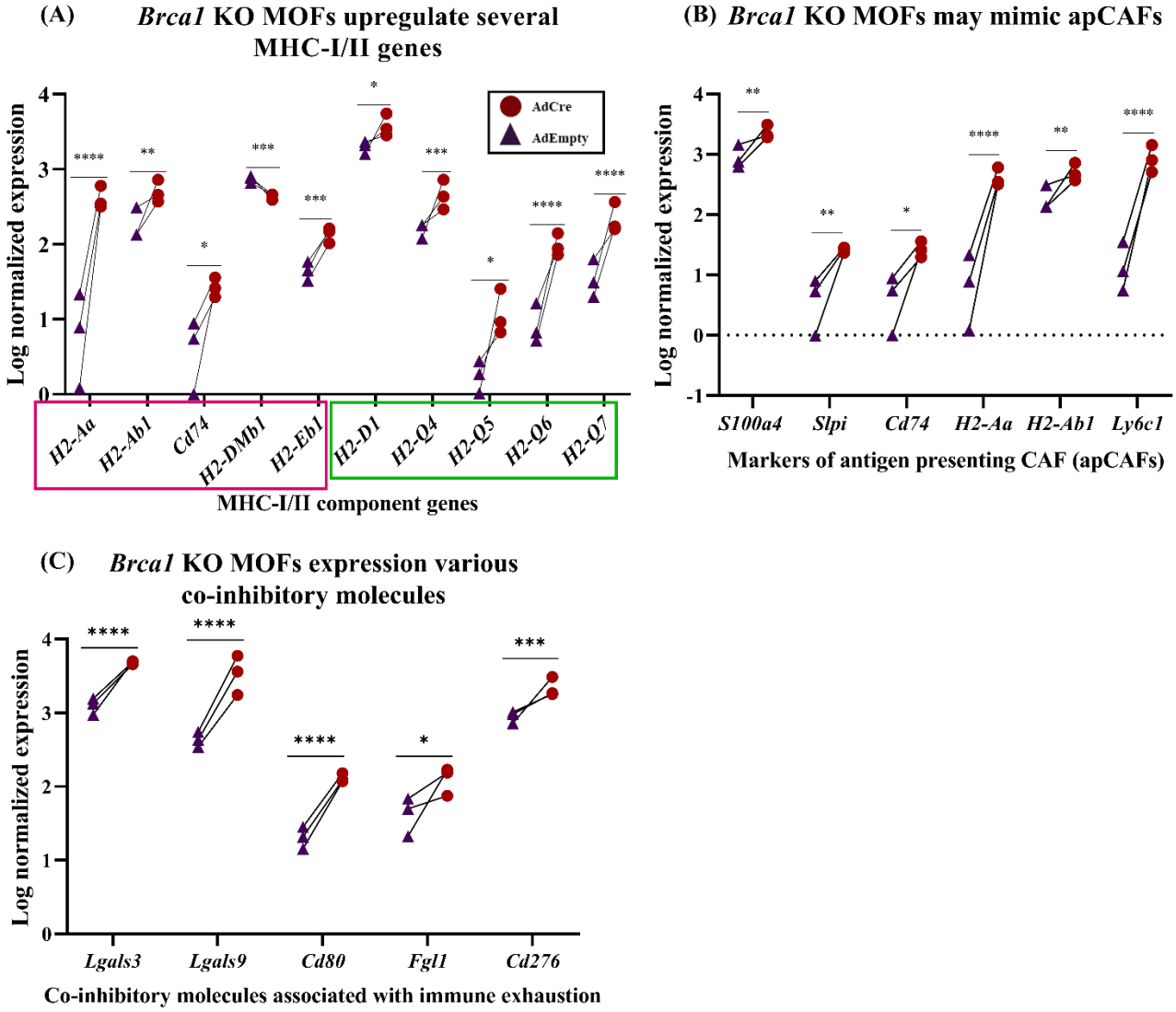

Figure 32: The loss of Brca1 in MOFs may facilitate the formation of an immunosuppressive niche. *Genes encoding for (A) components of the MHC-I/II complex (MHC-I associated genes highlighted in green and MHC-II associated genes highlighted in pink) and (B) markers of antigen presenting CAFs (apCAFs) were substantially upregulated by Brca1 KO. RNA-seq data was analyzed using DESeq2 (R project) to access differential expression of genes, which is presented as log normalized expression in Brca1 KO MOFs as compared to AdEmpty MOFs. Experiment was performed in triplicate (n=3). Gene list for "Markers of antigen presenting CAFs" was custom built using data generated by Friedman et al. 2020*[186]*. All differentially expressed genes meet the threshold described in figure 18. Unpaired student's T-test was applied using R; * = p-value < 0.05; ** = p-value ≤ 0.01; ***= p-value ≤ 0.001; ****= p-value <0.0001.*

Chapter 4: Discussion

The homozygous deletion of *Brca1* from primary MOFs induced a myofibroblastic phenotype that was characterized by increased expression of *Acta2*, formation of α-smooth muscle actin stress fibers and increased expression of genes encoding for structural ECM proteins such as *Col11a1, Col18a1*, *Col8a1*, *Col14a1, Col4a1*, *Col2a1* and *Eln*. This was accompanied by the development of cellular senescence, which was confirmed by reduced proliferation, enlarged and flattened morphology, increased expression of cell cycle inhibitors, and positive staining for SA-β-gal activity. These changes resulted in a mildly-inflammatory SASP that appears to be enriched with immune modulators, components of the MHC-I/II complex and various components of the ECM, specifically CAMs, matricellular proteins, and remodelling and cross-linking enzymes. While there have been numerous studies to investigate the consequences of loss of BRCA1 in the transformation of epithelial cells, our results suggest that loss of BRCA1 function in ovarian fibroblasts has the potential to create a pro-fibrotic microenvironment, which we hypothesize may also be a contributing to the earlier onset of ovarian cancer in *BRCA1* mutation carriers.

4.1 Induction of senescence in *Brca1* KO MOFs is likely associated with post-translational modification of p53 at lysine 320.

Cellular senescence is defined as irreversible growth arrest in response to a variety of stressors, such as DNA damage, oxidative stress, mitochondrial dysfunction, all of which are primary hallmarks of cellular aging[90]. Our findings that the loss of *Brca1* in ovarian fibroblasts is associated with the development of cellular senescence are consistent with those documented in literature. Mouse embryonic fibroblasts isolated from *Brca1*$^{\Delta 11/\Delta 11}$ mice exhibited flattened and enlarged morphology, reduced proliferation, and strong SA-β-gal staining as compared to wt mouse embryonic fibroblasts in culture[169]. Given the integral role of BRCA1 as orchestrator of

dsDNA damage repair, the loss of BRCA1 was associated with impaired dsDNA damage repair, genomic instability, and accumulation of DNA damage[169]. Cao and colleagues proposed that the accumulation of DNA damage due to the loss of BRCA1 function was likely to evoke a physiological response through the activation of p53, initially resulting in cell cycle arrest, followed either by apoptotic clearance of genetically compromised cells or survival through the onset of cellular senescence. In response to DNA damage, p53 is acetylated at one of two C-terminal lysine residues, K320 and K373, in a mutually exclusive manner[183,196,197]. Acetylation at K373 (K373-Ac) is associated with immediate response to severe DNA damage, and leads to apoptotic clearance of compromised cells, while acetylation at K320 (K320-Ac) is associated with persistent DNA damage and promotes survival through the induction of cellular senescence[183,198]. It can therefore be speculated that the induction of apoptosis, peaking at 48h after AdCre transduction, in response to sudden loss of *Brca1* in MOFs, (**Figure 13**) may be attributed to p53 K373-Ac in response to abrupt impairment of dsDNA damage repair (**Figures 20 B, C**) and subsequent accumulation of damaged DNA. However, as apoptosis started to taper off at day 11, surviving *Brca1* KO MOFs adopted a flattened, enlarged morphology (**Figure 24)**, which may be attributed to p53 K320-Ac, promoting survival of *Brca1* KO MOFs through the induction of senescence. This is consistent with increased expression of genes activated and decreased expression of those repressed by p53 K320-Ac (**Figure 27B**). Interestingly, we observed significantly decreased expression of *Mki67*, a gene encoding for Ki67, a marker of cell proliferation, that is transcriptionally activated by p53 K320-Ac. In support of our findings, senescence-associated cell cycle arrest and lack of proliferation are characterized by decreased expression of *Mki67*. It has been shown that the acetyltransferase P300/Cbp-associated factor is responsible for K320-Ac on p53, and is known to do so to a greater extent under hypoxic

conditions[183,199]. It may be possible that preferential K320-Ac of p53 and consequent onset of senescence in *Brca1* KO MOFs is due, at least in part, to being cultured in hypoxic conditions to mimic relatively low blood oxygenation levels in the ovary. This collectively suggests that the sudden and extended loss of *Brca1* is likely stabilized by distinct acetylation patterns of p53 acetylation, initially via apoptotic clearance (K373-Ac) and then through cell cycle arrest (K320-Ac) and subsequent onset of senescence in *Brca1* KO MOFs (**Figure 33**).

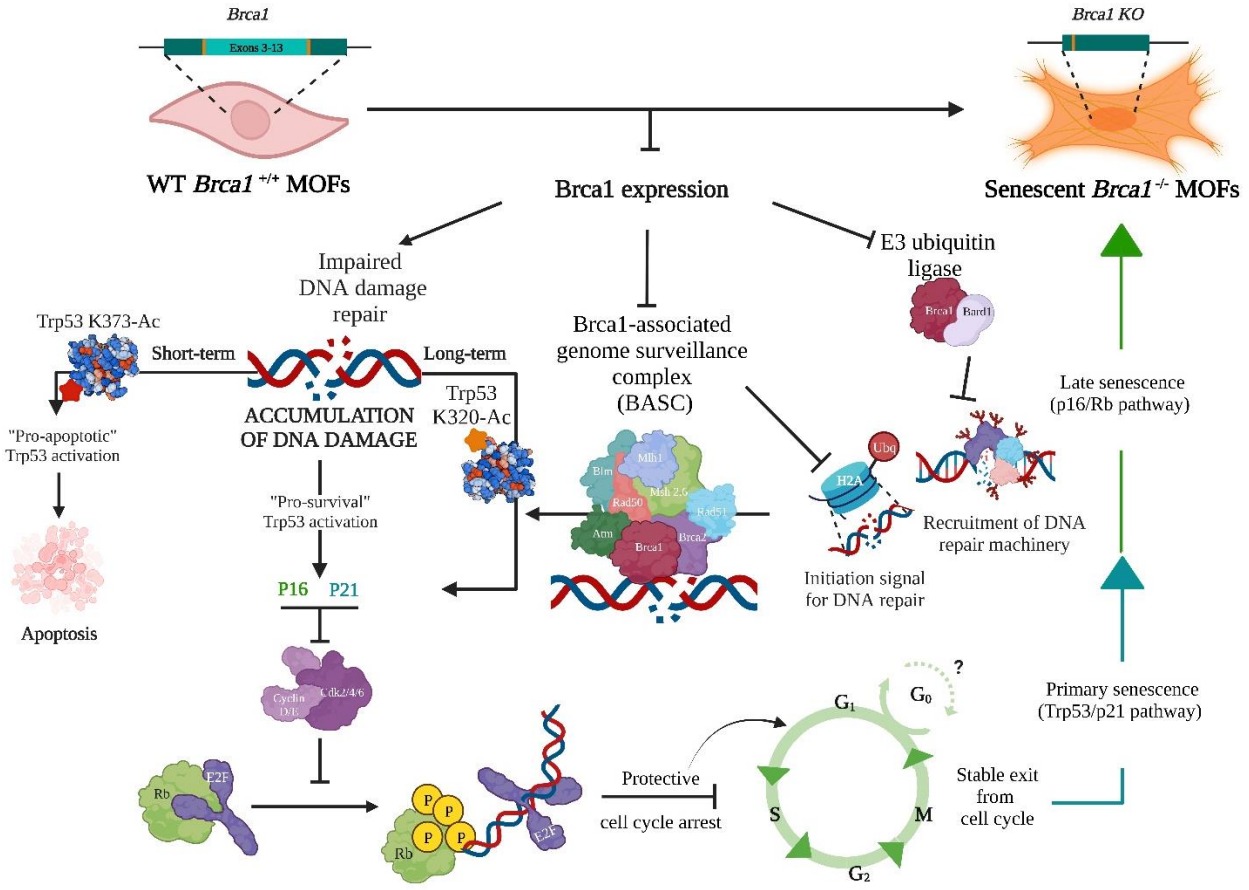

Figure 33: Onset of senescence in Brca1 KO MOFs may be attributed to the induction of p53 K320-Ac in response to sustained DNA damage. *Deletion of Brca1 and hence loss of BRCA1 function, specifically as a mediator of DNA repair, poses as a stressor and induces cellular stress responses. The sudden (short-term) loss of Brca1 likely promotes acetylation at lysine 373 of p53 (p53 K373-Ac), a post-translational modification that results in hyperphosphorylation of the N-terminal of p53, leading to increased stability and nuclear retention, thereby enhancing its*

interaction with low-affinity promoters for pro-apoptotic genes, potentially explaining the sudden increase in apoptosis with loss of Brca1. Prolonged impairment of DNA repair, however, preferences acetylation of lysine 320 of p53 (p53 K320-Ac), a post-translational modification that blocks hyperphosphorylation at the N-terminal and consequently promotes nuclear export, rendering p53 capable of binding only to high-affinity promoters such as that for p21. The expression of p21 and p16 (triggered directly by DNA damage), inhibitors of cyclin-dependent kinase/cyclin complexes prevent hyperphosphorylation of the protein retinoblastoma (Rb), thereby preventing release of the transcription factor E2f, that is responsible for the transcription of DNA replication machinery required for the S phase to prepare for mitosis.

4.2 SASP of *Brca1* KO MOFs is associated with immune evasion and may facilitate the formation of an immunosuppressive microenvironment.

The development of cellular senescence is bipartite in nature. Primary senescence, which is the early, reversible state of cell cycle arrest that is dominated by p53 activity, is followed by late senescence that is primarily mediated by p16/Rb pathway. Late senescence is characterized by irreversible cell cycle arrest, elevated expression of p21 and p16, presence of SA-β-gal activity, decreased expression of Ki67 (*Mki67*)[198], and production of SASP[200], all of which appears to be exhibited by *Brca1* KO MOFs. The production of SASP is a key pathogenic feature of senescent cells. Though the components and functions of SASP are diverse, production of inflammatory cytokines, chemokines and interleukins is a marked feature that is often associated with recognition and clearance of senescent cells by the immune system, to restore tissue homeostasis[201]. While the transcription factor NFκB is responsible for the production of a pro-inflammatory SASP, the components of SASP are to a large extent modulated by the activity of p53, with inactivation of p53 in human fibroblasts being associated with the production of strongly inflammatory SASP, thereby suggesting an inhibitory role of p53 in modulating the inflammatory nature of SASP. In the case of *Brca1* KO MOFs, we did not observe any significant changes in the

expression of pro-inflammatory cytokines associated with immune clearance, such as, IL-6, IL-1α, IL-8, and TNF-α, suggesting that the production of SASP in response to the loss of *Brca1* is not dependent on NFκB (**Figure 28D**). Given that pro-inflammatory SASP is associated with immune recognition and clearance of senescent cells, *Brca1* deficient ovarian fibroblasts may be subject to reduced recognition and clearance by the immune system, allowing them to persist in the ovary. The expression of *Cdkn1a*, the p21 encoding gene, in response to stress induced activation of p53 hinders cell cycle progression at G1/S and G2/M phases of the cell cycle by inhibiting the activity of cyclin D/E-CDK2/4/6 complexes[202,203], while simultaneously inhibiting apoptosis by binding to apoptotic agents, such as caspases[202], thereby preventing apoptotic clearance of *Brca1* KO MOFs, which is believed to be a hallmark characteristic of senescent cells[204].

Recent evidence has shown that the expression of the non-classical MHC class 1b molecule, H2-q, on senescent cells allows them to evade immune clearance by inhibiting the activity of NK and $CD8^+$ T-cells[205]. H2-q binds to stimulatory NKG2c and inhibitory NKG2a receptors to regulate the cytotoxic activity of NK and $CD8^+$ T-cells[205]. However, the binding affinity of H2-q for NKG2a is greater than that for NKG2c. Therefore, when the two receptors are co-expressed on a single effector cell, inhibitory signals override activation signals, rendering NK and $CD8^+$ T-cells functionally exhausted[206]. This suggests an additional mechanism by which *Brca1* KO MOFs may evade immune clearance and persist. Consistent with this, we observed upregulation of genes encoding for subunits (*Serpinb9 -b, -c, -d, -e, -f, -g, -h*) of SERPINb9 (**Figure 29B**), a protease inhibitor that blocks the activity of granzyme B, a mediator of cytotoxicity imparted by NK and T-cells, thereby allowing *Brca1* deficient MOFs to persist by resisting immune clearance[207].

The ability to evade immune clearance is further supported by increased expression of markers of antigen-presenting cancer associated fibroblasts (apCAFs), which includes the MHC-II related genes *H2-Aa*, *H2-Ab1* and *Cd74*, as well as *S100a4*, *Slpi*, and *Ly6c1*. As the name suggests, apCAFs modulate immune activity and have been identified to be immunosuppressive in models of breast and pancreatic cancers, and tumor suppressive in a model of non-small cell lung cancer [186,208,209]. While increased expression of MHC-I and -II molecules allow CAFs to interact with cells of the innate (NK cells) and adaptive immune system, it is the co-expression of stimulatory and inhibitory molecules that dictate the outcome of antigen presentation, which is the activation or exhaustion of immune cells. Specifically, co-expression of antigen presenting machinery with stimulatory molecules results in NK/ T-cell activation, while that with inhibitory molecules results in NK/T-cell exhaustion. In murine and human models of breast and pancreatic cancers, apCAFs are believed to confer immunosuppression by preventing the activation of T-cells due to the absence of co-stimulatory molecules[208]. Much like apCAFs observed in models of breast and pancreatic cancer, *Brca1* KO MOFs exhibited upregulation of various MHC-II genes (**Figure 32**). In support of our findings, Friedman et al. (2020) reported that in cases of triple negative breast cancer, patients with *BRCA1/2* mutations had significantly higher proportions of $S100a4^+$ apCAFs as compared to BRCA1 wt patients, suggesting an association between the loss of BRCA1 and expression of antigen presenting machinery genes[186]. However unlike apCAFs described in models of breast and pancreatic cancers, we detected significantly increased expression of genes encoding for co-inhibitory molecules, such as *Lgals3*, *Fgl1*, *Cd80*, *Lgals9*, *Cd276* as well as for various components of MHC-I complex- *H2-d1*, *H2-q4*, *H2-q6*, *H2-q7* (**Figure 32**), which may convey upon *Brca1* deficient MOFs the ability to not only interact with, but also negatively modulate the activity of NK as well as, $CD4^+$ and $CD8^+$ T-cells.

Lgals3 and *Fgl1* encode for galectin 3 (GAL3) and fibrinogen-like protein 1 (FGL1), respectively, both of which are ligands for LAG-3, a potent inhibitory receptor expressed by previously activated $CD4^+$ and $CD8^+$ T and NK cells. As such, binding of GAL3 and FGL1 to LAG-3 renders $CD4^+$, $CD8^+$ T and NK cells functionally exhausted, thereby negatively regulating innate and adaptive immune responses[210–214]. Additionally, GAL3 is known to inhibit T-cell activation in a LAG-3 independent manner by hampering the formation of an immunological synapse, and its expression has been correlated to apoptosis of T-cells in primary and metastatic melanomas, thereby highlighting the role of GAL3 in mediating immunosuppression through inhibition of T-cell activtiy[215,216]. CD74, an accessory molecule for MHC-II, is also upregulated by *Brca1* KO MOFs and is known to support slow processing, peptide loading, and assembly, resulting in the surface expression of a highly stable peptide-MHC-II complex (pMHC-II), a high affinity ligand for LAG-3[217]. Binding of CD4 to MHC-II in the presence of TCR/MHC-II complex stimulates the activation of T helper cells, promoting proliferation and cytokine production, while binding of LAG-3 to pMHC-II inhibits signalling through the TCR, rendering T-cells functionally exhausted[218,219]. The interaction of pMHC-II/CD4 is mutually exclusive to that of pMHC-II/LAG-3, with pMHC-II complex binding to LAG-3 with significantly higher affinity than to CD4. Belonging to the same family of proteins as GAL3, galectin-9 (GAL9) encoded by *Lgals9* has been shown to interact with and facilitate crosslinking and aggregation of Tim-3, an inhibitory receptor highly expressed on $CD4^+$ T helper cells to induce apoptosis, thereby limiting T-cell activity. Additionally, binding of GAL9 to checkpoint receptor, PD-1 attenuates TIM-3/GAL9 mediated apoptosis, while promoting T-cell exhaustion[220,221]. Upregulation of genes encoding for co-inhibitory molecules, such as *Lgals3* and *Fgl1* along with pMHC-II renders *Brca1* KO MOFs capable of inhibiting immune responses through direct exhaustion of $CD4^+$ T-cells, thus limiting

immune surveillance and contributing to the formation of an immunosuppressive microenvironment.

It can therefore be speculated that the concurrent surface expression of stable H2-q, a non-classical MHC class Ib molecule, MHC-II (pMHC-II), and co-inhibitory molecules (GAL3, FGL1 and GAL9) by *Brca1* deficient MOFs confers them with the ability to evade immune responses, allowing for the accumulation of senescent myofibroblasts that are able to render NK, cytotoxic ($CD8^+$) and effector ($CD4^+$) T-cells functionally exhausted, thereby facilitating the formation of immunosuppressive microenvironment (**Figure 34**). We recently identified a population of fibroblasts expressing components of SASP as well as non-classical MHCI/II molecules, namely, *H2-Aa*, *H2-Ab1*, *H2-Eb1*, *H2-D1* and *H2-K1* (SASP fibroblasts) in fibrotic aged murine ovaries that were absent in young counterparts, suggesting a possible association between aged/senescent cells and immunosuppression[61]. The expression of non-classical MHC-I/-II genes by non-immune cells has been described as a gene signature for aging and cellular senescence and has been previously observed in aging hepatocytes and now in aging ovarian fibroblasts[61,88]. Increased expression of genes associated aging and cellular senescence by *Brca1* KO MOFs suggests an association between *Brca1* and aging.

Impaired immune clearance leads to accumulation of senescent cells and as such, components of SASP in tissues, which are known to exacerbate pathology and accelerate aging[222,223]. Comprised of remodelling enzymes such as MMPs/ TIMPs and inflammatory cytokines, SASP can induce chronic low-grade inflammation and promote abnormal fibrotic remodelling of the ECM, yielding the formation of a pathogenic microenvironment that facilitates migration, survival, and proliferation of disseminated cancer cells. The loss of *Brca1* in MOFs enhanced the expression of various secretory components, such as structural and matricellular

proteins (**Figures 19, 30**) cell adhesion molecules (**Figure 29A**) and remodelling enzymes (**Figure 29B**), and immunomodulatory cytokines and chemokines (**Figure 31**), the accumulation of which may collectively render the ovarian ECM an optimal niche for metastatic invasion.

4.3 Myofibroblastic senescent *Brca1* KO MOFs likely resist apoptotic clearance.

Activation of myofibroblasts in response to wound healing is essential for tissue repair and function. Just as important is the elimination myofibroblastic phenotype, either through de-differentiation of myofibroblasts into fibroblasts or through apoptotic clearance, to retain the normal physiologic state. Accumulation of activated myofibroblasts due to impaired de-differentiation of myofibroblasts or resistance to apoptosis has been implicated in the pathology of fibrotic disorders[224]. In this study we showed that the loss of *Brca1* in MOFs in vitro triggers the development of a myofibroblastic phenotype that is characterized by increased expression of *Acta2* and various collagen encoding genes. Increased mRNA expression of *Acta2* was consistent with the formation of stress fibers in *Brca1* KO MOFs, but not wt (AdEmpty) MOFs. The transcription factor myoblast determination protein 1 (MyoD) is a critical switch for the differentiation and de-differentiation of myofibroblasts, with sustained upregulation of MyoD preceding that of *Acta2* during myofibroblast differentiation, and declining levels of MyoD preceding those of α-SMA as myofibroblasts de-differentiate into fibroblasts[224,225]. Additionally, declining levels of MyoD correlate with susceptibility of apoptosis in myofibroblasts, resulting in elimination of myofibroblast activity[225]. Senescent myofibroblasts with elevated MyoD expression fail to undergo de-differentiation and display resistance to apoptosis, while genetic silencing of MyoD restores susceptibility of these myofibroblasts to apoptosis and partially reversed age-associated pulmonary fibrosis in vivo[225], thereby highlighting the contribution of MyoD to the persistence of the myofibroblastic phenotype and its contribution of age-associated fibrosis.

Additionally, growing evidence attributes age-associated tissue fibrosis to the accumulation of senescent myofibroblasts[226–228]. Consistently, we observed substantial upregulation of MyoD encoding gene, *Myod1* (**Figure 19A**), suggesting that the development of senescence and elevated expression of MyoD likely renders *Brca1* deficient MOFs resistant to apoptotic clearance. Should this accumulation of myofibroblastic senescent cells occur in the ovary, it could contribute to accelerated aging and onset of ovarian fibrosis, through enhanced expression of structural proteins, cross-linking and remodelling enzymes. In addition to expression of H2-q, pMHC-II, co-inhibitory molecules and Serpinb9 that collectively facilitate immune evasion of myofibroblastic senescent *Brca1* KO MOFs, we observed upregulation of *Lgals1*, *Mcam*, *Igfbp3*, *Sphk1*, *S100b* and downregulation of *Casp6*, *Casp2*, *Casp9* and *Casp12*, all of which have been implicated in inhibition of apoptosis. Specifically, extracellular interaction of GAL1 with CD146, and IGFBP3 induced expression of *Sphk1* have been shown to inhibit apoptosis[229,230]. Expression of S100b in mesenchymal cells and inhibited expression of initiating and executioner caspases can prevent apoptosis independently, and can be hypothesized to synergistically resist apoptosis (**Figure 34**)[231]. Mechanisms that confer resistance to apoptosis or prevent immune clearance are likely to facilitate the accumulation of "pro-fibrotic" myofibroblastic senescence in tissues, which has been implicated with aging, and fibrosis, both of which confer increased risk for cancers[173,232–237]. Additionally, senescent normal ovarian fibroblasts can induce neoplastic transformation, proliferation, and migration of pre-malignant immortalized OSE cells in vitro, while senescent peritoneal mesothelial cells supported the proliferation, migration, and invasion of ovarian cancer cells in vitro, and enhanced peritoneal metastases in vivo, likely through the activity of the SASP and direct cell-cell interactions[238,239]. Moreover, identification of senescent fibroblasts with tumor promoting potential adjacent to ovarian cancer cells suggests a positive correlation between

presence of senescent cells and tumorigenesis[240]. It can therefore be speculated that the accumulation of *Brca1* deficient senescent myofibroblasts in the ovary may facilitate ovarian aging through the accumulation of SASP, the components of which may result in dysregulated structure and composition of the ECM, resulting in impaired tissue function. The accumulation of senescent myofibroblasts may also prime malignant transformation of compromised epithelial cells, thereby posing increased risk for the onset of cancer.

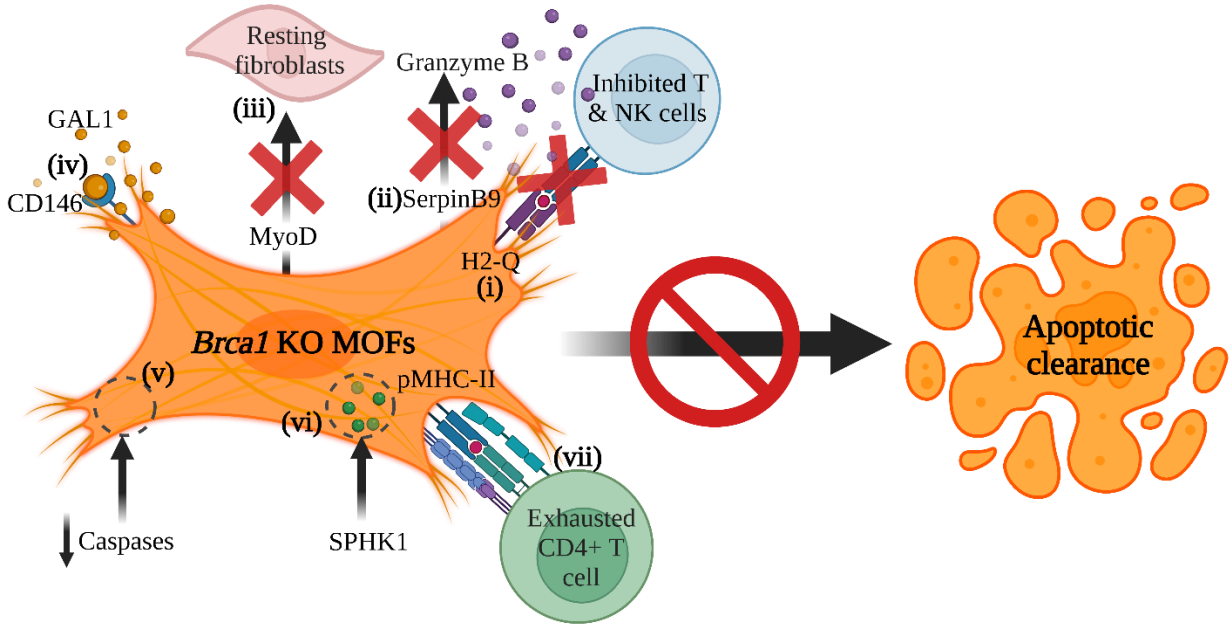

Figure 34: Deletion of Brca1 renders senescent MOFs resistant to apoptotic and immune mediated clearance. *Several factors/mechanisms likely contribute to impaired clearance of these Brca1 deficient cells:* ***(i)*** *The onset of cellular senescence that is accompanied by upregulation of non-classical MHC-II, that binds to Nkg2a on NK and aging populations of CD8$^+$ T-cells to inactivate their cytotoxic activity;* ***(ii)*** *Upregulation of serpinb9, an inhibitor of granzyme B mediated apoptosis;* ***(iii)*** *Myofibroblast activation- Upregulation of MyoD blocks de-differentiation of apoptosis resistant myofibroblasts into resting fibroblasts that are sensitive to apoptosis;* ***(iv)*** *GAL1 secreted by Brca1 KO MOFs may act into an autocrine manner to inhibit apoptosis in a CD146 dependent manner;* ***(v)*** *Expression of p21 directly blocks transcription of various caspases to reduce apoptotic clearance;* ***(vi)*** *IGFBP3 mediated upregulation of Sphk1 has*

been shown to block apoptosis; ***(vii)*** *Co-expression of MHC-II and co-inhibitory molecules may render CD4+ T cells functionally exhausted, thus preventing immune clearance. Collectively, all of the above-mentioned mechanisms may confer protection against apoptotic clearance of Brca1 KO MOFs.*

4.4 Accumulation of senescent *Brca1* deficient myofibroblasts in the ovary likely facilitates the development of an immunosuppressive, pathogenic microenvironment capable of supporting metastatic colonization.

Impaired mechanical homeostasis of the ECM is believed to drive the onset and progression of tissue fibrosis. While myofibroblasts are key mediators of fibrotic tissue remodelling[241,242], components of SASP can also contribute to age-associated tissue fibrosis, as is observed in models of lung, kidney, and heart fibrosis[243–247]. Myofibroblast mediated overproduction, disordered arrangement and extensive cross-linking of collagens and elastic fibers, as well as accumulation of mucopolysaccharides, such as hyaluronan, have been observed and demonstrated to result in pathological lung fibrosis[248–250].

4.4.1 Collagen microarchitecture as a driver of ECM stiffness

Collagens are the most abundant proteins in vertebrates and serve as structural scaffolding for virtually all organs, holding together various tissues and constituent cells that cooperate to confer functionality to organs. Tissue resident fibroblasts deposit monomeric collagen α chains into the interstitial ECM, where they interact with one and other to assemble into various supramolecular structures through a process termed fibrillogenesis. Alpha chains of fibrillar collagens (types I, II, III, V, and XI) assemble into homo/heterotrimers, referred to as collagen microfibrils. Other types of collagens, such types XII and XIV associate with the surface of collagen fibrils, to regulate fibril diameter, fibrillogenesis, and mediate interactions with various

components of the ECM[251,252]. The α chains of fibrillar collagens are synthesized as N- and C-terminal telopeptide containing procollagens, that associate with Sparc, a molecular chaperone that promotes intracellular cleavage of telopeptides by various members of ADAMTS/ADAMTS-like proteinases and facilitates proper deposition in the ECM[253]. The loss of *Brca1* in MOFs resulted in significant upregulation of *Col2a1*, *Col11a1*, *Col14a1*, *Col8a1*, *Col18a1*, *Sparc*, and *Adamtsl5* and downregulation of *Col12a1* (**Figure 20**). Microfibrils of collagens II and XI are known to associate with each other to form dense supramolecular collagen fibrils that provide cartilage with its characteristic semi-rigid structure[254]. Collagen XIV is known to bridge fibrillar collagens and is present in areas of mechanical stress, such as in bleomycin induced fibrotic lesions in the lungs[255]. Increased expression of genes associated with molecular chaperones, collagen maturation enzymes and cartilage specific fibrillar collagens by *Brca1* deficient MOFs likely suggests enhanced deposition of fibrillar collagens into the surrounding ovarian extracellular matrix.

Decorin, a small leucine-rich proteoglycan bearing multiple collagen binding sites, has been deemed a structural spacer[256] that simultaneously interacts with various collagens (type I, II, II, IV, VI, XII and XIV) to limit the anisotropic assembly of collagen fibers[257,258]. As such, substantially decreased expression of the decorin encoding gene, *Dcn*, by *Brca1* KO MOFs may promote anisotropic arrangement of collagen fibrils, a defining characteristic of tissue fibrosis. In support of our findings, *Dcn* null animals displayed enhanced experimental hepatic fibrosis, as compared to wt animals[259].

Fibrillar collagens that form the frame-work of tissues greatly contribute to the molecular architecture and provide mechanical properties for tissue function. Proteoglycans (PGs) interact with collagen fibrils in a non-covalent manner to create a network of collagens, which is then reinforced via cross-linking for stability[260,261]. Cross-linking of collagens, catalyzed by families of

cross-linking enzymes, such as Lysyl hydroxylases (LH) and oxidases (Lox; encoded by *Lox*), its paralogs, Lox-like enzymes (Loxl; encoded by *Loxl1-4*) and transglutaminases (TG)[242]. Cross-linking of collagens occurs among side chain residues of (i) collagen α chains, (ii) triple helical microfibrils and (ii) supramolecular collagen fibers. In each case, formation of a covalent link reinforces the overall structure, that is a disulphide bond between residues of an α chain strengthen the triple helix structure, while covalent bonds linking microfibrils and supramolecular fibers reinforce the arrangement of the collagen network, thereby stabilizing the structure of the ECM by limiting flexibility[262,263]. As such excessive cross-linking is a major driving force of age- and fibrosis-associated tissue stiffness and mechanical stress[264–266]. This is illustrated by increased expression of transglutaminase 2 (*Tgm2*), Lox and Loxl enzymes in idiopathic pulmonary fibrosis[267,268], which was then ameliorated in murine models of bleomycin induced pulmonary fibrosis by inhibition or absence of these cross-linking enzymes[268,269]. Moreover, TGF-β mediated activation of lung fibroblasts was accompanied with the production of cross-linking enzyme Loxl4, thereby linking myofibroblast activation to Loxl4 mediated fibrotic remodeling[267]. Additionally, inhibition of Loxl4 antagonized fibrogenic hallmarks in vitro and similar phenotypes in murine models of systemic sclerosis[270]. Loxl enzymes secreted into the matrix as zymogens are activated by proprotein convertases through proteolytic cleavage[271]. In the case of *Brca1* KO MOFs, we observed significant upregulation of cross-linking enzyme encoding genes, *Loxl4* and *Tgm2*, that are responsible for crosslinking fibrils of collagens II/II, II/XI and XI/XI, respectively, as well as proprotein convertase encoding genes, *Pcsk-6* and *Pcsk-1* (**Figures 29B and 30**).

Hyaluronan, also known as hyaluronic acid (HA), a unique glycosaminoglycan (GAG) composed of repeated disaccharides, plays a vital role in maintaining tissue structure and providing adequate hydration through its ability to interact with water molecules. HAS2, the primary HA

synthase, is known to be upregulated by TGF-β mediated myofibroblast activation, and the enhanced synthesis of HA is believed to indirectly contribute to tissue fibrosis[272]. In a previous separate study, expression of Has2 rendered myofibroblasts resistant to apoptotic clearance, thereby promoting survival and persistant activation, which was directly associated with pathological fibrosis[273]. Moreover, the development of lung fibrosis is dependent on the expression of HAS2 and CD44 in fibroblasts[274]. Interestingly, transcripts for *Has2*, *Has3* and pro-fibrotic cell surface HA receptor, *Cd44* were upregulated in *Brca1* deficient MOFs (**Figure 30**), suggesting increased production of HA. Moreover, due to its ability to interact with and trap water molecules, excessive accumulation of HA is accompanied by edema that contributes to tissue stiffness and frequently impairs organ function[242,275]. It may therefore be speculated that the accumulation of HA and possible pro-fibrotic signalling through CD44, *Brca1* deficient MOFs may contribute to increased stiffness of the ovarian ECM.

HA is known to bind to and interact with hyalectans, a family of large chondroitin sulfate proteoglycans, such as versican (encoded by *Vcan*) and aggrecan (encoded by *Acan*) through hyaluronan and proteoglycan link proteins (HAPLN) to form large stable aggregates in the ECM[256,276,277]. According to the human protein atlas, while versican is universally expressed in most tissues, including ovaries, aggrecan is exclusively expressed in the brain and in soft connective tissues, particularly cartilage, but not in ovaries. The interaction between aggrecan and HA mediated by HAPLN proteins is crucial in maintain cell-ECM interactions, with overexpression of aggrecan and HAPLN by NIH3T3 fibroblasts yielding destabilized cell-ECM interactions, likely due to restricted motility imparted by aggrecans[276,278]. As is the case with HA, high concentration of aggrecans in the ECM can draw water into tissues, causing edema, which, as previously mentioned is a driver of ECM stiffness and impaired organ function. While aggrecan

can interact with various collagen fibrils, aggrecan/collagen II interaction, unique to cartilage, produces a network that is especially stiff, dense, resistant to deformation and equips cartilage with its characteristic viscosity and mechanical properties, allowing it to behave as a stiff elastic polymer[276,279]. Consistent with increased expression of cartilage specific fibrillar collagens II and XI, we observed significant upregulation of *Acan* & *Hapln1*, but downregulated expression of *Vcan* by *Brca1* deficient MOFs (**Figure 30**). It can therefore be speculated that the formation of stiff cartilage specific supramolecular structures, such as Collagen II/XI fibrils, aggrecan/Collagen II networks, and HA-Hapln1-Aggrecan aggregates within the ovarian ECM may impair proper ovarian function due to increased stiffness and rigidity of the ovarian matrix. Decreased expression of aggrecanase-1 encoding gene, *Adamts4* is likely to facilitate the deposition of aggrecan aggregates, which contribute to increased stiffness of the ECM. Additionally, we observed significantly increased expression of *Fbn1* and *Eln*, which encode for fibrillin and elastin monomers that polymerize to form the backbone and core of elastic fibers, respectively. While elastic fibers confer tissues with recoil ability and flexibility, active synthesis and accumulation of elastic fibers has been shown to increase stiffness and is associated with fibrosis[248,249]. Specifically, in human models of idiopathic pulmonary fibrosis, increased proportions of elastic fibers negatively correlated with lung function due to increased stiffness[248].

It can therefore be speculated that through enhanced expression of fibrillar collagens, glycoproteins (HA and Aggrecan), impaired organizational units (reduced decorin), and enhanced cross-linking of matrix proteins (Tgm2 & Loxl4), the accumulation of myofibroblastic senescent *Brca1* deficient MOFs in the ovary may prime the onset of ovarian fibrosis through increased stiffness of the ovarian extracellular matrix[242].

4.4.2 Immunomodulatory elements associated with activation of Type II immunity may facilitate fibrotic remodelling of the ECM.

The expression of mildly inflammatory chemokines and cytokines, such as *Cxcl13*, *Csf-1*, *Il-25*, *Il-13α2*, *Tnfsf10*, as well as various death, *Tnfrsf21*, and decoy death receptors, *Tnfrsf11b*, *Tnfrsf22* and *Tnfrsf23* was found to significantly increase with the loss of *Brca1* in MOFs (**Figure 31**).

Brca1 KO MOFs also upregulated the expression of a unique member of the IL-17 family of cytokines, *Il-25* (**Figure 31**). IL-25 is an initiator of type-II immune response that facilitates wound healing and tissue repair through resolution of inflammation and dampens adaptive immune responses[193–195]. Binding of IL25 to its heterodimeric receptor, composed of IL-17RA and IL-17RB, drives the differentiation of T-helper (Th) cells, innate lymphoid cells (ILC) into Th2 cells and type 2 ILC, respectively, to induce the production of characteristic type-II cytokines- IL-4, IL-5, IL-9, IL-13, IL-25, and IL-33, that elicit anti-inflammatory effects associated with type II immunity[280–282]. Persistent activation of type II immune response, however, has been documented to drive pathological fibrosis and tumor progression[283–286]. Il-4, Il-5 and I-13 secreted by Th2 cells and type 2 ILC induce eosinophil proliferation and activation to yield in eosinophilic inflammation that has been associated with fibrotic remodelling of tissues[287–289]. Additionally, Il-25 may also act directly on eosinophils to promote Th2 differentiation through the activation of their secondary antigen presenting function[290]. While Il-4 and Il-13 function to suppress inflammation, they have been identified as potent mediators of fibrosis. Il-13 has been observed to promote fibrosis through activation of TGF-β signalling in fibroblasts and through TGF-β independent mechanisms that are yet to be characterized[291–293]. Fibrotic activity of Il-13 is regulated by the relative expression of Il-13rα1, the signalling receptor that promotes fibrosis and Il-13rα2, the decoy receptor that is

believed to ameliorate fibrosis. Activation of type II immune response and development of hepatic fibrosis resulted in the expression of Il-13rα2, that was absent prior to the onset of fibrosis. Interestingly, mice deficient of Il-13rα2 showed exacerbated fibrosis as compared to Il-13rα2 expressing mice, suggesting that onset the onset of Il-13 induced fibrosis triggers the expression of Il-13rα2, which in turn functions to limit the progression of fibrosis[294]. Similarly, it is possible that increased expression of *Il-13rα2* by *Brca1* deficient MOFs (**Figure 31**) may be indicative of active fibrotic signalling and may prevent exacerbation of fibrosis by limiting fibrotic tendencies of Il-13. Moreover, Il-4 and Il-13 also promote alternate (M2a) activation of resident macrophages that are mediators of type II inflammation and are characterized by increased expression of antigen presenting machinery, co-inhibitory molecules and anti-inflammatory cytokines[295–297]. It can therefore be speculated that persistent production of IL-25 may result in activation of type II immune responses that have been implicated in the development of organ fibrosis through activation of eosinophils and M2a macrophage polarization, the latter of which may also be primed by Csf1[298], a growth factor encoded by the gene *Csf1* upregulated by *Brca1* KO MOFs (**Figure 31**).

4.5 Accumulation of *Brca1* deficient ovarian fibroblasts may confer increased risk for the onset of cancer through accelerated development of an immunosuppressive pre-metastatic niche.

Tissue fibrosis that naturally accompanies aging has been observed to enhance the metastatic potential of tissues. The association between fibrosis and cancer risk is well established. The presence of pathological fibrosis in lungs and liver has been positively correlated to increased arrival and growth of disseminated cancer cells in fibrotic niches due to lysyl oxidase mediated cross-linking of collagens[79,299]. Given that the risk of cancer increases with age and that age-

associated fibrotic remodelling has been linked to increased risk for cancer, it is unsurprising that the ECM associated with a potent premetastatic niche shares substantial resemblance to fibrosis[300]. Dense anisotropic fibers of the matrix, such as those characteristic of fibrotic niches, provide migratory tracks for cancer cells, thereby promoting invasion and colonization[75]. Due to the commonalities between fibrotic and pre-metastatic matrices, it can be suggested that the presence of pathological fibrosis may facilitate metastatic invasion through the formation of a pre-metastatic niche. The pre-metastatic ECM is characterized by increased rigidity and stiffness due to extensive deposition of structural proteins, proteoglycans, enhanced expression and activity of cross-linking and remodelling enzymes, such as lysyl oxidases and MMPs, that are produced by resident /myofibroblasts[301]. It is as such rich in anisotropic, highly cross-linked collagens, HA, its cell surface receptor CD44, and numerous CAMs that interact with cancer cells to facilitate invasion.

Our findings collectively suggest that the loss of *Brca1* may trigger reprogramming of ovarian fibroblasts into a unique subtype of senescent CAFs with myofibroblastic and antigen presenting activity and employ mechanisms to resist apoptosis and evade immune clearance, resulting in the accumulation of myofibroblastic senescent *Brca1* deficient MOFs, that may facilitate the formation of a pre-metastatic niche, a pathogenic microenvironment characterized by fibrotic remodelling of the matrix, and immunosuppressive reprogramming of stromal cells to support metastatic progression of malignancies (**Figure 35**). Marked increase in risk for cancer beyond middle age may as such be attributed to the accumulation of senescent cells in tissues[302–304].

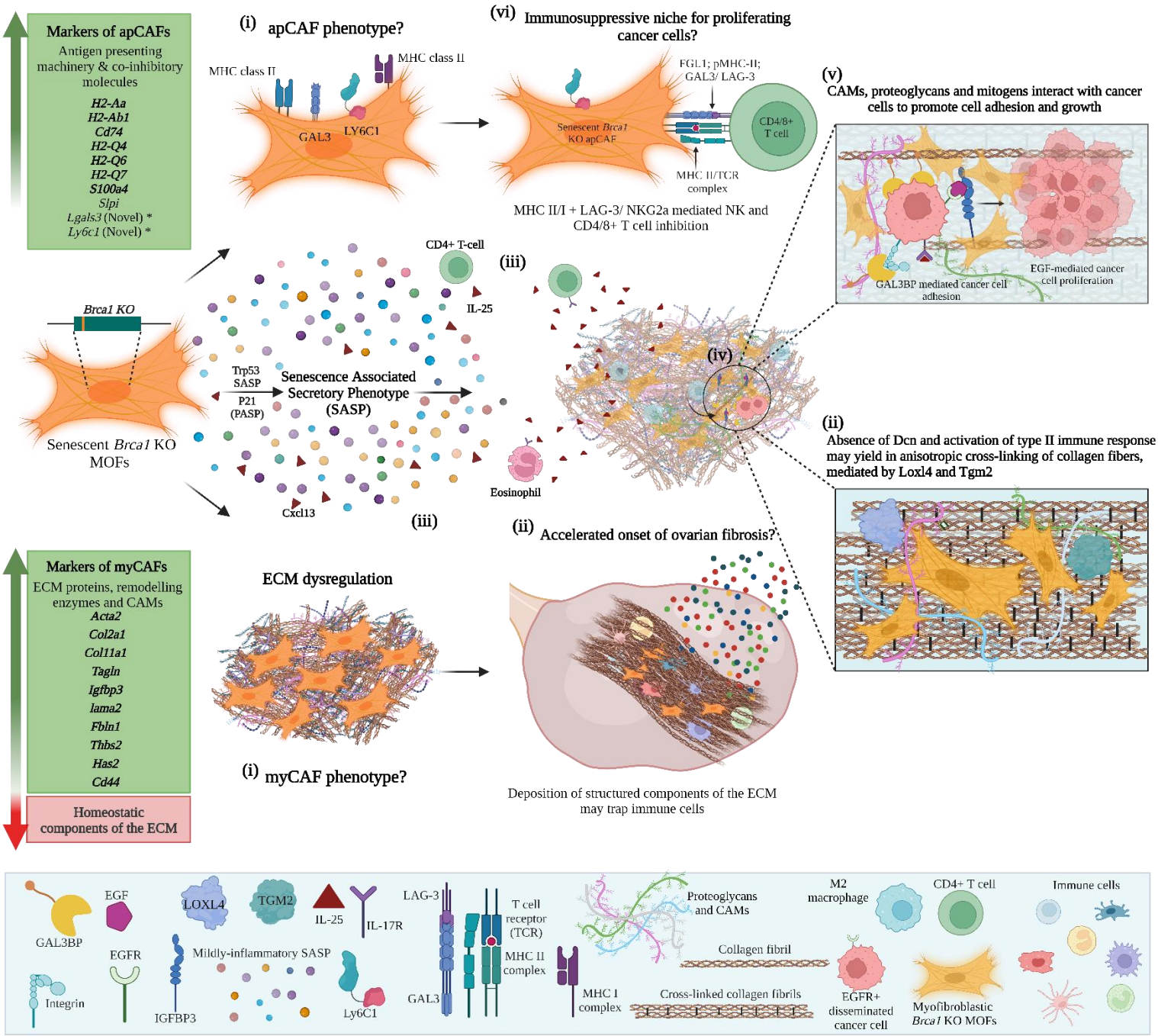

Figure 35: Accumulation of Brca1 KO MOFs facilitate metastatic invasion and colonization. *Brca1 KO MOFs that resist apoptotic clearance develop a senescence-like morphology that is accompanied by* ***(i)*** *myofibroblastic and antigen presenting CAF phenotype, the former of which* ***(ii)*** *increases the deposition of GAG-Aggrecan and HA that increase water retention, as well as structural proteins (collagens and elastin) that collectively result in increased stiffness and*

dysregulation of the ovarian ECM, thereby contributing to the pre-mature development of ovarian fibrosis, which may in turn negatively impact ovarian function; ***(iii)*** *SASP of Brca1 KO MOFs is composed of potent chemokines, namely IL-25, among others such as S100a2, S100a4 and CXCL13, all of which have been documented to recruit a variety of immune cells including eosinophils, B and T lymphocytes; IL-25 can prime Th2 activation of CD4+ T-cells and macrophages, which in turn is known to drive tissue fibrosis; Upregulation of CAM, mitogens, along with fibrosis-like ovarian ECM collectively facilitates metastatic invasion* ***(iv)*** *through enhanced migration and adhesion of infiltrating cancer cells,* ***(v)*** *while growth factor binding proteins that retain mitogenic molecules like EGF in the ECM likely induce proliferation of infiltrating cancer cells. This is further supported by* ***(vi)*** *apCAF-like immunosuppressive activity of MOFs that is through the upregulation of antigen presenting machinery, and co-inhibitory molecules such as H2-Q, Gal3, Fgl1, pMHC-II, CD80 and CD276 that render CD4+, CD8+ T and NK cells functionally exhausted. Collectively, this creates a microenvironment permissive of cancer by limiting anti-tumor activity.*

4.6 The accumulation of senescent *Brca1* deficient ovarian myofibroblasts may accelerate ovarian aging.

Mechanical properties of tissues, such as stiffness and elasticity have evolved to support organ function. For example, the dense and non-elastic nature of the ECM of bones allows them to provide structural support and weight bearing ability, while the dense, yet elastic nature of cartilage ECM allows them to resist compressive forces and provide flexibility to joints. Ovarian function, defined as repetitive folliculogenesis and atresia, ovulation, formation, and regression of the CL, is largely compartmentalized to medulla and is heavily dependent on the loose organization of the medullar ECM that must undergo robust and dynamic changes throughout the ovarian cycle to facilitate intracellular communication required for proper ovarian function[305,306]. Such reliance of organ function on the structure of the ECM is best exemplified by vastly different organization and arrangement of medullar and cortical ECM. Quiescent primordial follicles reside in the ovarian

cortex, which is a region of functional dormancy, and is characterized by a tightly packed, stiff ECM, which in turn maintains the quiescent nature of primordial follicles[306]. Increased stiffness of the ECM promotes quiescence of primordial follicles and impaired follicular development and growth, while enzymatic loosening of the ovarian ECM triggers the activation of follicular development. Methods that physically loosen tissues are used in clinical settings to relieve inhibited follicular growth in women with POI and PCOS, thereby highlighting the importance of ECM structure, organization and stiffness on ovarian function[307,308]. It is therefore unsurprising that tissue fibrosis, characterized by increased stiffness and reduced elasticity of the ECM, can have detrimental effects on tissue function and may contribute to aging. As previously mentioned, gene expression associated with SASP and myofibroblastic phenotype of *Brca1* deficient MOFs is likely to result in increased stiffness and dysregulated organization of the ovarian extracellular matrix[309], possibility impairing ovarian function[63].

Stromal fibroblasts dynamically remodel the ECM to accommodate growing follicles, permit ovulation and mediate ovulatory wound healing. As such, stromal fibroblasts are indispensable for proper ovarian function. Inflammatory post-ovulatory conditions prime the activation of myofibroblasts that undergo proliferation and produce a matrix to promote wound healing of the OSE. Formation of the progesterone secreting corpus luteum (CL) from remnants of the ovulatory follicle requires rapid remodelling, growth and differentiation[310] that is largely mediated by stromal fibroblasts, that undergo rapid proliferative expansion as the CL continues to grow during the ovine estrous cycle[311]. Given the heavy involvement of stromal fibroblasts in mediating proper ovarian function, the accumulation of myofibroblastic senescent *Brca1* KO ovarian fibroblasts in the ovary may lead to increased stiffness of the ovarian ECM and impede all

aspects of ovarian function requiring proliferative stromal fibroblasts, leading to pre-maturely diminished ovarian function, and thereby contributing to accelerated ovarian aging.

4.7 Functionality of the gene expression profile of *Brca1* KO MOFs mirrors characteristics of ovarian aging.

In healthy tissue, the onset of cellular senescence counteracts cancer and aging to reinforce tissue homeostasis. However, under conditions of perpetual damage and reduced repair (aging), the onset of cellular senescence has robust pro-aging outcomes at the tissue level through the induction of excessive inflammation, reduced tissue function and exhaustion of stem cells, and is regarded as a driver of organismal aging[201,312,313]. The gene expression profile of *Brca1* KO MOFs indicates impaired DNA damage repair (**Figure 20B, C**), which is a primary hallmark of aging. Consistently, we observed decreased expression of *Rad51c*, a protein essential for DNA damage repair that confers high risk for breast and ovarian cancers with loss-of-function mutations. Impaired DNA damage repair is a potent inducer of inflammation, compromises the integrity of the genome, likely triggering the onset of senescence[87]. As such, it can be speculated that loss of *Brca1* in MOFs may mimic characteristics of cellular aging, ultimately leading to p53 and p16 induced cellular senescence (**Figure 36**). While the activation of p53 and p16 confers protection from potentially malignant transformation of genetically compromised cells, the accumulation of senescent cells in tissue has been positively correlated to physiological aging[87].

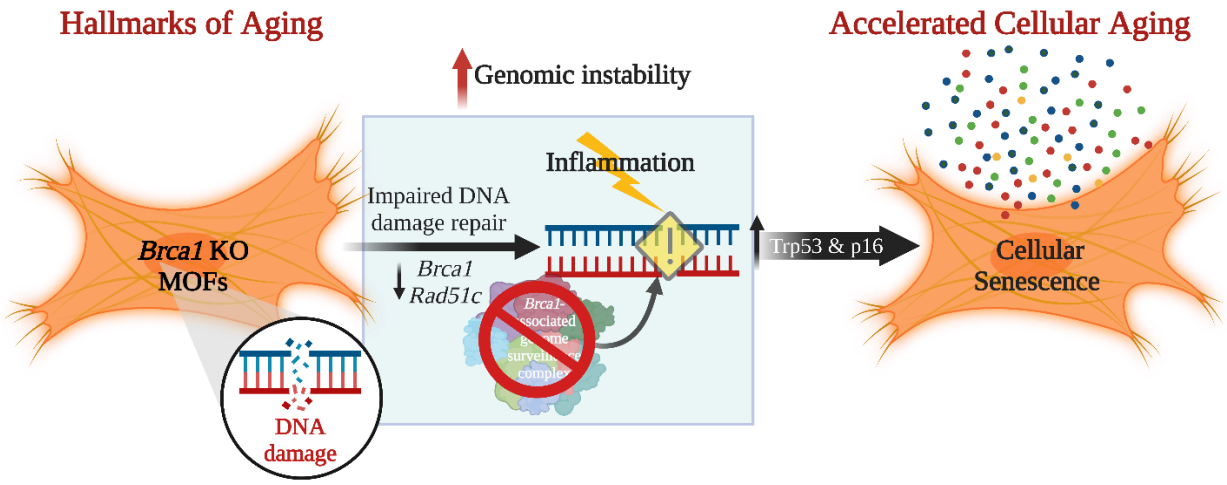

Figure 36: Loss of Brca1 likely mimics cellular aging through the induction of hallmarks of aging. *Loss of Brca1 appears to impair DNA repair, resulting in accumulation of damaged DNA, which is a hallmark of cellular aging, and a known triggers for the onset of cellular senescence through the activation of p53 and p16 pathways. The loss of Brca1 and onset of cellular senescence in ovarian fibroblasts may consequently facilitate pre-mature ovarian aging.*

The accumulation of senescent cells and presentation of progeroid syndromes in mutant mice with extensive and persistant DNA damage was ameliorated by the elimination of Trp53 or p16[169,314,315]. These findings highlight the role of p53 and p16 mediated onset of senescence in aging. The levels of p16 have been positively correlated to ovarian aging, with p16 positive cells being localized to the stroma in aged murine ovaries[316]. Additionally, the levels of insulin-like growth factor binding protein 3 (IGFBP3) were found to be increased in the plasma of aged rats and have been directly associated with cellular aging and senescence in vitro[317]. We observed a 3.5-fold increase in expression of the p16 encoding gene *Cdkn2a* and a 4.5-fold increase in *Igfbp3* expression in *Brca1* KO MOFs as compared to *Brca1* wt MOFs, suggesting that *Brca1* deficiency in MOFs may mimic a state reflective of physiological aging.

The ovarian stroma is composed of various components, such as blood and lymphatic vessels, nerves, and immune cells as well as the OSE, ECM, and tissue-resident fibroblasts[51]. The ovarian immune population consists of a variety of cells, namely eosinophils, macrophages, B and T lymphocytes, NK cells, dendritic cells, neutrophils and mast cells, with macrophages being the predominant immune cell type within the ovary. Both tissue-resident fibroblasts and macrophages are responsible for the dynamic reorganization of the ECM, as well as for priming and mediating inflammatory and wound healing responses to facilitate folliculogenesis, ovulation and reproductive homeostasis[51,318]. Cross-talk among stromal fibroblasts and macrophages can alter the activity of the other and is essential for maintaining tissue homeostasis. While both classically activated inflammatory M1 macrophages and alternatively activated tissue remodelling M2 macrophages are normally present in the ovary, aging murine ovaries were found to have increased proportions of M2 macrophages[62,319]. The polarization and infiltration of M2 macrophages in murine models of lung and kidney disease lead to the accumulation of α-SMA positive cells and promote tissue fibrosis[320,321]. While a variety of stimuli promote M2 polarization, one stimulus is CSF-1 (encoded by *Csf1*), a growth factor that primarily regulates differentiation, proliferation and survival of macrophages and may be produced by both immune and non-immune cells[298]. We report a 3-fold increase in the mRNA expression of *Csf1* in *Brca1* KO MOFs, as compared to *Brca1* wt (AdEmpty) MOFs (**Figure 31**), suggesting a possible means by which fibroblasts may facilitate organ aging in a paracrine manner. It can therefore be speculated that fibroblast derived CSF-1 may act on macrophages to promote the activation of pro-fibrotic M2 macrophages that are found in increased proportions in the aging ovary. This is supported by the finding that fibroblast-macrophage interaction via the CSF-1/CSF-1r axis has been implicated with onset of lung fibrosis[322]. Additionally, M2 macrophages can promote myofibroblast differentiation, leading to

excessive deposition of ECM proteins, which then act to provide survival signals in macrophages, thereby creating a positive feedback loop, eventually resulting in tissue fibrosis[323].

Currently, the fibrotic nature and inflammatory microenvironment of the aged murine ovary are yet to be linked to the accumulation of senescent cells. Age-associated lung fibrosis has been linked to the accumulation of senescent cells and production of SASP[324], so the identification of SASP fibroblasts in aged murine ovaries may potentially bridge this gap[61]. *Brca1* KO MOFs were found to increase the expression of components of SASP, such as chemoattractants, interleukins and immunomodulatory cell surface receptors and upregulate genes encodings for CAMs, ECM proteins, as well as remodelling and cross-linking enzymes, suggesting that the onset of senescence in *Brca1* deficient MOFs is accompanied by the production of SASP and may yield in dysregulation of the matrix, which is believed to drive the progression of fibrosis. This highlights the striking resemblance of *Brca1* deficiency in ovarian fibroblasts to characteristics observed in aged ovaries.

For most organs, tissue stiffness increases with age due to the accumulation of fibrosis[309]. Activated myofibroblasts that are responsible for mediating tissue repair are characterized by increased expression of α-SMA and various ECM proteins such as fibrillar collagen, fibronectin, and elastin, which are the primary culprits for the onset of fibrosis. Specifically, the accumulation of senescent myofibroblasts is believed to drive the progression of lung fibrosis and were found to be prevalent in age-related fibrotic conditions[325].This is consistent with the presence of $p16^+$ cells in the stroma, and SASP- and $\alpha\text{-SMA}^+$- fibroblast populations in the fibrotic murine aging ovary[61,62,316].

Parallels observed between the functionality of the gene expression prolife of *Brca1* deficient ovarian fibroblasts and characteristics of ovarian aging collectively suggest the

possibility that *Brca1* deficiency in MOFs mimics a cellular state that mirrors aging conditions and may thereby contribute to accelerated ovarian aging, likely through the onset of senescence, its associated inflammatory secretome, myofibroblast activation, matrix dysregulation and paracrine priming of pro-fibrotic M2 macrophage, likely resulting in the accelerated onset of ovarian fibrosis (**Figure 37**).

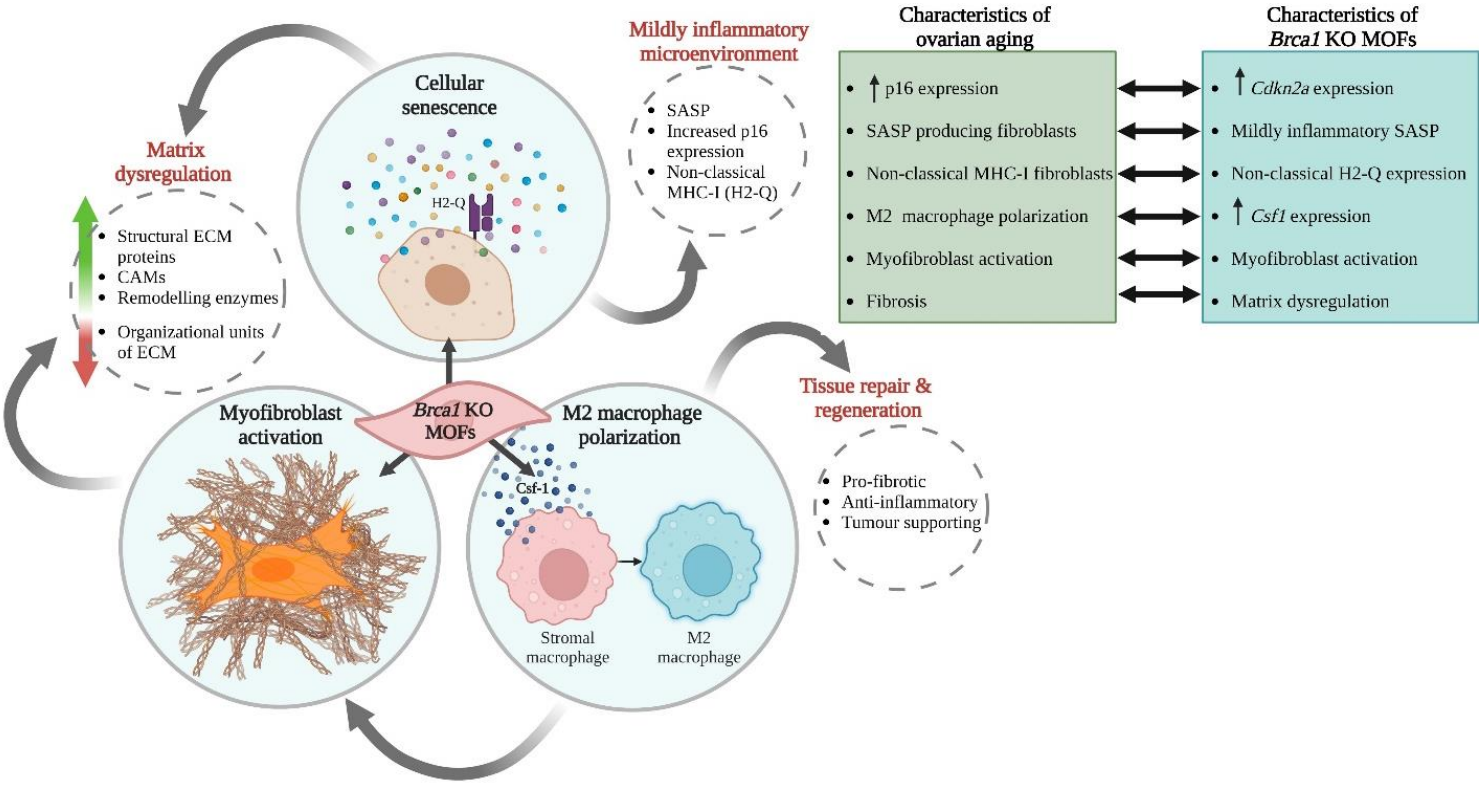

Figure 37: Brca1 KO MOFs have a transcriptome that reflects a cellular state of similar to that observed in aging ovaries. *Similarities among gene expression profile of MOFs and aspects of aging ovaries include: Myofibroblast activation (responsible for production of ECM) as well as induction of cellular senescence that is associated with increased expression of p16, non-classical MHC components, as well as SASP, enriched in cytokines such as CSF-1, that may act on ovarian macrophages to promote alternative M2 activation, predominantly observed in the aging ovary.*

4.8 Limitations

The results of this study provide a fundamental understanding of mechanisms through which *Brca1* KO MOFs may contribute to the development of a pre-metastatic niche, which in turn increases the risk for OC. While experimental conditions were optimized to stimulate a native tissue environment as best as possible, in vitro experiments are unable to account for the complex multifactorial nature of physiological phenomena. As such, the findings and conclusions drawn from these in-vitro experiments represent a singular aspect that may contribute to a complex physiological outcome, namely the accelerated development of an age-associated pre-metastatic microenvironment in the ovaries of *BRCA1* mutation carriers. The majority of the experiments in this study have assessed mRNA expression (qPCR and RNA-seq), as such all interpretations and speculations have been drawn with the assumption that altered transcription results in altered protein expression. Any discrepancies between transcription and translation are limiting factors of this study.

4.9 Future directions: Confirming the role of *Brca1* deficient ovarian stromal fibroblasts in accelerating ovarian aging, fibrosis, and cancer risk.

Given the in-vitro nature and transcriptomic reliance of our study, it is pertinent to assess the relevance of our findings at a proteomic level. As such, while we have confirmed reduced mRNA expression of *Brca1* using qPCR/RNA-seq, the lack of BRCA1 protein and, consequently, BRCA1 activity would truly confirm loss of *Brca1* in MOFs. Our data suggest that *Brca1* KO induced accumulation of DNA damage activates stress-response pathways involving p53, p16 and p21, which ultimately result in the onset of senescence, and its associated secretory phenotype. As such, we plan on confirming the onset of cellular senescence through detection of markers of senescence, namely p16 and p21, and K320-Ac of p53 using SDS-PAGE and immunoblotting. Additionally,

senescence associated-growth arrest of *Brca1* deficient MOFs could be assessed using the BrdU cell proliferation assay. In combination with positive staining for acidic SA-β-galactosidase activity, detection of p16, p21, K320-Ac p53 and inhibited cell proliferation of *Brca1* deficient MOFs would confirm the onset of cellular senescence. Given that *Brca1* deficient fibroblasts appear to facilitate premature ovarian aging and establishment of a (pre)metastatic niche through their SASP, it will therefore be necessary to characterize the nature and functionality of SASP. This can be achieved with a targeted cytokine array/ELISA to confirm the secretion of Il-25, Cxcl13, Egf, Fgf, Gal3, Gal1, Fgl1, Csf-1, S100a4 and HA, all of which are components that contribute towards the establishment of a (pre)metastatic niche. Given that ovarian fibrosis physiologically accompanies ovarian aging and that fibroblasts are the primary cell type responsible for the synthesis and degradation of the ECM, it will be important to explore the contribution of *Brca1* KO ovarian fibroblasts to accelerating ovarian fibrosis using immunofluorescence to visualize the deposition of structural matrix proteins such as collagens 2/11 and matricellular proteins such as IGFBP3. As previously mentioned, organ fibrosis has been positively correlated with increased risk of cancer; as such, increased deposition and ordered arrangement of the surrounding matrix (examined in vitro using immunofluorescence) by *Brca1* deficient MOFs would potentially provide insight into enhanced risk for OC in *Brca1* mutation carriers. As such, a Transwell matrigel invasion assay could be used to assess whether colorectal and breast cancer cell lines (most common non-gynaecological metastases to the ovary) are attracted to *Brca1* deficient MOFs. In a separate experiment, treating these cancer cell lines with conditioned media from *Brca1* KO MOFs could assess the proliferative effects of their SASP. Extensive literature evidence suggests that not only do senescent mesenchymal cells facilitate metastatic invasion of cancer cells by creating a cancer favouring niche, but the interaction of

senescent fibroblasts with genetically compromised epithelial cells promotes transformation and growth of these epithelial cells[102,238,239,326–328]. To study the contribution of *Brca1* deficient MOFs in promoting transformation of genetically compromised epithelial cells, we propose to co-culture *Brca1* MOFs with *Brca1* deficient murine OSE cells (mOSE cells). Should senescent *Brca1* deficient MOFs successfully promote invasion, stimulate proliferation of cancer cells, as well as facilitate malignant transformation of the mOSE cells, this would suggest a potential mechanism to explain early onset of ovarian cancer in *Brca1* mutation carriers. Last but not least, flow cytometry could be used to detect surface expression of components of MHC-I/II to provide insight into the potential mechanisms by which *Brca1* deficient MOFs may confer immunosuppression.

Conclusion

We had originally hypothesized that the loss of *Brca1* in MOFs may accelerate the onset of ovarian fibrosis and consequently accelerate ovarian aging through myofibroblast hyperactivation. Using primary murine ovarian fibroblasts as a model system to study the effects of *Brca1* deficiency, we discovered that the sudden loss of *Brca1* in MOFs immediately induced cell death via apoptosis. However, MOFs surviving the loss of *Brca1* adopted a flat morphology and were identified to be senescent. The gene expression profile of these cells was found to align with that of myofibroblasts, thereby confirming our hypothesis that the loss of *Brca1* renders ovarian fibroblasts hyperactive. We speculate the onset of senescence to be attributed to the expression of the cyclin-CDK inhibitors, p16 and p21 in response to accumulation of damaged DNA due to impaired dsDNA repair pathways. Using RNA-sequencing, the gene expression prolife of *Brca1* KO ovarian myofibroblasts were found to mimic characteristics of aged ovarian fibroblasts (increased expression of p16 and non-classical MHC-I), as well as matrix producing myofibroblasts (increased expression of collagens and matrix remodelling enzymes. Additionally, the gene expression profile of these *Brca1* deficient MOFs may function to prime characteristics of premature ovarian aging in vivo. Collectively, we speculate that the loss of *Brca1* in ovarian fibroblasts mimics characteristics of cellular aging and may facilitate premature ovarian aging through diminished proliferation and increased stiffness of the ovarian ECM, that not only hampers ovarian function but may render the ovary an appealing niche for metastatic cancer cells. In support of this, *Brca1* KO MOFs were found to upregulate components that support different aspects of metastatic invasion, including chemokines, cell adhesion molecules (integrins, galectins, CAMs), mitogens (EGF, FGF), and inhibitory antigen presenting machinery (MHC-I/II, GAL3, GAL9,

CD80, CD276), that collectively facilitate the recruitment, adhesion, and proliferation of metastatic cancer cells, and enhance tumorigenesis through reduced adaptive immune activity.

References

1. Lee, S. Ovarian cancer statistics. *Canadian Cancer Society* https://cancer.ca/en/cancer-information/cancer-types/ovarian/statistics.
2. Survival statistics for ovarian cancer - Canadian Cancer Society. *www.cancer.ca* https://www.cancer.ca:443/en/cancer-information/cancer-type/ovarian/prognosis-and-survival/survival-statistics/?region=on.
3. Ovarian Cancer Risk Factors - Ovarian Cancer Research Alliance. *OCRA* https://ocrahope.org/patients/about-ovarian-cancer/risk-factors/.
4. Lee, S. Survival statistics for ovarian cancer. *Canadian Cancer Society* https://cancer.ca/en/cancer-information/cancer-types/ovarian/prognosis-and-survival/survival-statistics.
5. Kim, J. *et al.* Cell Origins of High-Grade Serous Ovarian Cancer. *Cancers (Basel)* **10**, 433 (2018).
6. Karnezis, A. N. *et al.* The disparate origins of ovarian cancers: pathogenesis and prevention strategies. *Nature Reviews Cancer* **17**, 65–74 (2017).
7. Parkinson, C. A., Hatcher, H. M. & Ajithkumar, T. V. Management of malignant ovarian germ cell tumors. *Obstet Gynecol Surv* **66**, 507–514 (2011).
8. Boussios, S. *et al.* Non-epithelial Ovarian Cancer: Elucidating Uncommon Gynaecological Malignancies. *Anticancer Res* **36**, 5031–5042 (2016).
9. What is high grade serous carcinoma? *OCRA* https://ocrahope.org/2021/07/high-grade-serous-carcinoma/ (2021).
10. Cronin, K. A. *et al.* Annual Report to the Nation on the Status of Cancer, part I: National cancer statistics: Annual Report National Cancer Statistics. *Cancer* **124**, 2785–2800 (2018).
11. Koshiyama, M., Matsumura, N. & Konishi, I. Recent Concepts of Ovarian Carcinogenesis: Type I and Type II. *Biomed Res Int* **2014**, 934261 (2014).
12. Hirst, J. *et al.* Ovarian Cancer Genetics: Subtypes and Risk Factors. in *Ovarian Cancer - From Pathogenesis to Treatment* (IntechOpen, 2018). doi:10.5772/intechopen.72705.

13. Gibson, E. & Mahdy, H. Anatomy, Abdomen and Pelvis, Ovary. in *StatPearls* (StatPearls Publishing, 2022).
14. Fathalla, M. F. INCESSANT OVULATION—A FACTOR IN OVARIAN NEOPLASIA ? *The Lancet* **298**, 163 (1971).
15. Crum, C. P., McKeon, F. D. & Xian, W. BRCA, the Oviduct, and the Space and Time Continuum of Pelvic Serous Carcinogenesis. *International Journal of Gynecologic Cancer* **22**, (2012).
16. Dubeau, L. & Drapkin, R. Coming into focus: the nonovarian origins of ovarian cancer. *Ann Oncol* **24**, viii28–viii35 (2013).
17. Kurman, R. J. & Shih, I.-M. Molecular Pathogenesis and Extraovarian Origin of Epithelial Ovarian Cancer. Shifting the Paradigm. *Hum Pathol* **42**, 918–931 (2011).
18. Ducie, J. *et al.* Molecular analysis of high-grade serous ovarian carcinoma with and without associated serous tubal intra-epithelial carcinoma. *Nat Commun* **8**, 990 (2017).
19. Pearce, C. L. *et al.* Association between endometriosis and risk of histological subtypes of ovarian cancer: a pooled analysis of case–control studies. *Lancet Oncol* **13**, 385–394 (2012).
20. Doğanay, M. *et al.* Krukenberg carcinoma metastasized from stomach resembling mucinous cystadenocarcinoma of the ovary. *J Exp Ther Oncol* **11**, 23–26 (2015).
21. de Waal, Y. R. P., Thomas, C. M. G., Oei, A. L. M., Sweep, F. C. G. J. & Massuger, L. F. A. G. Secondary ovarian malignancies: frequency, origin, and characteristics. *Int J Gynecol Cancer* **19**, 1160–1165 (2009).
22. Yada-Hashimoto, N. *et al.* Metastatic ovarian tumors: a review of 64 cases. *Gynecol Oncol* **89**, 314–317 (2003).
23. Zhang, J.-J., Cao, D.-Y., Yang, J.-X. & Shen, K. Ovarian metastasis from nongynecologic primary sites: a retrospective analysis of 177 cases and 13-year experience. *J Ovarian Res* **13**, 128 (2020).
24. Whittemore, A. S. Characteristics relating to ovarian cancer risk: implications for prevention and detection. *Gynecol Oncol* **55**, S15-19 (1994).

25. So, W.-K., Cheng, J.-C., Poon, S.-L. & Leung, P. C. K. Gonadotropin-releasing hormone and ovarian cancer: a functional and mechanistic overview. *The FEBS Journal* **275**, 5496–5511 (2008).
26. Ovarian Cancer Statistics. *OCRA* https://ocrahope.org/patients/about-ovarian-cancer/statistics/.
27. Ovarian Cancer Signs & Symptoms. *OCRA* https://ocrahope.org/patients/about-ovarian-cancer/.
28. Moyer, V. A. Screening for Ovarian Cancer: U.S. Preventive Services Task Force Reaffirmation Recommendation Statement. *Ann Intern Med* **157**, 900–904 (2012).
29. Sölétormos, G. *et al.* Clinical Use of Cancer Biomarkers in Epithelial Ovarian Cancer. *Int J Gynecol Cancer* **26**, 43–51 (2016).
30. Patni, R. Screening for Ovarian Cancer: An Update. *J Midlife Health* **10**, 3–5 (2019).
31. Gupta, D. & Lis, C. G. Role of CA125 in predicting ovarian cancer survival - a review of the epidemiological literature. *Journal of Ovarian Research* **2**, 13 (2009).
32. Daoud, E. & Bodor, G. CA-125 concentrations in malignant and nonmalignant disease. *Clin Chem* **37**, 1968–1974 (1991).
33. Buamah, P. K. & Skillen, A. W. Serum CA 125 concentrations in patients with benign ovarian tumours. *J Surg Oncol* **56**, 71–74 (1994).
34. Jacobs, I. & Bast, R. C. The CA 125 tumour-associated antigen: a review of the literature. *Hum Reprod* **4**, 1–12 (1989).
35. *OVARIAN CANCER SCREENING. Genetic Susceptibility to Breast and Ovarian Cancer: Assessment, Counseling and Testing Guidelines* (American College of Medical Genetics, 1999).
36. Risks and causes of ovarian cancer | Cancer Research UK. https://www.cancerresearchuk.org/about-cancer/ovarian-cancer/risks-causes.
37. Salehi, F., Dunfield, L., Phillips, K. P., Krewski, D. & Vanderhyden, B. C. Risk Factors for Ovarian Cancer: An Overview with Emphasis on Hormonal Factors. *Journal of Toxicology and Environmental Health, Part B* **11**, 301–321 (2008).
38. Purdie, D. M., Bain, C. J., Siskind, V., Webb, P. M. & Green, A. C. Ovulation and risk of epithelial ovarian cancer. *Int. J. Cancer* **104**, 228–232 (2003).

39. Population, N. R. C. (US) C. on. *Contraceptive Benefits and Risks*. *Contraception and Reproduction: Health Consequences for Women and Children in the Developing World* (National Academies Press (US), 1989).

40. Burkman, R., Schlesselman, J. J. & Zieman, M. Safety concerns and health benefits associated with oral contraception. *Am. J. Obstet. Gynecol.* **190**, S5-22 (2004).

41. Bassuk, S. S. & Manson, J. E. Oral contraceptives and menopausal hormone therapy: relative and attributable risks of cardiovascular disease, cancer, and other health outcomes. *Ann Epidemiol* **25**, 193–200 (2015).

42. Wentzensen, N. & de Gonzalez, A. B. The Pill's gestation: from birth control to cancer prevention. *The Lancet Oncology* **16**, 1004–1006 (2015).

43. Holesh, J. E., Bass, A. N. & Lord, M. Physiology, Ovulation. in *StatPearls* (StatPearls Publishing, 2022).

44. Duffy, D. M., Ko, C., Jo, M., Brannstrom, M. & Curry, T. E. Ovulation: Parallels With Inflammatory Processes. *Endocrine Reviews* **40**, 369–416 (2019).

45. Clancy, K. B. H., Baerwald, A. R. & Pierson, R. A. Systemic Inflammation Is Associated with Ovarian Follicular Dynamics during the Human Menstrual Cycle. *PLOS ONE* **8**, e64807 (2013).

46. Park, C. J. *et al.* Progesterone Receptor Serves the Ovary as a Trigger of Ovulation and a Terminator of Inflammation. *Cell Reports* **31**, 107496 (2020).

47. Richards, J. S., Russell, D. L., Ochsner, S. & Espey, L. L. Ovulation: New Dimensions and New Regulators of the Inflammatory-Like Response. *Annu. Rev. Physiol.* **64**, 69–92 (2002).

48. Cox, E. & Takov, V. Embryology, Ovarian Follicle Development. in *StatPearls* (StatPearls Publishing, 2022).

49. Mikhael, S., Punjala-Patel, A. & Gavrilova-Jordan, L. Hypothalamic-Pituitary-Ovarian Axis Disorders Impacting Female Fertility. *Biomedicines* **7**, 5 (2019).

50. 26.6B: Ovarian Cycle. *Medicine LibreTexts* https://med.libretexts.org/Bookshelves/Anatomy_and_Physiology/Book%3A_Anatomy_and_Physi

ology_(Boundless)/26%3A_The_Reproductive_System/26.6%3A_Physiology_of_the_Female_Reproductive_System/26.6B%3A_Ovarian_Cycle (2018).

51. Kinnear, H. M. *et al.* The Ovarian Stroma as a New Frontier. *Reproduction* **160**, R25–R39 (2020).
52. Turner, E. C. *et al.* Conditional ablation of macrophages disrupts ovarian vasculature. *Reproduction* **141**, 821–831 (2011).
53. Care, A. S. *et al.* Macrophages regulate corpus luteum development during embryo implantation in mice. *J Clin Invest* **123**, 3472–3487 (2013).
54. McIntush, E. W. & Smith, M. F. Matrix metalloproteinases and tissue inhibitors of metalloproteinases in ovarian function. *Rev Reprod* **3**, 23–30 (1998).
55. Zhang, Z., Huang, L. & Brayboy, L. Macrophages: an indispensable piece of ovarian health. *Biol Reprod* **104**, 527–538 (2020).
56. Espey, L. L. Ovulation as an Inflammatory Reaction-A Hypothesis. *Biology of Reproduction* 73–106 (1980).
57. Boots, C. E. & Jungheim, E. S. Inflammation and Human Ovarian Follicular Dynamics. *Semin Reprod Med* **33**, 270–275 (2015).
58. Zamah, A. M., Hassis, M. E., Albertolle, M. E. & Williams, K. E. Proteomic analysis of human follicular fluid from fertile women. *Clin Proteomics* **12**, 5 (2015).
59. Tomasek, J. J., Gabbiani, G., Hinz, B., Chaponnier, C. & Brown, R. A. Myofibroblasts and mechano-regulation of connective tissue remodelling. *Nat Rev Mol Cell Biol* **3**, 349–363 (2002).
60. McCloskey, C. W. *et al.* Metformin Abrogates Age-Associated Ovarian Fibrosis. *Clin Cancer Res* **26**, 632–642 (2020).
61. Landry, D. A. *et al.* Metformin prevents age-associated ovarian fibrosis by modulating the immune landscape in female mice. *Sci Adv* **8**, eabq1475 (2022).
62. Briley, S. M. *et al.* Reproductive age-associated fibrosis in the stroma of the mammalian ovary. *Reproduction* **152**, 245–260 (2016).

63. Mara, J. N. *et al.* Ovulation and ovarian wound healing are impaired with advanced reproductive age. *Aging (Albany NY)* **12**, 9686–9713 (2020).

64. White, E. S. & Mantovani, A. R. Inflammation, wound repair, and fibrosis: reassessing the spectrum of tissue injury and resolution. *J Pathol* **229**, 141–144 (2013).

65. Evans, M. C. & Diegelmann, R. F. Wound healing: an overview of acute, fibrotic and delayed healing. *FBL* **9**, 283–289 (2004).

66. Ho, C. Y. *et al.* Myocardial Fibrosis as an Early Manifestation of Hypertrophic Cardiomyopathy. *New England Journal of Medicine* **363**, 552–563 (2010).

67. Alam, A., Chun Suen, K. & Ma, D. Acute-on-chronic liver failure: recent update. *J Biomed Res* **31**, 283–300 (2017).

68. Mannon, R. B. Therapeutic Targets in the Treatment of Allograft Fibrosis. *American Journal of Transplantation* **6**, 867–875 (2006).

69. Wells, R. G. Tissue Mechanics and Fibrosis. *Biochim Biophys Acta* **1832**, 884–890 (2013).

70. Bains, W. Transglutaminse 2 and EGGL, the Protein Cross-Link Formed by Transglutaminse 2, As Therapeutic Targets for Disabilities of Old Age. *Rejuvenation Res* **16**, 495–517 (2013).

71. Amargant, F. *et al.* Ovarian stiffness increases with age in the mammalian ovary and depends on collagen and hyaluronan matrices. *Aging Cell* **19**, e13259 (2020).

72. Sapudom, J. *et al.* The phenotype of cancer cell invasion controlled by fibril diameter and pore size of 3D collagen networks. *Biomaterials* **52**, 367–375 (2015).

73. Ray, A., Slama, Z. M., Morford, R. K., Madden, S. A. & Provenzano, P. P. Enhanced Directional Migration of Cancer Stem Cells in 3D Aligned Collagen Matrices. *Biophys J* **112**, 1023–1036 (2017).

74. Sapudom, J. *et al.* Fibril bending stiffness of 3D collagen matrices instructs spreading and clustering of invasive and non-invasive breast cancer cells. *Biomaterials* **193**, 47–57 (2019).

75. Conklin, M. W. *et al.* Aligned collagen is a prognostic signature for survival in human breast carcinoma. *Am J Pathol* **178**, 1221–1232 (2011).

76. Mantovani, A., Allavena, P., Sica, A. & Balkwill, F. Cancer-related inflammation. *Nature* **454**, 436–444 (2008).

77. Germano, G., Allavena, P. & Mantovani, A. Cytokines as a key component of cancer-related inflammation. *Cytokine* **43**, 374–379 (2008).

78. Colotta, F., Allavena, P., Sica, A., Garlanda, C. & Mantovani, A. Cancer-related inflammation, the seventh hallmark of cancer: links to genetic instability. *Carcinogenesis* **30**, 1073–1081 (2009).

79. Olaso, E. *et al.* Tumor-dependent activation of rodent hepatic stellate cells during experimental melanoma metastasis. *Hepatology* **26**, 634–642 (1997).

80. Cox, T. R. & Erler, J. T. Fibrosis, cancer and the premetastatic niche. *Breast Cancer Management* **3**, 453–455 (2014).

81. Bilimoria, M. M. *et al.* Underlying liver disease, not tumor factors, predicts long-term survival after resection of hepatocellular carcinoma. *Arch Surg* **136**, 528–535 (2001).

82. Rangarajan, S. *et al.* Metformin reverses established lung fibrosis in a bleomycin model. *Nat Med* **24**, 1121–1127 (2018).

83. Shankaraiah, R. C. *et al.* Metformin prevents liver tumourigenesis by attenuating fibrosis in a transgenic mouse model of hepatocellular carcinoma. *Oncogene* **38**, 7035–7045 (2019).

84. Xiao, H. *et al.* Metformin attenuates cardiac fibrosis by inhibiting the TGFbeta1-Smad3 signalling pathway. *Cardiovasc. Res.* **87**, 504–513 (2010).

85. Xu, S. *et al.* Metformin Suppresses Tumor Progression by Inactivating Stromal Fibroblasts in Ovarian Cancer. *Mol Cancer Ther* **17**, 1291–1302 (2018).

86. Tseng, C.-H. Metformin reduces ovarian cancer risk in Taiwanese women with type 2 diabetes mellitus: Metformin and Ovarian Cancer. *Diabetes Metab Res Rev* **31**, 619–626 (2015).

87. López-Otín, C., Blasco, M. A., Partridge, L., Serrano, M. & Kroemer, G. The Hallmarks of Aging. *Cell* **153**, 1194–1217 (2013).

88. Tabula Muris Consortium. A single-cell transcriptomic atlas characterizes ageing tissues in the mouse. *Nature* **583**, 590–595 (2020).

89. McHugh, D. & Gil, J. Senescence and aging: Causes, consequences, and therapeutic avenues. *J Cell Biol* **217**, 65–77 (2018).

90. van der Rijt, S., Molenaars, M., McIntyre, R. L., Janssens, G. E. & Houtkooper, R. H. Integrating the Hallmarks of Aging Throughout the Tree of Life: A Focus on Mitochondrial Dysfunction. *Front Cell Dev Biol* **8**, 594416 (2020).

91. Hernandez-Segura, A., Nehme, J. & Demaria, M. Hallmarks of Cellular Senescence. *Trends in Cell Biology* **28**, 436–453 (2018).

92. Ben-Porath, I. & Weinberg, R. A. The signals and pathways activating cellular senescence. *Int J Biochem Cell Biol* **37**, 961–976 (2005).

93. Kumari, R. & Jat, P. Mechanisms of Cellular Senescence: Cell Cycle Arrest and Senescence Associated Secretory Phenotype. *Frontiers in Cell and Developmental Biology* **9**, (2021).

94. Franceschi, C. & Campisi, J. Chronic inflammation (inflammaging) and its potential contribution to age-associated diseases. *J Gerontol A Biol Sci Med Sci* **69 Suppl 1**, S4-9 (2014).

95. Franceschi, C., Garagnani, P., Parini, P., Giuliani, C. & Santoro, A. Inflammaging: a new immune-metabolic viewpoint for age-related diseases. *Nat Rev Endocrinol* **14**, 576–590 (2018).

96. Xue, W. *et al.* Senescence and tumour clearance is triggered by p53 restoration in murine liver carcinomas. *Nature* **445**, 656–660 (2007).

97. Kang, T.-W. *et al.* Senescence surveillance of pre-malignant hepatocytes limits liver cancer development. *Nature* **479**, 547–551 (2011).

98. Krizhanovsky, V. *et al.* Senescence of activated stellate cells limits liver fibrosis. *Cell* **134**, 657–667 (2008).

99. Atala, A. Re: Tumour-Infiltrating Gr-1+ Myeloid Cells Antagonize Senescence in Cancer. *Journal of Urology* **193**, 2146–2147 (2015).

100. Eggert, T. *et al.* Distinct functions of senescence-associated immune responses in liver tumor surveillance and tumor progression. *Cancer Cell* **30**, 533–547 (2016).

101. Coppé, J.-P. *et al.* Secretion of Vascular Endothelial Growth Factor by Primary Human Fibroblasts at Senescence *. *Journal of Biological Chemistry* **281**, 29568–29574 (2006).

102. Krtolica, A., Parrinello, S., Lockett, S., Desprez, P.-Y. & Campisi, J. Senescent fibroblasts promote epithelial cell growth and tumorigenesis: A link between cancer and aging. *Proc Natl Acad Sci U S A* **98**, 12072–12077 (2001).

103. van Deursen, J. M. The role of senescent cells in ageing. *Nature* **509**, 439–446 (2014).

104. Nikolich-Žugich, J. Ageing and life-long maintenance of T-cell subsets in the face of latent persistent infections. *Nat Rev Immunol* **8**, 512–522 (2008).

105. Camaioni, A. *et al.* The process of ovarian aging: it is not just about oocytes and granulosa cells. *J Assist Reprod Genet* **39**, 783–792 (2022).

106. Li, Q. *et al.* Current understanding of ovarian aging. *Sci. China Life Sci.* **55**, 659–669 (2012).

107. Wu, J. *et al.* Aging conundrum: A perspective for ovarian aging. *Frontiers in Endocrinology* **13**, (2022).

108. Toss, A. *et al.* Hereditary Ovarian Cancer: Not Only BRCA 1 and 2 Genes. *Biomed Res Int* **2015**, 341723 (2015).

109. Ovarian Cancer Risk Factors. https://www.cancer.org/cancer/ovarian-cancer/causes-risks-prevention/risk-factors.html.

110. NAKAMURA, K. *et al.* Features of ovarian cancer in Lynch syndrome (Review). *Mol Clin Oncol* **2**, 909–916 (2014).

111. Pietragalla, A., Arcieri, M., Marchetti, C., Scambia, G. & Fagotti, A. Ovarian cancer predisposition beyond BRCA1 and BRCA2 genes. *Int J Gynecol Cancer* **30**, 1803–1810 (2020).

112. Ahmed, A. A. *et al.* Driver mutations in TP53 are ubiquitous in high grade serous carcinoma of the ovary. *J Pathol* **221**, 49–56 (2010).

113. Sorrell, A. D., Espenschied, C. R., Culver, J. O. & Weitzel, J. N. TP53 Testing and Li-Fraumeni Syndrome: Current Status of Clinical Applications and Future Directions. *Mol Diagn Ther* **17**, 31–47 (2013).

114. Vasen, H. F. *et al.* MSH2 mutation carriers are at higher risk of cancer than MLH1 mutation carriers: a study of hereditary nonpolyposis colorectal cancer families. *J Clin Oncol* **19**, 4074–4080 (2001).

115. Petrucelli, N., Daly, M. B. & Pal, T. BRCA1- and BRCA2-Associated Hereditary Breast and Ovarian Cancer. in *GeneReviews*® (eds. Adam, M. P. et al.) (University of Washington, Seattle, 1993).

116. Matta, B. P. *et al.* Familial history and prevalence of BRCA1, BRCA2 and TP53 pathogenic variants in HBOC Brazilian patients from a public healthcare service. *Sci Rep* **12**, 18629 (2022).

117. Momenimovahed, Z., Tiznobaik, A., Taheri, S. & Salehiniya, H. Ovarian cancer in the world: epidemiology and risk factors. *Int J Womens Health* **11**, 287–299 (2019).

118. Pearce, C. L. *et al.* Population Distribution of Lifetime Risk of Ovarian Cancer in the United States. *Cancer Epidemiol Biomarkers Prev* **24**, 671–676 (2015).

119. Kuchenbaecker, K. B. *et al.* Risks of Breast, Ovarian, and Contralateral Breast Cancer for BRCA1 and BRCA2 Mutation Carriers. *JAMA* **317**, 2402–2416 (2017).

120. Lakhani, S. R. *et al.* Pathology of Ovarian Cancers in BRCA1 and BRCA2 Carriers. *Clin Cancer Res* **10**, 2473–2481 (2004).

121. Ashworth, A. BRCA1/BRCA2. in *Brenner's Encyclopedia of Genetics (Second Edition)* (eds. Maloy, S. & Hughes, K.) 381–383 (Academic Press, 2013). doi:10.1016/B978-0-12-374984-0.00171-6.

122. Deng, C.-X. & Brodie, S. G. Roles of BRCA1 and its interacting proteins. *BioEssays* **22**, 728–737 (2000).

123. Clark, S. L., Rodriguez, A. M., Snyder, R. R., Hankins, G. D. V. & Boehning, D. Structure-Function of the Tumor Suppressor BRCA1. *Comput Struct Biotechnol J* **1**, e201204005 (2012).

124. Chen, Y. *et al.* BRCA1 is a 220-kDa nuclear phosphoprotein that is expressed and phosphorylated in a cell cycle-dependent manner. *Cancer Res* **56**, 3168–3172 (1996).

125. Brca1 - Breast cancer type 1 susceptibility protein homolog - Mus musculus (Mouse) | UniProtKB | UniProt. https://www.uniprot.org/uniprotkb/P48754/entry#structure.

126. Brca1 MGI Mouse Gene Detail - MGI:104537 - breast cancer 1, early onset. https://www.informatics.jax.org/marker/MGI:104537.

127. Sharan, S. K., Wims, M. & Bradley, A. Murine Brca1: sequence and significance for human missense mutations. *Hum Mol Genet* **4**, 2275–2278 (1995).

128. Szabo, C. Human, canine and murine BRCA1 genes: sequence comparison among species. *Human Molecular Genetics* **5**, 1289–1298 (1996).

129. Xu, X. *et al.* Centrosome Amplification and a Defective G2–M Cell Cycle Checkpoint Induce Genetic Instability in BRCA1 Exon 11 Isoform–Deficient Cells. *Molecular Cell* **3**, 389–395 (1999).

130. Wang, Y. *et al.* BASC, a super complex of BRCA1-associated proteins involved in the recognition and repair of aberrant DNA structures. *Genes & Development* **14**, 927 (2000).

131. Simhadri, S. *et al.* Male Fertility Defect Associated with Disrupted BRCA1-PALB2 Interaction in Mice. *J Biol Chem* **289**, 24617–24629 (2014).

132. Sy, S. M. H., Huen, M. S. Y. & Chen, J. PALB2 is an integral component of the BRCA complex required for homologous recombination repair. *Proc Natl Acad Sci U S A* **106**, 7155–7160 (2009).

133. Zhang, F. *et al.* PALB2 Links BRCA1 and BRCA2 in the DNA-Damage Response. *Curr Biol* **19**, 524–529 (2009).

134. Orthwein, A. *et al.* A mechanism for the suppression of homologous recombination in G1 cells. *Nature* **528**, 422–426 (2015).

135. Yarden, R. I., Pardo-Reoyo, S., Sgagias, M., Cowan, K. H. & Brody, L. C. BRCA1 regulates the G2/M checkpoint by activating Chk1 kinase upon DNA damage. *Nat Genet* **30**, 285–289 (2002).

136. Liu, Y. & Lu, L.-Y. BRCA1 and homologous recombination: implications from mouse embryonic development. *Cell & Bioscience* **10**, 49 (2020).

137. Zhao, W. *et al.* BRCA1–BARD1 promotes RAD51-mediated homologous DNA pairing. *Nature* **550**, 360–365 (2017).

138. Moynahan, M. E. & Jasin, M. Mitotic homologous recombination maintains genomic stability and suppresses tumorigenesis. *Nat Rev Mol Cell Biol* **11**, 196–207 (2010).

139. Chapter 12: DNA Damage and Repair – Chemistry. https://wou.edu/chemistry/courses/online-chemistry-textbooks/ch450-and-ch451-biochemistry-defining-life-at-the-molecular-level/chapter-12-dna-damage-repair-and-mutations/.

140. Zhao, X. *et al.* Cell cycle-dependent control of homologous recombination. *Acta Biochim Biophys Sin (Shanghai)* **49**, 655–668 (2017).

141. Guo, T. *et al.* Harnessing accurate non-homologous end joining for efficient precise deletion in CRISPR/Cas9-mediated genome editing. *Genome Biology* **19**, 170 (2018).

142. Wu, S. *et al.* Molecular Mechanisms of PALB2 Function and Its Role in Breast Cancer Management. *Frontiers in Oncology* **10**, (2020).

143. Powell, S. N. & Kachnic, L. A. Roles of BRCA1 and BRCA2 in homologous recombination, DNA replication fidelity and the cellular response to ionizing radiation. *Oncogene* **22**, 5784–5791 (2003).

144. Prakash, R., Zhang, Y., Feng, W. & Jasin, M. Homologous Recombination and Human Health: The Roles of BRCA1, BRCA2, and Associated Proteins. *Cold Spring Harb Perspect Biol* **7**, a016600 (2015).

145. Buisson, R. & Masson, J.-Y. PALB2 self-interaction controls homologous recombination. *Nucleic Acids Research* **40**, 10312–10323 (2012).

146. Xia, B. *et al.* Control of BRCA2 Cellular and Clinical Functions by a Nuclear Partner, PALB2. *Molecular Cell* **22**, 719–729 (2006).

147. Krais, J. J. *et al.* RNF168-mediated localization of BARD1 recruits the BRCA1-PALB2 complex to DNA damage. *Nat Commun* **12**, 5016 (2021).

148. Jazayeri, A. *et al.* ATM- and cell cycle-dependent regulation of ATR in response to DNA double-strand breaks. *Nat Cell Biol* **8**, 37–45 (2006).

149. Mallery, D. L., Vandenberg, C. J. & Hiom, K. Activation of the E3 ligase function of the BRCA1/BARD1 complex by polyubiquitin chains. *The EMBO Journal* **21**, 6755–6762 (2002).

150. Witus, S. R. *et al.* BRCA1/BARD1 site-specific ubiquitylation of nucleosomal H2A is directed by BARD1. *Nat Struct Mol Biol* **28**, 268–277 (2021).

151. Densham, R. M. *et al.* Human BRCA1-BARD1 Ubiquitin ligase activity counters chromatin barriers to DNA resection. *Nat Struct Mol Biol* **23**, 647–655 (2016).

152. Shabbeer, S. *et al.* BRCA1 Targets G2/M Cell Cycle Proteins for Ubiquitination and Proteasomal Degradation. *Oncogene* **32**, 5005–5016 (2013).

153. Wu, W. *et al.* BRCA1 Ubiquitinates RPB8 in Response to DNA Damage. *Cancer Research* **67**, 951–958 (2007).

154. Horwitz, A. A., Affar, E. B., Heine, G. F., Shi, Y. & Parvin, J. D. A mechanism for transcriptional repression dependent on the BRCA1 E3 ubiquitin ligase. *Proc Natl Acad Sci U S A* **104**, 6614–6619 (2007).

155. Kwiatkowski, F. *et al.* BRCA Mutations Increase Fertility in Families at Hereditary Breast/Ovarian Cancer Risk. *PLOS ONE* **10**, e0127363 (2015).

156. Szabo, C. I., Worley, T. & Monteiro, A. N. A. Understanding Germ-Line Mutations in *BRCA1*. *Cancer Biology & Therapy* **3**, 515–520 (2004).

157. Berchuck, A. *et al.* Frequency of germline and somatic BRCA1 mutations in ovarian cancer. *Clin Cancer Res* **4**, 2433–2437 (1998).

158. Lin, W. T. *et al.* COMPARISON OF AGE AT NATURAL MENOPAUSE IN BRCA1/2 MUTATION CARRIERS TO A NON-CLINIC-BASED SAMPLE OF WOMEN IN NORTHERN CALIFORNIA. *Cancer* **119**, 1652–1659 (2013).

159. Finch, A. *et al.* Frequency of premature menopause in women who carry a BRCA1 or BRCA2 mutation. *Fertility and Sterility* **99**, 1724–1728 (2013).

160. Pavone, M. E. *et al.* Human Ovarian Tissue Cortex Surrounding Benign and Malignant Lesions. *Reprod Sci* **21**, 582–589 (2014).

161. Oktay, K., Kim, J. Y., Barad, D. & Babayev, S. N. Association of BRCA1 Mutations With Occult Primary Ovarian Insufficiency: A Possible Explanation for the Link Between Infertility and Breast/Ovarian Cancer Risks. *J Clin Oncol* **28**, 240–244 (2010).

162. Wang, E. T. *et al.* BRCA1 Germline Mutations May Be Associated With Reduced Ovarian Reserve. *Fertil Steril* **102**, 1723–1728 (2014).

163. Titus, S. *et al.* Impairment of BRCA1-related DNA Double Strand Break Repair Leads to Ovarian Aging in Mice and Humans. *Sci Transl Med* **5**, 172ra21 (2013).

164. Zhang, X. *et al.* Fertility preservation in BRCA mutation carriers—efficacy and safety issues: a review. *Reproductive Biology and Endocrinology* **18**, 11 (2020).

165. Derks-Smeets, I. A. P. *et al.* BRCA1 mutation carriers have a lower number of mature oocytes after ovarian stimulation for IVF/PGD. *J Assist Reprod Genet* **34**, 1475–1482 (2017).

166. Nelson, L. M. Primary Ovarian Insufficiency. *N Engl J Med* **360**, 606–614 (2009).

167. Albright, F., Smith, P. H. & Fraser, R. A SYNDROME CHARACTERIZED BY PRIMARY OVARIAN INSUFFICIENCY AND DECREASED STATURE: Report of 11 Cases With a Digression on Hormonal Control of Axillary and Pubic Hair. *The American Journal of the Medical Sciences* **204**, 625–648 (1942).

168. Welt, C. K. Primary ovarian insufficiency: a more accurate term for premature ovarian failure. *Clin Endocrinol* **68**, 499–509 (2008).

169. Cao, L., Li, W., Kim, S., Brodie, S. G. & Deng, C.-X. Senescence, aging, and malignant transformation mediated by p53 in mice lacking the Brca1 full-length isoform. *Genes Dev* **17**, 201–213 (2003).

170. Vogel, H., Lim, D.-S., Karsenty, G., Finegold, M. & Hasty, P. Deletion of Ku86 causes early onset of senescence in mice. *Proc Natl Acad Sci U S A* **96**, 10770–10775 (1999).

171. de Boer, J. *et al.* Premature Aging in Mice Deficient in DNA Repair and Transcription. *Science* **296**, 1276–1279 (2002).

172. Mohaghegh, P. & Hickson, I. D. DNA helicase deficiencies associated with cancer predisposition and premature ageing disorders. *Human Molecular Genetics* **10**, 741–746 (2001).

173. White, M. C. *et al.* Age and Cancer Risk. *Am J Prev Med* **46**, S7-15 (2014).

174. Pedersen, J. K., Engholm, G., Skytthe, A. & Christensen, K. Cancer and Aging: Epidemiology and Methodological Challenges. *Acta Oncol* **55**, 7–12 (2016).

175. Aunan, J. R., Cho, W. C. & Søreide, K. The Biology of Aging and Cancer: A Brief Overview of Shared and Divergent Molecular Hallmarks. *Aging Dis* **8**, 628–642 (2017).

176. Estapé, T. Cancer in the Elderly: Challenges and Barriers. *Asia Pac J Oncol Nurs* **5**, 40–42 (2018).

177. Berben, L., Floris, G., Wildiers, H. & Hatse, S. Cancer and Aging: Two Tightly Interconnected Biological Processes. *Cancers (Basel)* **13**, 1400 (2021).

178. Salazar, H. *et al.* Microscopic benign and invasive malignant neoplasms and a cancer-prone phenotype in prophylactic oophorectomies. *J Natl Cancer Inst* **88**, 1810–1820 (1996).

179. Etzold, A. *et al.* CAF-like state in primary skin fibroblasts with constitutional *BRCA1* epimutation sheds new light on tumor suppressor deficiency-related changes in healthy tissue. *Epigenetics* **11**, 120–131 (2016).

180. Love, M. I., Huber, W. & Anders, S. Moderated estimation of fold change and dispersion for RNA-seq data with DESeq2. *Genome Biol* **15**, 550 (2014).

181. Foroutan, M. *et al.* Single sample scoring of molecular phenotypes. *BMC Bioinformatics* **19**, 404 (2018).

182. Bhuva, D. D., Cursons, J. & Davis, M. J. Stable gene expression for normalisation and single-sample scoring. *Nucleic Acids Research* **48**, e113–e113 (2020).

183. Knights, C. D. *et al.* Distinct p53 acetylation cassettes differentially influence gene-expression patterns and cell fate. *J Cell Biol* **173**, 533–544 (2006).

184. Sturmlechner, I. *et al.* p21 produces a bioactive secretome that places stressed cells under immunosurveillance. *Science* **374**, eabb3420 (2021).

185. Lopes-Paciencia, S. *et al.* The senescence-associated secretory phenotype and its regulation. *Cytokine* **117**, 15–22 (2019).

186. Friedman, G. *et al.* Cancer-associated fibroblast compositions change with breast cancer progression linking the ratio of S100A4+ and PDPN+ CAFs to clinical outcome. *Nat Cancer* **1**, 692–708 (2020).

187. Biernacka, A., Dobaczewski, M. & Frangogiannis, N. G. TGF-β signaling in fibrosis. *Growth Factors* **29**, 196–202 (2011).

188. Yeung, T.-L. *et al.* TGF-β Modulates Ovarian Cancer Invasion by Upregulating CAF-Derived Versican in the Tumor Microenvironment. *Cancer Res* **73**, 5016–5028 (2013).

189. Ren, B. *et al.* E2F integrates cell cycle progression with DNA repair, replication, and G2/M checkpoints. *Genes Dev* **16**, 245–256 (2002).

190. Prakash, R. *et al.* Homologous recombination–deficient mutation cluster in tumor suppressor RAD51C identified by comprehensive analysis of cancer variants. *Proceedings of the National Academy of Sciences* **119**, e2202727119 (2022).

191. Witus, S. R., Stewart, M. D. & Klevit, R. E. The BRCA1/BARD1 ubiquitin ligase and its substrates. *Biochem J* **478**, 3467–3483 (2021).

192. González-Gualda, E., Baker, A. G., Fruk, L. & Muñoz-Espín, D. A guide to assessing cellular senescence in vitro and in vivo. *The FEBS Journal* **288**, 56–80 (2021).

193. Fort, M. M. *et al.* IL-25 Induces IL-4, IL-5, and IL-13 and Th2-Associated Pathologies In Vivo. *Immunity* **15**, 985–995 (2001).

194. Liu, Y., Shao, Z., Shangguan, G., Bie, Q. & Zhang, B. Biological Properties and the Role of IL-25 in Disease Pathogenesis. *Journal of Immunology Research* **2018**, e6519465 (2018).

195. Tamachi, T. *et al.* IL-25 enhances allergic airway inflammation by amplifying a TH2 cell–dependent pathway in mice. *Journal of Allergy and Clinical Immunology* **118**, 606–614 (2006).

196. Kruse, J.-P. & Gu, W. Modes of p53 Regulation. *Cell* **137**, 609–622 (2009).

197. Reed, S. M. & Quelle, D. E. p53 Acetylation: Regulation and Consequences. *Cancers (Basel)* **7**, 30–69 (2014).

198. Mijit, M., Caracciolo, V., Melillo, A., Amicarelli, F. & Giordano, A. Role of p53 in the Regulation of Cellular Senescence. *Biomolecules* **10**, 420 (2020).

199. Xenaki, G. *et al.* PCAF is a HIF-1α cofactor that regulates p53 transcriptional activity in hypoxia. *Oncogene* **27**, 5785–5796 (2008).

200. Kulaberoglu, Y., Gundogdu, R. & Hergovich, A. The Role of p53/p21/p16 in DNA-Damage Signaling and DNA Repair. in *Genome Stability* 243–256 (Elsevier, 2016). doi:10.1016/B978-0-12-803309-8.00015-X.

201. Jeyapalan, J. C. & Sedivy, J. M. Cellular senescence and organismal aging. *Mech Ageing Dev* **129**, 467–474 (2008).

202. Rufini, A., Tucci, P., Celardo, I. & Melino, G. Senescence and aging: the critical roles of p53. *Oncogene* **32**, 5129–5143 (2013).

203. Al Bitar, S. & Gali-Muhtasib, H. The Role of the Cyclin Dependent Kinase Inhibitor p21cip1/waf1 in Targeting Cancer: Molecular Mechanisms and Novel Therapeutics. *Cancers (Basel)* **11**, 1475 (2019).

204. Hu, L. *et al.* Why Senescent Cells Are Resistant to Apoptosis: An Insight for Senolytic Development. *Frontiers in Cell and Developmental Biology* **10**, (2022).

205. Pereira, B. I. *et al.* Senescent cells evade immune clearance via HLA-E-mediated NK and CD8+ T cell inhibition. *Nat Commun* **10**, 2387 (2019).

206. Béziat, V. *et al.* Human NKG2A overrides NKG2C effector functions to prevent autoreactivity of NK cells. *Blood* **117**, 4394–4396 (2011).

207. Law, R. H. *et al.* An overview of the serpin superfamily. *Genome Biol* **7**, 216 (2006).

208. Elyada, E. *et al.* Cross-Species Single-Cell Analysis of Pancreatic Ductal Adenocarcinoma Reveals Antigen-Presenting Cancer-Associated Fibroblasts. *Cancer Discovery* **9**, 1102–1123 (2019).

209. Kerdidani, D. *et al.* Lung tumor MHCII immunity depends on in situ antigen presentation by fibroblasts. *J Exp Med* **219**, e20210815 (2022).

210. Wang, M. *et al.* LAG3 and its emerging role in cancer immunotherapy. *Clinical and Translational Medicine* **11**, e365 (2021).

211. Kouo, T. *et al.* Galectin-3 Shapes Antitumor Immune Responses by Suppressing CD8+ T Cells via LAG-3 and Inhibiting Expansion of Plasmacytoid Dendritic Cells. *Cancer Immunol Res* **3**, 412–423 (2015).

212. Wang, J. *et al.* Fibrinogen-like protein 1 is a major immune inhibitory ligand of LAG3. *Cell* **176**, 334-347.e12 (2019).

213. Huard, B., Tournier, M., Hercend, T., Triebel, F. & Faure, F. Lymphocyte-activation gene 3/major histocompatibility complex class II interaction modulates the antigenic response of CD4+ T lymphocytes. *Eur J Immunol* **24**, 3216–3221 (1994).

214. Cifaldi, L. *et al.* DNAM-1 Activating Receptor and Its Ligands: How Do Viruses Affect the NK Cell-Mediated Immune Surveillance during the Various Phases of Infection? *Int J Mol Sci* **20**, 3715 (2019).

215. Gilson, R. C., Gunasinghe, S. D., Johannes, L. & Gaus, K. Galectin-3 modulation of T-cell activation: mechanisms of membrane remodelling. *Prog Lipid Res* **76**, 101010 (2019).

216. Zubieta, M. R. *et al.* Galectin-3 expression correlates with apoptosis of tumor-associated lymphocytes in human melanoma biopsies. *Am J Pathol* **168**, 1666–1675 (2006).

217. Landsverk, O. J. B., Ottesen, A. H., Berg-Larsen, A., Appel, S. & Bakke, O. Differential regulation of MHC II and invariant chain expression during maturation of monocyte-derived dendritic cells. *Journal of Leukocyte Biology* **91**, 729–737 (2012).

218. Huard, B., Prigent, P., Tournier, M., Bruniquel, D. & Triebel, F. CD4/major histocompatibility complex class II interaction analyzed with CD4- and lymphocyte activation gene-3 (LAG-3)-Ig fusion proteins. *Eur J Immunol* **25**, 2718–2721 (1995).

219. Hannier, S., Tournier, M., Bismuth, G. & Triebel, F. CD3/TCR complex-associated lymphocyte activation gene-3 molecules inhibit CD3/TCR signaling. *J Immunol* **161**, 4058–4065 (1998).

220. Yang, R. *et al.* Galectin-9 interacts with PD-1 and TIM-3 to regulate T cell death and is a target for cancer immunotherapy. *Nat Commun* **12**, 832 (2021).

221. Simons, K. H. *et al.* T cell co-stimulation and co-inhibition in cardiovascular disease: a double-edged sword. *Nat Rev Cardiol* **16**, 325–343 (2019).

222. Selman, M. & Pardo, A. Fibroageing: An ageing pathological feature driven by dysregulated extracellular matrix-cell mechanobiology. *Ageing Research Reviews* **70**, 101393 (2021).

223. Ovadya, Y. *et al.* Impaired immune surveillance accelerates accumulation of senescent cells and aging. *Nat Commun* **9**, 5435 (2018).

224. Hecker, L., Jagirdar, R., Jin, T. & Thannickal, V. J. Reversible Differentiation of Myofibroblasts by MyoD. *Exp Cell Res* **317**, 1914–1921 (2011).

225. Kato, K. *et al.* Impaired Myofibroblast Dedifferentiation Contributes to Nonresolving Fibrosis in Aging. *Am J Respir Cell Mol Biol* **62**, 633–644 (2020).

226. Mora, A. L., Rojas, M., Pardo, A. & Selman, M. Emerging therapies for idiopathic pulmonary fibrosis, a progressive age-related disease. *Nat Rev Drug Discov* **16**, 755–772 (2017).

227. Álvarez, D. *et al.* IPF lung fibroblasts have a senescent phenotype. *Am J Physiol Lung Cell Mol Physiol* **313**, L1164–L1173 (2017).

228. Cui, H. *et al.* miR-34a Inhibits Lung Fibrosis by Inducing Lung Fibroblast Senescence. *Am J Respir Cell Mol Biol* **56**, 168–178 (2017).

229. Wang, Z. *et al.* CD146, from a melanoma cell adhesion molecule to a signaling receptor. *Sig Transduct Target Ther* **5**, 1–15 (2020).

230. Granata, R. *et al.* Dual effects of IGFBP-3 on endothelial cell apoptosis and survival: involvement of the sphingolipid signaling pathways. *FASEB J* **18**, 1456–1458 (2004).

231. Tubaro, C., Arcuri, C., Giambanco, I. & Donato, R. S100B in myoblasts regulates the transition from activation to quiescence and from quiescence to activation and reduces apoptosis. *Biochim Biophys Acta* **1813**, 1092–1104 (2011).

232. Tripathi, U., Misra, A., Tchkonia, T. & Kirkland, J. L. Impact of Senescent Cell Subtypes on Tissue Dysfunction and Repair: Importance and Research Questions. *Mechanisms of Ageing and Development* **198**, 111548 (2021).

233. Yousefzadeh, M. J. *et al.* Tissue specificity of senescent cell accumulation during physiologic and accelerated aging of mice. *Aging Cell* **19**, e13094 (2020).

234. Yang, J., Liu, M., Hong, D., Zeng, M. & Zhang, X. The Paradoxical Role of Cellular Senescence in Cancer. *Frontiers in Cell and Developmental Biology* **9**, (2021).

235. Radisky, D. C., Kenny, P. A. & Bissell, M. J. Fibrosis and Cancer: Do Myofibroblasts Come Also From Epithelial Cells Via EMT? *J Cell Biochem* **101**, 830–839 (2007).

236. Chandler, C., Liu, T., Buckanovich, R. & Coffman, L. G. The double edge sword of fibrosis in cancer. *Translational Research* **209**, 55–67 (2019).

237. Piersma, B., Hayward, M. K. & Weaver, V. M. Fibrosis and cancer: A strained relationship. *Biochim Biophys Acta Rev Cancer* **1873**, 188356 (2020).

238. Lawrenson, K. *et al.* Senescent Fibroblasts Promote Neoplastic Transformation of Partially Transformed Ovarian Epithelial Cells in a Three-dimensional Model of Early Stage Ovarian Cancer. *Neoplasia* **12**, 317–325 (2010).

239. Mikuła-Pietrasik, J. *et al.* Senescent peritoneal mesothelium creates a niche for ovarian cancer metastases. *Cell Death Dis* **7**, e2565 (2016).

240. Yang, G. *et al.* The chemokine growth-regulated oncogene 1 (Gro-1) links RAS signaling to the senescence of stromal fibroblasts and ovarian tumorigenesis. *Proceedings of the National Academy of Sciences* **103**, 16472–16477 (2006).

241. Verderio, E. A. M., Johnson, T. & Griffin, M. Tissue transglutaminase in normal and abnormal wound healing: Review article. *Amino Acids* **26**, (2004).

242. Pehrsson, M. *et al.* Enzymatic cross-linking of collagens in organ fibrosis – resolution and assessment. *Expert Review of Molecular Diagnostics* **21**, 1049–1064 (2021).

243. Tang, X., Li, P.-H. & Chen, H.-Z. Cardiomyocyte Senescence and Cellular Communications Within Myocardial Microenvironments. *Frontiers in Endocrinology* **11**, (2020).

244. Schafer, M. J., Haak, A. J., Tschumperlin, D. J. & LeBrasseur, N. K. Targeting Senescent Cells in Fibrosis: Pathology, Paradox, and Practical Considerations. *Curr Rheumatol Rep* **20**, 3 (2018).

245. Xu, J., Zhou, L. & Liu, Y. Cellular Senescence in Kidney Fibrosis: Pathologic Significance and Therapeutic Strategies. *Frontiers in Pharmacology* **11**, (2020).

246. Pardo, A. & Selman, M. The Interplay of the Genetic Architecture, Aging, and Environmental Factors in the Pathogenesis of Idiopathic Pulmonary Fibrosis. *Am J Respir Cell Mol Biol* **64**, 163–172 (2021).

247. Levi, N., Papismadov, N., Solomonov, I., Sagi, I. & Krizhanovsky, V. The ECM path of senescence in aging: components and modifiers. *The FEBS Journal* **287**, 2636–2646 (2020).

248. Enomoto, N. *et al.* Amount of elastic fibers predicts prognosis of idiopathic pulmonary fibrosis. *Respiratory Medicine* **107**, 1608–1616 (2013).

249. Kanta, J. Elastin in the Liver. *Frontiers in Physiology* **7**, (2016).

250. Scallan, J., Huxley, V. H. & Korthuis, R. J. *Pathophysiology of Edema Formation. Capillary Fluid Exchange: Regulation, Functions, and Pathology* (Morgan & Claypool Life Sciences, 2010).

251. Manon-Jensen, T. & Karsdal, M. A. Chapter 12 - Type XII Collagen. in *Biochemistry of Collagens, Laminins and Elastin* (ed. Karsdal, M. A.) 81–85 (Academic Press, 2016). doi:10.1016/B978-0-12-809847-9.00012-X.

252. Manon-Jensen, T. & Karsdal, M. A. Chapter 14 - Type XIV Collagen. in *Biochemistry of Collagens, Laminins and Elastin* (ed. Karsdal, M. A.) 93–95 (Academic Press, 2016). doi:10.1016/B978-0-12-809847-9.00014-3.

253. Ricard-Blum, S. The Collagen Family. *Cold Spring Harb Perspect Biol* **3**, a004978 (2011).

254. Holmes, D. F. & Kadler, K. E. The 10+4 microfibril structure of thin cartilage fibrils. *Proceedings of the National Academy of Sciences of the United States of America* **103**, 17249 (2006).

255. Tzortzaki, E. G. *et al.* Expression of FACIT collagens XII and XIV during bleomycin-induced pulmonary fibrosis in mice. *The Anatomical Record Part A: Discoveries in Molecular, Cellular, and Evolutionary Biology* **275A**, 1073–1080 (2003).

256. Chen, D. *et al.* Distinct effects of different matrix proteoglycans on collagen fibrillogenesis and cell-mediated collagen reorganization. *Sci Rep* **10**, 19065 (2020).

257. Zhu, W., Robey, P. G. & Boskey, A. L. CHAPTER 9 - The Regulatory Role of Matrix Proteins in Mineralization of Bone. in *Osteoporosis (Third Edition)* (eds. Marcus, R., Feldman, D., Nelson, D. A. & Rosen, C. J.) 191–240 (Academic Press, 2008). doi:10.1016/B978-012370544-0.50011-2.

258. Kalamajski, S. & Oldberg, Å. The role of small leucine-rich proteoglycans in collagen fibrillogenesis. *Matrix Biology* **29**, 248–253 (2010).

259. Baghy, K. *et al.* Ablation of the decorin gene enhances experimental hepatic fibrosis and impairs hepatic healing in mice. *Lab Invest* **91**, 439–451 (2011).

260. Tanzer, M. L. Cross-linking of collagen. *Science* **180**, 561–566 (1973).

261. Garnero, P. The contribution of collagen crosslinks to bone strength. *Bonekey Rep* **1**, 182 (2012).

262. Theocharis, A. D., Manou, D. & Karamanos, N. K. The extracellular matrix as a multitasking player in disease. *The FEBS Journal* **286**, 2830–2869 (2019).

263. Junqueira, L. C. & Montes, G. S. Biology of collagen-proteoglycan interaction. *Arch Histol Jpn* **46**, 589–629 (1983).

264. Liu, B., McNally, S., Kilpatrick, J. I., Jarvis, S. P. & O'Brien, C. J. Aging and ocular tissue stiffness in glaucoma. *Survey of Ophthalmology* **63**, 56–74 (2018).

265. Snedeker, J. G. & Gautieri, A. The role of collagen crosslinks in ageing and diabetes - the good, the bad, and the ugly. *Muscles Ligaments Tendons J* **4**, 303–308 (2014).

266. González, A., López, B., Ravassa, S., San José, G. & Díez, J. The complex dynamics of myocardial interstitial fibrosis in heart failure. Focus on collagen cross-linking. *Biochimica et Biophysica Acta (BBA) - Molecular Cell Research* **1866**, 1421–1432 (2019).

267. Aumiller, V. *et al.* Comparative analysis of lysyl oxidase (like) family members in pulmonary fibrosis. *Sci Rep* **7**, 149 (2017).

268. Philp, C. J. *et al.* Extracellular Matrix Cross-Linking Enhances Fibroblast Growth and Protects against Matrix Proteolysis in Lung Fibrosis. *Am J Respir Cell Mol Biol* **58**, 594–603 (2018).

269. Olsen, K. C. *et al.* Transglutaminase 2 and its role in pulmonary fibrosis. *Am J Respir Crit Care Med* **184**, 699–707 (2011).

270. Huang, M. *et al.* Lysyl oxidase enzymes mediate TGF-β1-induced fibrotic phenotypes in human skin-like tissues. *Laboratory Investigation* **99**, 514–527 (2019).

271. Okada, K., Moon, H.-J., Finney, J., Meier, A. & Mure, M. Extracellular Processing of Lysyl Oxidase-like 2 and Its Effect on Amine Oxidase Activity. *Biochemistry* **57**, 6973–6983 (2018).

272. Albeiroti, S., Soroosh, A. & de la Motte, C. A. Hyaluronan's Role in Fibrosis: A Pathogenic Factor or a Passive Player? *BioMed Research International* **2015**, e790203 (2015).

273. Wang, Y., Lauer, M. E., Anand, S., Mack, J. A. & Maytin, E. V. Hyaluronan Synthase 2 Protects Skin Fibroblasts against Apoptosis Induced by Environmental Stress *. *Journal of Biological Chemistry* **289**, 32253–32265 (2014).

274. Li, Y. *et al.* Severe lung fibrosis requires an invasive fibroblast phenotype regulated by hyaluronan and CD44. *Journal of Experimental Medicine* **208**, 1459–1471 (2011).

275. Petrey, A. & de la Motte, C. Hyaluronan, a Crucial Regulator of Inflammation. *Frontiers in Immunology* **5**, (2014).

276. Kiani, C., Chen, L., Wu, Y. J., Yee, A. J. & Yang, B. B. Structure and function of aggrecan. *Cell Res* **12**, 19–32 (2002).

277. Evanko, S. P. *et al.* A Role for HAPLN1 During Phenotypic Modulation of Human Lung Fibroblasts In Vitro. *J Histochem Cytochem* **68**, 797–811 (2020).

278. Yang, B. B., Zhang, Y., Cao, L. & Yang, B. L. Aggrecan and link protein affect cell adhesion to culture plates and to type II collagen. *Matrix Biol* **16**, 541–561 (1998).

279. Shi, Y. *et al.* A small molecule promotes cartilage extracellular matrix generation and inhibits osteoarthritis development. *Nat Commun* **10**, 1914 (2019).

280. Elenkov, I. J. & Chrousos, G. P. Stress Hormones, Th1/Th2 patterns, Pro/Anti-inflammatory Cytokines and Susceptibility to Disease. *Trends in Endocrinology & Metabolism* **10**, 359–368 (1999).

281. Deng, C. *et al.* Roles of IL-25 in Type 2 Inflammation and Autoimmune Pathogenesis. *Front Immunol* **12**, 691559 (2021).

282. Opal, S. M. & DePalo, V. A. Anti-Inflammatory Cytokines. *Chest* **117**, 1162–1172 (2000).

283. Dong, J. & Ma, Q. Type 2 Immune Mechanisms in Carbon Nanotube-Induced Lung Fibrosis. *Frontiers in Immunology* **9**, (2018).

284. Chang-Ni Lin, Chih-Yen Chien, & Hui-Ching Chung. Are Friends or Foes? New Strategy for Head and Neck Squamous Cell Carcinoma Treatment via Immune Regulation. *International Journal of Head and Neck Science* **1**, (2017).

285. Spellberg, B. & Edwards, J. E., Jr. Type 1/Type 2 Immunity in Infectious Diseases. *Clinical Infectious Diseases* **32**, 76–102 (2001).

286. Gieseck, R. L., Wilson, M. S., Wynn, T. A., Wilson, M. S. & Wynn, T. A. Type 2 immunity in tissue repair and fibrosis. *Nat Rev Immunol* **18**, 62–76 (2018).

287. Aceves, S. S. & Ackerman, S. J. Relationships Between Eosinophilic Inflammation, Tissue Remodeling and Fibrosis in Eosinophilic Esophagitis. *Immunol Allergy Clin North Am* **29**, 197–xiv (2009).

288. Aceves, S. S. Remodeling and fibrosis in chronic eosinophil inflammation. *Dig Dis* **32**, 15–21 (2014).

289. Jacobs, I. *et al.* Role of Eosinophils in Intestinal Inflammation and Fibrosis in Inflammatory Bowel Disease: An Overlooked Villain? *Frontiers in Immunology* **12**, (2021).

290. Peng, B. *et al.* Role of IL-25 on Eosinophils in the Initiation of Th2 Responses in Allergic Asthma. *Front. Immunol.* **13**, 842500 (2022).

291. Gieseck, R. L. *et al.* Interleukin-13 Activates Distinct Cellular Pathways Leading to Ductular Reaction, Steatosis, and Fibrosis. *Immunity* **45**, 145–158 (2016).

292. Kaviratne, M. *et al.* IL-13 Activates a Mechanism of Tissue Fibrosis That Is Completely TGF-β Independent. *The Journal of Immunology* **173**, 4020–4029 (2004).

293. Liu, Y. *et al.* IL-13 Induces Connective Tissue Growth Factor in Rat Hepatic Stellate Cells via TGF-β–Independent Smad Signaling. *The Journal of Immunology* **187**, 2814–2823 (2011).

294. Chiaramonte, M. G. *et al.* Regulation and Function of the Interleukin 13 Receptor α 2 During a T Helper Cell Type 2–dominant Immune Response. *J Exp Med* **197**, 687–701 (2003).

295. Lech, M. & Anders, H.-J. Macrophages and fibrosis: How resident and infiltrating mononuclear phagocytes orchestrate all phases of tissue injury and repair. *Biochimica et Biophysica Acta (BBA) - Molecular Basis of Disease* **1832**, 989–997 (2013).

296. Stout, R. D. *et al.* Macrophages Sequentially Change Their Functional Phenotype in Response to Changes in Microenvironmental Influences1. *The Journal of Immunology* **175**, 342–349 (2005).

297. Lang, R., Patel, D., Morris, J. J., Rutschman, R. L. & Murray, P. J. Shaping Gene Expression in Activated and Resting Primary Macrophages by IL-10. *The Journal of Immunology* **169**, 2253–2263 (2002).

298. Jones, C. V. & Ricardo, S. D. Macrophages and CSF-1. *Organogenesis* **9**, 249–260 (2013).

299. Cox, T. R. *et al.* LOX-Mediated Collagen Crosslinking Is Responsible for Fibrosis-Enhanced Metastasis. *Cancer Research* **73**, 1721–1732 (2013).

300. Cox, T. R. & Erler, J. T. Molecular Pathways: Connecting Fibrosis and Solid Tumor Metastasis. *Clinical Cancer Research* **20**, 3637–3643 (2014).

301. Bonnans, C., Chou, J. & Werb, Z. Remodelling the extracellular matrix in development and disease. *Nat Rev Mol Cell Biol* **15**, 786–801 (2014).

302. Campisi, J. Aging, Cellular Senescence, and Cancer. *Annu Rev Physiol* **75**, 685–705 (2013).

303. Krishnamurthy, J. *et al.* p16INK4a induces an age-dependent decline in islet regenerative potential. *Nature* **443**, 453–457 (2006).

304. Campisi, J. Cellular senescence: putting the paradoxes in perspective. *Curr Opin Genet Dev* **21**, 107–112 (2011).

305. Woodruff, T. K. & Shea, L. D. The Role of the Extracellular Matrix in Ovarian Follicle Development. *Reprod Sci* **14**, 6–10 (2007).

306. Grosbois, J., Bailie, E. C., Kelsey, T. W., Anderson, R. A. & Telfer, E. E. Spatio-temporal remodelling of the composition and architecture of the human ovarian cortical extracellular matrix during in vitro culture. *Human Reproduction* **38**, 444–458 (2023).

307. Nagamatsu, G., Shimamoto, S., Hamazaki, N., Nishimura, Y. & Hayashi, K. Mechanical stress accompanied with nuclear rotation is involved in the dormant state of mouse oocytes. *Sci Adv* **5**, eaav9960 (2019).

308. Xu, M., West, E., Shea, L. D. & Woodruff, T. K. Identification of a stage-specific permissive in vitro culture environment for follicle growth and oocyte development. *Biol Reprod* **75**, 916–923 (2006).

309. Handorf, A. M., Zhou, Y., Halanski, M. A. & Li, W.-J. Tissue Stiffness Dictates Development, Homeostasis, and Disease Progression. *Organogenesis* **11**, 1–15 (2015).

310. Stocco, C., Telleria, C. & Gibori, G. The molecular control of corpus luteum formation, function, and regression. *Endocr Rev* **28**, 117–149 (2007).

311. Niswender, G. D., Juengel, J. L., Silva, P. J., Rollyson, M. K. & McIntush, E. W. Mechanisms Controlling the Function and Life Span of the Corpus Luteum. *Physiological Reviews* **80**, 1–29 (2000).

312. Bhatia-Dey, N., Kanherkar, R. R., Stair, S. E., Makarev, E. O. & Csoka, A. B. Cellular Senescence as the Causal Nexus of Aging. *Frontiers in Genetics* **7**, (2016).

313. Diwan, B. & Sharma, R. Nutritional components as mitigators of cellular senescence in organismal aging: a comprehensive review. *Food Sci Biotechnol* **31**, 1089–1109 (2022).

314. Varela, I. *et al.* Accelerated ageing in mice deficient in Zmpste24 protease is linked to p53 signalling activation. *Nature* **437**, 564–568 (2005).

315. Baker, D. J. *et al.* Clearance of p16Ink4a-positive senescent cells delays ageing-associated disorders. *Nature* **479**, 232–236 (2011).

316. Krishnamurthy, J. *et al.* Ink4a/Arf expression is a biomarker of aging. *J Clin Invest* **114**, 1299–1307 (2004).

317. Kim, K. S. *et al.* Regulation of replicative senescence by insulin-like growth factor-binding protein 3 in human umbilical vein endothelial cells. *Aging Cell* **6**, 535–545 (2007).

318. Wu, R., Van der Hoek, K. H., Ryan, N. K., Norman, R. J. & Robker, R. L. Macrophage contributions to ovarian function. *Hum Reprod Update* **10**, 119–133 (2004).

319. Zhang, Z., Schlamp, F., Huang, L., Clark, H. & Brayboy, L. Inflammaging is associated with shifted macrophage ontogeny and polarization in the aging mouse ovary. *Reproduction* **159**, 325–337 (2020).

320. Hou, J. *et al.* M2 macrophages promote myofibroblast differentiation of LR-MSCs and are associated with pulmonary fibrogenesis. *Cell Communication and Signaling* **16**, 89 (2018).

321. Wang, X. *et al.* The Role of Macrophages in Kidney Fibrosis. *Frontiers in Physiology* **12**, (2021).

322. Meziani, L. *et al.* CSF1R inhibition prevents radiation pulmonary fibrosis by depletion of interstitial macrophages. *European Respiratory Journal* **51**, (2018).

323. Buechler, M. B., Fu, W. & Turley, S. J. Fibroblast-macrophage reciprocal interactions in health, fibrosis, and cancer. *Immunity* **54**, 903–915 (2021).

324. Schafer, M. J. *et al.* Cellular senescence mediates fibrotic pulmonary disease. *Nat Commun* **8**, 14532 (2017).

325. Hinz, B. & Lagares, D. Evasion of apoptosis by myofibroblasts: a hallmark of fibrotic diseases. *Nat Rev Rheumatol* **16**, 11–31 (2020).

326. Harper, E. I., Sheedy, E. F. & Stack, M. S. With Great Age Comes Great Metastatic Ability: Ovarian Cancer and the Appeal of the Aging Peritoneal Microenvironment. *Cancers (Basel)* **10**, (2018).

327. Parrinello, S., Coppe, J.-P., Krtolica, A. & Campisi, J. Stromal-epithelial interactions in aging and cancer: senescent fibroblasts alter epithelial cell differentiation. *J Cell Sci* **118**, 485–496 (2005).

328. Krtolica, A. & Campisi, J. Cancer and aging: a model for the cancer promoting effects of the aging stroma. *Int J Biochem Cell Biol* **34**, 1401–1414 (2002).